

# University of Naples Federico II



*PhD PROGRAM IN NEUROSCIENCE*

*XXXIII CYCLE*

**Beyond retigabine: Design, identification, and  
pharmacological characterization of novel neuronal Kv7  
channel activators**

***Coordinator:* Prof. Maurizio Tagliatela**

***Tutor***

**Prof. Maurizio Tagliatela**

***Candidate***

**Dr Piera Nappi**

**ACADEMIC YEAR 2020-21**

## Index

1. Introduction .....	1
1.1 Epilepsy: definition, classification, and cause .....	1
1.2 Epileptic Encephalopathies: an overview .....	4
1.3 Ion channels.....	6
1.3.1 Potassium channels .....	7
1.4 Kv7 potassium channel family .....	9
1.5 Structure of Kv7 channels.....	12
1.5.1 Electromechanical coupling .....	14
1.5.2 Regulation of Kv7 channels .....	16
1.6 Neuronal Kv7 channels; cellular, subcellular distribution.....	19
1.6.1 The functional role of neuronal Kv7 channels.....	20
1.6.2 M-channels regulation.....	22
1.7 KCNQ2 and KCNQ3 channelopathies.....	23
1.8 Animal models of KCNQ dysfunction.....	28
1.9 Pharmacology of Kv7 channels.....	31
1.9.1 $I_{KM}$ blockers .....	32
1.9.2 $I_{KM}$ Activator .....	35
1.9.2.1 Flupirtine, Retigabine and Derivatives .....	35
1.9.2.2 Acrylamide .....	49

1.9.2.3 Benzamides .....	53
1.9.2.4 Fenamates .....	56
1.9.2.5 Other chemotypes of neuronal Kv7 activators .....	58
1.9.2.6 Gaba, gabapentinoids, and ketogenic diet .....	61
1.9.2.7 Traditional medicine .....	63
1.10 Precision medicine in Epilepsy .....	64
2 Aim of the work .....	73
3. Materials and methods .....	75
3.1 Site-Directed Mutagenesis .....	75
3.2 Bacterial transformation and plasmidic DNA preparation.....	76
3.3 Cell cultures.....	77
3.4 Generation of stable cell lines .....	77
3.4.1 PiggyBac (PB) Transposon system .....	77
3.4.2 Generation of PB-RedPuro- Kv7.2 .....	79
3.4.3 Generation of PB-RedPuro- Kv7.3 .....	80
3.4.3 Generation of PB-RedPuro- Kv7.3 A315T .....	81
3.4.3 Generation of PB-RedPuro- Kv7.4 .....	82
3.5 Cell cultures and stable transfection with Lipofectamine .....	82
3.6 Whole-cell electrophysiology .....	83
3.6.1 CHO cells preparation and electrophysiology .....	83

3.7 FluxOR™ II Green Potassium Ion Channel Assay.....	85
3.8 Photochemical Stability Assay.....	87
3.9 Homology model.....	88
3.10 Protein preparation .....	88
3.11 Molecular docking.....	89
3.11.1 Ligand preparation .....	89
3.11.2 Glide .....	89
3.11.3 InducedFit.....	91
3.12 Molecular Dynamics Simulations .....	92
3.13 Statistics.....	95
4 Results .....	96
4.1 Ligand Docking.....	96
4.2 Molecular Dynamics Simulations of the Apo form .....	102
4.2.1 Selection of simulation timescale.....	102
4.2.2 Application of GCMC.....	105
4.3 Molecular Dynamics Simulations of the Holo form .....	105
4.4 Functional characterization of Kv7.2 S303A mutant.....	113
4.5 Synthetic strategy .....	116
4.6 Electrophysiological characterization of Kv7.2/Kv7.3, Kv7.2, Kv7.3, Kv7.3A315T, Kv7.4 stable cell lines .....	118

4.7 Screening of the compound library .....	125
4.7.1 Effects of known Kv7 activators and inhibitor on fluorescence in CHO-Kv7.2/Kv7.3 .....	125
4.7.2 Library screening on CHO-Kv7.2/Kv7.3 .....	128
4.7.3 Electrophysiological characterization of CP RET 46, 59, 63, and 86 on Kv7.2/Kv7.3 channels. ....	132
4.7.4 Photostability Assays .....	134
4.7.5 Library screening on CHO-Kv7.4 .....	136
4.7.6 Library screening on CHO-Kv7.3* .....	139
5 Discussion and conclusion .....	140
5.1 Evaluation of retigabine binding mode and refinement of ligand binding site.....	141
5.2 Screening of newly synthesized retigabine derivatives .....	144
5.2.1 Structure–Activity Relationship of retigabine derivatives.....	146
5.3 Search of selectivity .....	150
5.4 Conclusion and future direction .....	151
Referece.....	152

## Abbreviations

AEDs: antiepileptic drugs

AHP: afterhyperpolarization

AIS: axon initial segment

ankG: ankyrin G

AP: action potential

ASD: autism spectrum disorder

BFIS: Benign Familial Infantile Seizures

BFNIS: Benign Familial Neonatal-Infantile Seizures

BFNS: *Benign Familial Neonatal Seizures*

BHB:  $\beta$ -hydroxybutyric acid

CaM: Calmodulin

CHO: Chinese Hamster Ovary

CNS: central nervous system

Cryo-EM: Cryo-electron microscopy

DAG: diacylglycerol

DD: developmental disability

DE: developmental encephalopathy

DEE: developmental and epileptic encephalopathies

DFNA2: deafness nonsyndromic autosomal dominant 2

DN: dominant-negative

EC<sub>50</sub>: half maximal effective concentration

EE: Epileptic Encephalopathy

EEG: electroencephalogram

EIEE: early infantile epileptic encephalopathy

FCD: Focal cortical dysplasia

FDA: Food and Drug Administration

GABA:  $\gamma$ -amino-butyric acid

GABOB:  $\gamma$ -amino- $\beta$ -hydroxybutyric acid

GCMC: Grand canonical Monte Carlo

GoF: gain-of-function

GSK: GlaxoSmithKline

HTS: high-throughput screening

IC<sub>50</sub>: half maximal inhibitory concentration

ID: intellectual disability

I<sub>KM</sub>: M-current

ILAE: International League Against Epilepsy

IP3: inositol triphosphate

IVA: Isovaleric acid

KD: ketogenic diet

KO: knock-out

LoF: loss-of-function

LQTS: long QT syndrome

MEA: microelectrode array

MES: maximal electroshock seizures

MD: Molecular Dynamics

mTOR: mechanistic target of rapamycin

MTX: Mallotoxin

nAChR: nicotinic acetylcholine receptor

NDD: neurodevelopmental delay

NMD: non-sense mediated mRNA decay

NMDA: N-methyl-D-aspartate

OHCs: outer hair cells

PB: PiggyBac

PCR: Polymerase Chain Reaction

PD: pore domain

PDB: Protein Data Bank

PIP2: Phosphatidylinositol 4,5-bisphosphate

PKC: protein kinase C

PLC: phospholipase C

Po: maximal probability of opening

PTZ: pentylenetetrazole

RMSD: Root Mean Square Deviation

RMSF: Root Mean Square Fluctuation

SID: subunit interaction domain

SQTS: short QT syndrome

TSC: tuberous sclerosis complex

TEA: tetraethylammonium

Vrest: resting membrane potential

VSD: Voltage Sensing Domain

$V_{1/2}$ : half-activation potential

WHO: World Health Organization



## Abstract

The Kv7 subfamily of voltage-gated potassium channels includes 5 members (Kv7.1-Kv7.5) having distinct expression patterns and physiological roles. Kv7.2 and Kv7.3 subunits are mainly expressed in the nervous system, where they underlie the so-called M-current ( $I_{KM}$ ), a sub-threshold  $K^+$  current controlling action potential generation. Neuronal Kv7 potassium channels are critical regulators of neuronal excitability; indeed, loss-of-function mutations in the genes encoding for Kv7.2 and Kv7.3 are responsible for a wide spectrum of early-onset epilepsies.

On the other hand, retigabine is a strong activator of the Kv7 currents, representing the first antiepileptic drug acting on Kv7 channels. Approved in 2011 for adjunctive therapy in adults showing drug-resistant partial onset seizures with or without secondary generalization, retigabine suppresses neuronal hyperexcitability by shifting the Kv7.2/3 current activation threshold toward more hyperpolarized potentials, thereby increasing their maximal current. Unfortunately, retigabine, suffers from considerable drawbacks including poor selectivity for Kv7 subtypes, short half-life, poor brain penetration and chemical instability. The latter, represents one of the main clinical concern over retigabine; light exposure may cause photodegradation and oxidation, leading to dimer formation, which induces retinal and mucocutaneous blue-gray discoloration in patients taking the drugs more than 3 years. For these reasons, leading to a progressively reduced use of the drug, the manufacturing company (GSK) has decided to withdraw the drug from the market since June 2017.

Since no KCNQ activator is currently available for clinical use, this work originates from our effort to identify novel and safer  $I_{KM}$  activators. For this purpose, we synthesized a library of 41 retigabine derivatives, structurally characterized by modification that aim to overcome at least some of the limitations of retigabine and we developed a fluorescence-based assay to rapidly evaluate the effect of these derivatives on Kv7 channels.

# 1. Introduction

## 1.1 Epilepsy: definition, classification, and cause

Epilepsy is one of the most common chronic neurological disorders affecting approximately 50 million people worldwide (WHO, 2019). The International League Against Epilepsy (ILAE) defines epilepsy as a disorder of the brain characterized by an enduring predisposition to generate epileptic seizures and by the neurobiological, cognitive, psychological, and social consequences of this condition. The definition of epilepsy requires the occurrence of at least one epileptic seizure, which is defined as a transient occurrence of signs and/or symptoms due to abnormal excessive or synchronous neuronal activity in the brain (Fisher et al., 2005). In 2017, the ILAE published a new classification of epilepsy (Scheffer et al., 2017). The starting point of this multilevel classification is the definition of the seizure type; seizures are classified into focal onset, generalized onset, and unknown onset. Focal seizures (previously namely partial seizures) originate within networks limited to one hemisphere. Focal epileptic seizures are further distinguished according to the presence or absence of impaired awareness. Awareness means the ability of the subject to be aware of what is happening around him and what is going on during the crisis, being able to interact and report it later. Focal seizures with or without awareness optionally may be further characterized by one motor or nonmotor onset symptoms. Focal epileptic seizures in which abnormal neuronal electrical activity occurs may evolve to bilateral tonic-clonic seizures (previously called secondarily generalized seizures). Generalized seizures affect both cerebral hemispheres; manifestations can be asymmetrical, rendering difficult the distinction from focal-onset seizures. Generalized seizures are divided into motor (tonic-clonic, clonic, myoclonic, atonic, etc.) and nonmotor (typical or atypical absences, absences with myoclonus) seizures and are associated with impairment of awareness or complete loss of consciousness.

The second level is the definition of the epilepsy type. Also the different types of epilepsy can be classified in focal, generalized, mixed: focal and generalized, and unknown, depending on the type of epileptic seizures present.

Finally, the third level is represented by the identification of the epilepsy syndrome. An epilepsy syndrome refers to a collection of features including seizure types, EEG, and imaging features that tend to occur together. Often has age-dependent features such as age at onset and remission, seizure triggers, diurnal variation, and sometimes prognosis. It may also have distinctive comorbidities such as intellectual and psychiatric dysfunction, together with specific findings on EEG and imaging studies. Epileptic syndromes are therefore defined by a set of elements (clinical characteristics of the patient, type of epileptic seizures, etiology, etc.) that constitute and define a particular clinical condition; their correct classification allows to use of a more targeted treatment and define with more precision the prognosis.

Epilepsy may be the result of different etiologies (Berg et al., 2010):

- Genetic: the epileptic seizures are the direct result of a known or presumed genetic defect(s). Designation of the fundamental nature of the disorder as genetic does not exclude the possibility that environmental factors may contribute to the expression of the disease.
- Structural/metabolic: epilepsy is the result of structural (for example, stroke, trauma, infection) or metabolic conditions or diseases. They may also be of genetic origin; for instance, a patient with tuberous sclerosis has both a structural and a genetic etiology.
- “Unknown cause” in which the nature of the underlying cause is yet unknown.

Epilepsy incidence is bimodal, highest in both young children and older adults. Approximately 1 out of 150 children is diagnosed with epilepsy during the first 10 years of life, with highest incidence rate observed during infancy. In Norway, the incidence rate of epilepsy was 144 per 100 000 person-years in the first years of life and 58 per 100 000 for ages 1 to 10 years. The cumulative incidence of epilepsy was 0.66% at age 10 years (Aaberg KM et al., 2017).

Unfortunately, to date, despite the development in recent years of new anticonvulsant drugs (AEDs) with differing mechanisms of action, the pharmacological treatment of this neurological disorders remains a critical medical issue, with 30% of patients showing suboptimal response to treatment.

## 1.2 Epileptic Encephalopathies: an overview

Up to one-third of epilepsies are refractory to medical treatments, and a significant proportion of childhood intractable epilepsies have a significant detrimental effect on cognition and brain function. These conditions, in which the epileptiform abnormalities are thought to significantly contribute to the overall brain, are referred to as *epileptic encephalopathies (EE)* (Berg et al., 2010). The main features of EE include EEG abnormalities, seizures that are usually multi-form and intractable, developmental delay or intellectual disability, sometimes early death. More recently, in 2017, to highlight that the developmental impairment may not be necessary related to epileptic activity, the ILAE introduced the concept of “developmental and epileptic encephalopathies”.

DEE often have a genetic etiology, and the history of gene discovery in epileptic encephalopathies relates to gene discovery in epilepsies in general (Figure 1)

Starting from the era of family studies, several genes underlying relatively mild dominantly inherited familial epilepsies had been discovered, such as CHRNA4, SCN1A, SCN1B, KCNQ2, and GABRG2. Particularly, in 1995 the first gene identified was CHRNA4, encoding for the  $\alpha 4$ -subunit of the neuronal nicotinic acetylcholine receptor nAChR. Here, a S248F amino-acid exchange within the second transmembrane region was found in a patient with autosomal dominant nocturnal frontal lobe epilepsy (Steinlein et al., 1995). Later in 1998, mutations in the voltage-gated potassium channel genes KCNQ2 or KCNQ3 located on chromosome 20q13.3 and 8q24 respectively were identified in patients with Benign Familial Neonatal Seizures (Singh NA et al., 1998; Charlier C et al., 1998).

While these gene discoveries initially had no direct link to the more severe epileptic encephalopathies, they laid the general pathophysiological concept, such as the channelopathy concept of the human epilepsies.

Channelopathies are a heterogeneous group of disorders diseases that develop because of defects in ion channels. Mutations in genes encoding ion channels, which impair channel function, are the most common cause of channelopathies. Consistent with the distribution of ion channels throughout the human body, ion channel defects have been implicated in a wide variety of diseases, including epilepsy.

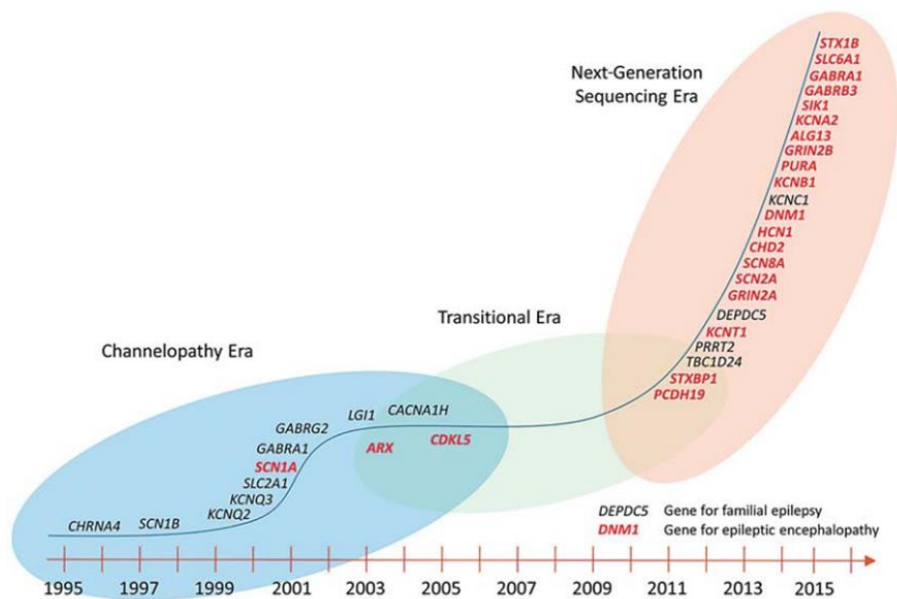


Figure 1. Timeline of gene discovery in human epilepsies (from Helbig et al., 2016).

### 1.3 Ion channels

Ion channels are transmembrane proteins that allow the diffusion of ions, across the plasma membrane. In excitable cells like neurons, muscle cells and endocrine cells, ion channels are responsible for generation and regulation of electrical signals required for coordinated neurotransmitter release, contraction of skeletal muscle, hormonal secretion, and furthermore, in all cells, they control cell volume and motility.

The classification of these proteins is based on the criteria of gating and ion selectivity. Depending on the type of gating trigger ion channels can be classified in different subfamilies, including voltage-gated ion channels (VGICs), ligand-gated ion channels, mechanosensitive ion channels and thermal-sensitive ion channels. Two main properties characterize the activity of a specific ion channel: the mechanism triggering its gating and the ion species flowing through it. In voltage-gated ion channels (VGICs), representing the third largest class of proteins involved in signal transduction, the gating trigger is represented by changes in transmembrane voltage. Other gating mechanisms are represented by changes in the chemical composition of the intra- or extracellular environment (ligand-gated ion channels (LGICs), in the applied mechanical force (mechanosensitive channels), or in the environmental temperature (thermosensitive channels). Permeation characteristics allow classifying ion channels based on their ion selectivity (with  $\text{Na}^+$ ,  $\text{K}^+$ ,  $\text{Ca}^{2+}$ , and  $\text{Cl}^-$  channels showing the greatest selectivity). Further classification criteria, such as cell- or tissue-specific expression or peculiar sensitivity to drugs and toxins, can further contribute to characterize ion channel classes.

### 1.3.1 Potassium channels

Given the pivotal role of voltage-dependent potassium ( $K^+$ ) channels in moderating neuronal excitability, it is not surprising that these channels are well represented among the channelopathies contributing to epilepsy.

Potassium channels represent the broadest and the most functionally heterogeneous class of ion channels present in both eukaryotic and prokaryotic cells. These channels play a very important role in the stabilization of membrane potential in the excitable tissues. Their activation reduces the frequency and the duration of the action potential (AP), as well decreases the susceptibility of the cell to excitatory stimuli. Moreover, in excitable and non excitable tissues,  $K^+$  channels are involved in the control of cell volume, proliferation, differentiation, and survival.

More than 70 genes encoding proteins serving as  $K^+$  channel subunits have been identified in humans. Based on their predicted structure,  $K^+$  channels could be classified in three main families (Figure 2): I) *Channels with six transmembrane segments (6TM)*; which includes voltage-gated  $K^+$  channels (Kv channels; Kv1–Kv12) and the small conductance  $Ca^{2+}$ -dependent  $K^+$  channels or SK. II) *Channels with two transmembrane segments (2TM)*, this family is composed by the inward-rectifier channels ( $K_{IR}1$ – $K_{IR}7$ ), structurally homologous to the S5 –S6 segments of the Kv channels and voltage-independent as they lack the VSD. III) *Channels with four transmembrane segments (4TM)*, including at least 15 different genes ( $K_{2P}1$ – $K_{2P}17$ ), topologically characterized by the tandem repetition of two pore domains.

However, structural, and functional heterogeneity of  $K^+$  channels is not restricted to these three groups. For example, large-conductance  $Ca^{2+}$ -dependent  $K^+$  channels (BK channels) assemble as tetramers of subunits containing *seven transmembrane segments*, which differ from Kv subunits for an extra transmembrane segment (S0) at the N-terminus.



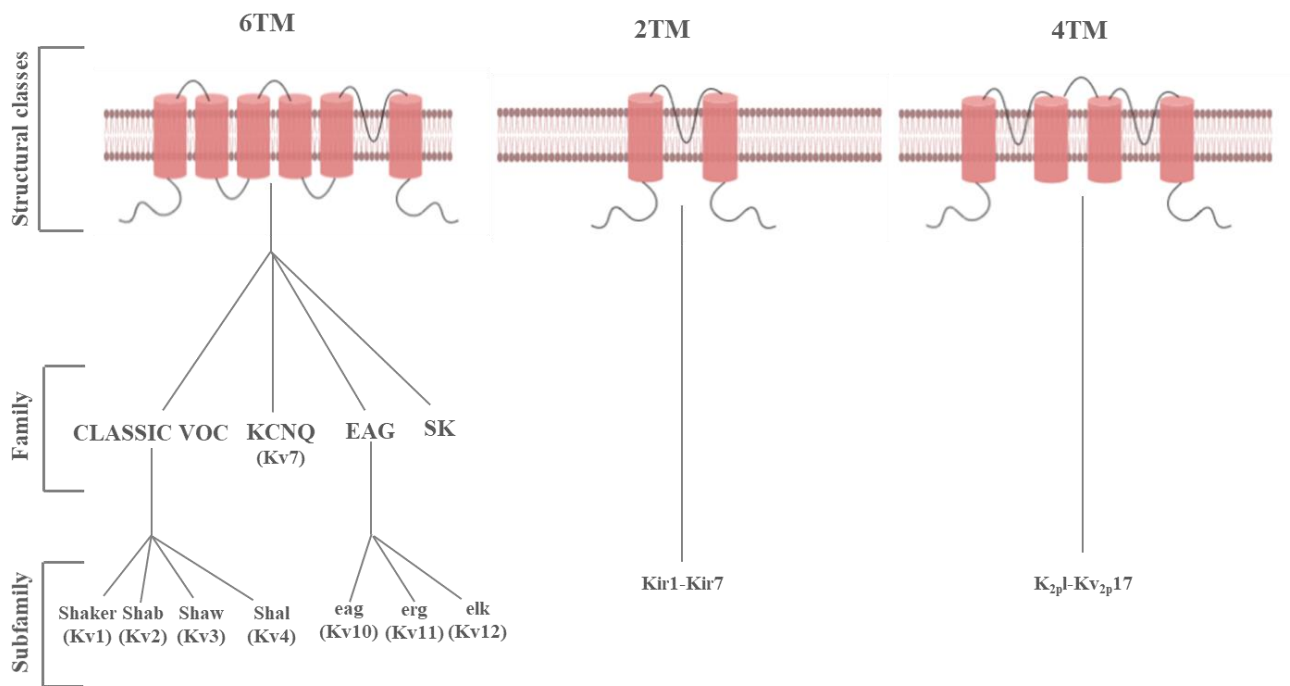


**Figure 2. Structure-based classification of ion channels.** 6TM channel families includes classical voltage-gated K<sup>+</sup> channels VGKCs (Kv 1, Kv 2, Kv 3, and Kv 4), KCNQ (Kv 7) channels, EAG channels (for ether-a-go-go, the name of a Drosophila mutant; Kv 10, Kv 11, and Kv 12). 2TM channel families includes Kir (inwardly rectifying) channels. 4TM (2-pore domain).

## 1.4 Kv7 potassium channel family

Channels belonging to the 6TM family are extremely heterogeneous and are classified into different subfamilies from Kv1 to Kv12. Among these subfamilies, the voltage-gated potassium ( $K^+$ ) channels Kv7 family, consists of 5 members (from Kv7.1 to Kv7.5) encoded by the KCNQ genes (KCNQ1–5).

The **Kv7.1** subunit, encoded by KCNQ1 gene, is mainly expressed in cardiomyocytes, where coupled with auxiliary KCNE1 subunits, underlies the slow component of *delayed rectifying  $K^+$  current* ( $I_{Ks}$ ) involved in ventricular repolarisation (Sanguinetti et al., 1996). The pathophysiological importance of  $I_{Ks}$  in cardiac is demonstrated by the fact that mutations in the KCNQ1 genes are responsible for the long QT syndrome (LQTS), an inherited arrhythmic disease characterized by delayed repolarization, syncopal episodes, and sudden death. Most of the mutations causing QT syndrome are loss-of-function variants causing a reduction of  $I_{Ks}$  current, but more recently, gain-of-function mutations (leading to increased activity of  $I_{Ks}$ ) in this gene have been identified as the cause of the short QT syndrome (SQTS) and/or atrial fibrillation (Dvir et al., 2014). In addition, Kv7.1 subunits are localized in non-cardiac tissues, such as the inner ear, gastrointestinal tract, thyroid gland, pancreas, and assemble also with KCNE2 and KCNE3 ancillary subunits. In gastric parietal cells, Kv7.1/KCNE2 channels are involved in the apical  $K^+$  recycling coupled to the  $H^+$ - $K^+$ -ATPase, essential for acid secretion, while in thyrocytes, regulates the synthesis of thyroid hormones (Roepke et al., 2006). Contrary to Kv7.1/KCNE1 heteromers, Kv7.1/KCNE2 and Kv7.1/KCNE3 complexes generate channels that are constitutively-open in the voltage range between - 80 to +80 mV (Abbot et al. 2015).

Contrary to Kv7.1 channel, the Kv7.2- Kv7.5 subunits are most known for their roles in the nervous system, as essential regulators of neuronal excitability (Brown et Passmore, 2009). In particular, **Kv7.2** and **Kv7.3** are co-expressed in many areas of the brain, including the cerebral cortex, hippocampus, cerebellum, and thalamus, suggesting the formation of heteromeric Kv7.2/7.3 channels (Schroeder et al., 1998; Tinel et al., 1998) which underline a voltage-dependent K<sup>+</sup> current, M-current (I<sub>KM</sub>). Mutations in KCNQ2 or KCNQ3 genes, encoding for Kv7.2 or Kv7.3 subunits respectively, have been associated to Benign Familial Neonatal Epilepsy (BFNE), an autosomal dominant idiopathic epilepsy of newborns (Plouin, 1994), and more recently mutations in KCNQ3 gene have also been associated in rare families with epileptic encephalopathy (Miceli et al, 2015b), nonsyndromic sporadic intellectual disability (Rauch et al., 2012; McRae et al., 2017), and intellectual disability with seizures and cortical visual impairment (Bosch et al., 2016)

KCNQ4 encodes for the **Kv7.4** subunit, which is highly expressed in the cochlea, specifically in sensory outer hair cells (OHCs), where it is involved in the regulation of their intrinsic excitability (Housley et al. 1992). Kv7.4 subunits are also expressed in the inner hair cells (IHCs) but at a lower level than OHCs (Kimitsuki et al.,2010). Loss-of-function mutations in the KCNQ4 gene result in autosomal-dominant non-syndromic deafness (DFNA2), a rare condition in which hearing loss is caused by a slow degeneration of OHCs induced by their chronic depolarization (Kubisch et al.,1999). Kv7.4 subunits have also been detected in vascular and visceral smooth muscle, where they are involved in the control of basal tone and in response to myogenic stimuli (Ipavec et al.,2011; Jepps et al.,2011; Svalø et al., 2013), and in skeletal muscle cells, where they regulate proliferation, differentiation, and response to myotoxic stimuli (Iannotti et al., 2010; 2013)

**Kv7.5** channel subunit, encoded by the KCNQ5 gene, is the last member of the Kv7 family to be identified. Kv7.5 channels are broadly expressed in the brain and show an overlapping

cellular pattern expression with Kv7.2 and Kv7.3 subunits. Also, these channel subunits are found in non-neuronal tissue, like skeletal and smooth muscle cells (Lerche et al., 2000; Schroeder et al., 2000). Recently, both gain-of-function and loss-of-function mutations in the KCNQ5 gene have been discovered in patients affected with severe epilepsy conditions (Lehman et al., 2017)

### 1.5 Structure of Kv7 channels.

Structurally, Kv7 channels are tetramers composed of identical or compatible subunits; each subunit shows a common architecture, with six transmembrane domains (from S1 to S6), and an intracellular -NH<sub>2</sub> and -COOH termini. The region encompassing S1-S4 segments forms the *Voltage Sensing Domain* (VSD), whereas the region between the S5-S6 segments forms the *Pore Domain* (PD) (Figure 3). Interestingly, the VSD of each subunit interacts with the pore module of the adjacent subunit: this results in the so-called *domain-swapped architecture*, which is typical of many families of Kv channels.

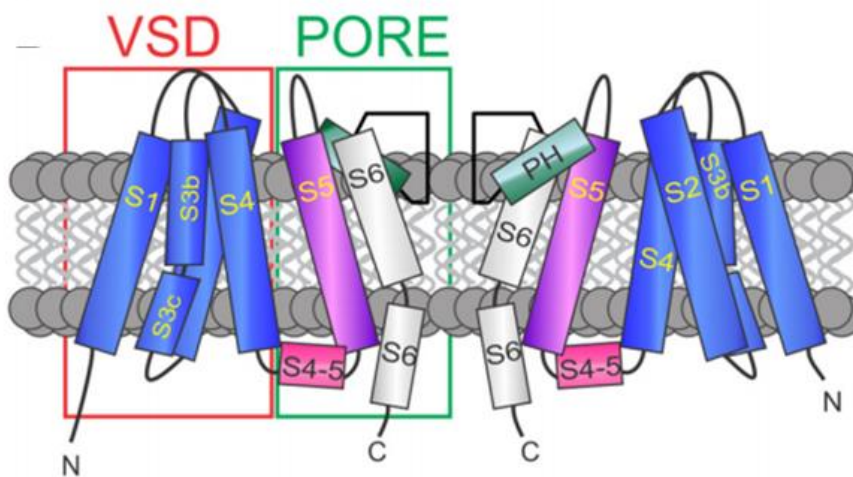


**Figure 3. Kv7 channel subunit.** The architecture of a Kv7 channel subunit. Cylinders are helical segments. VSD, voltage sensing domain; PH, pore helix. (From Abbot et al., 2020)

The VSD plays a crucial role in switching the channel from a resting to an activated configuration in response to changes in membrane potential. In particular, the S4 segment, which contains from four to six positively charged arginine (Rs) separated by uncharged residues, plays a key role in the voltage-sensitivity.

However, the precise rearrangements occurring in the voltage sensor during activation are not fully understood yet. Since structural studies have been performed in the absence of transmembrane potential, thus in “depolarizing” conditions, most of the information is relative to the activated (up) conformation of the sensor, whereas much less information is known about the resting (down) conformation. Three major conceptual models have been proposed to describe the movements of the sensor: I) *helical-screw/sliding-helix*, II) *transporter model* and III) *paddle model* (Tombola et al., 2006). Even if this proposed model differs in the extent and nature of S4 transmembrane movements, the consolidated hypothesis is that the resting and activated states are stabilized by ionized hydrogen bonds occurring between the S4 positive residues and two clusters of highly conserved negatively charged residues: an external negative cluster consisting of S1 helix and S2 helix, and an internal negative cluster consisting of glutamate S0 helix, S2 helix, and S3a helix (Long et al. 2007). A phenylalanine residue, located near the midpoint of the membrane, separates the external and internal negative has been proposed to form the charge-transfer center that catalyzes the gating charges movement (Tao et al.,2010).

As report previously, the S5 and S6 segments and the interconnecting loop (P region) participate in the formation of the pore domain (PD). A major contribution to the formation of the so-called *selectivity filter* is given by the P region that consists of about 20 amino acids and contains the molecular determinants of ion selectivity, the glycine–tyrosine–glycine (GYG) sequence, essential for discrimination between the various ionic species.

### 1.5.1 Electromechanical coupling

During depolarization, S4 moves outward, pulling the intracellular S4 –S5 linker, which in turn transfers these mechanical forces to the distal region of S6 of a neighbor subunit, leading to pore opening.

Analyses of crystal structures of several mammalian K<sup>+</sup> channels have revealed that hinges motif, localized at the level of the C-terminal region of S6, governing pore opening and closing. In Kv7 channels, this hinge function is ascribed to **PAG** (proline-adenine-glycine) motif. In particular, the PAG sequence of each subunit creates a bundle of four flexible helices that dislocate radially during pore opening and converge centrally during the closing, thereby interrupting ion flux (Seebold et al., 2006). In the bacterial MthK channels (Jiang et al., 2002a,b), missing the characteristic PAG sequence, a similar hinge function is attributable to a glycine residue in a homologous position.

Thus, direct contacts between the S4–S5 linker and the C-terminal region of S6 seem to be required for efficient electromechanical coupling between voltage sensor dislocation and pore opening during depolarization, but not sufficient. More information was provided by the recent comparison between the crystal structure of the chimeric Kv1.2/2.1 channel and the Cryo-EM structure of KCNQ1 (*Xenopus laevis*) (Sun and MacKinnon, 2017).

Crystal structure of chimeric Kv1.2/2.1 channel exhibit an activated VSD and an open PD by contrast KCNQ1<sub>EM</sub>, show an activated VSD, consistent with the absence of an applied field, but a close PD. The reason for the “decoupled” conformation on KCNQ1 is justified by the fact that Kv7 channels are both voltage and phosphatidylinositol-(4,5)-bisphosphate (PIP2) dependent. As described by Zaydman et al. (2013), membrane depolarization opens the pore only in the presence of PIP2, but gating charge displacement currents still occur in the absence of PIP2. Thus, in the absence of PIP2, the voltage sensors gain an activated conformation while the pore does not. Compared to its position in Kv1.2-2.1, the S4-S5 linker tilts by 25 degrees away from S6 in KCNQ1<sub>EM</sub> hypothesizing that, the reduced interaction

between the S4-S5 linker and the segment S6 on KCNQ1 seems consistent with the uncoupled pore and voltage sensor probably due to the absence of PIP2. (Sun and MacKinnon, 2017). This hypothesis was recently confirmed through the Cryo-EM structures of the human KCNQ1/KCNE3-CaM in the presence of PIP2 (Sun and MacKinnon, 2020). However, PIP2 depletion and consequently loss of VSD-pore coupling were also previously predicted from molecular dynamic simulations performed by Kasimova et al. in 2015.



### 1.5.2 Regulation of Kv7 channels

Kv7 channels exhibit a very long intracellular C-terminal region, organized into four  $\alpha$ -helical regions (called A-D helices), which are conserved in all Kv7 family members (Yus-Najera et al., 2002). The C-terminus represents an important platform for the interaction with different molecules and proteins, which plays a critical role in Kv7 channel function and regulation (Figure 3).

**Calmodulin** (calcium-modulated protein, or CaM) CaM is a small, soluble, and thermostable protein able to binds calcium ions. Structurally, CaM presents two globular domains, the N-lobe and the C-lobe, and each lobe is composed of two EF-hands, which are responsible for the binding of up to four  $\text{Ca}^{2+}$  ions per CaM molecule.

All members of Kv7 family subunits (Kv7.1-5) interacts CaM, which binds two different sites located respectively in helices A and B; the first one in helix A is formed by a canonical IQ-binding motif (IQXXRXXXXR), whereas the second in helix B displays two overlapping consensus 1-5-10 CaM-binding motifs (Yus-Näjera et al., 2002),

CaM plays an important role in surface trafficking; mutation on Kv7.2-CaM binding sites can reduce the export from the endoplasmic reticulum to the plasma membrane (Exteberria et al., 2008). In hippocampal neurons, CaM regulates the trafficking and the enrichment of Kv7.2/Kv7.3 channels at the axonal initial segment (AIS) (Liu and Devaux., 2014).

Moreover, CaM is essential in the generation of functional M-current (Gamper et al., 2005).

**Phosphatidylinositol-(4,5)-bisphosphate (PIP2)** is a phospholipid negatively charged present in the intracellular leaflet of the plasma membrane essential for the activation of all KCNQ channels. Moreover, PIP2 increases the opening probability of both homomeric and heteromeric channels; differences in the single-channel open probability are dependent on their intrinsic affinities for intracellular PIP2 (Li et al., 2005).

The earliest study on Kv7.2 identified an interaction site of PIP2 in the junction between S6 and the first C-terminal “A helix”, the so call the S6Jx domain: here, replacement of the histidine at position 328 (His367 in Kv7.3) by a cysteine reduced the sensitivity of the channel to PIP2 (Zhang, H et al. 2003). Subsequently, Hernandez and coll. highlighted, in both Kv7.2 and Kv7.3, a second PIP2-interaction domains in the A–B helix linker suggesting that negatively charged phosphate headgroups of PIP2 molecules formed electrostatic bond whit the “cationic cluster” identified in that region (Hernandez et al., 2009). Lastly, two binding sites have been detected in the S2-S3 and in the S4-S5 loop, respectively. Particularly, PIP2 binds S2- S3 loop in the closed state in Kv7.2, whereas, upon channel activation, PIP2 interacts with the S4-S5, modulating channel gating. (Zhang et al., 2013). The recently published cryo-EM structure of the hKCNQ1 showed that PIP2, also in this channel, could bind to S2–S3 loop, as well S4–S5 loop and S6C (Sun and MacKinnon, 2020).

Kv7 function could be modulated by the **A-kinase Anchoring 79/150 or AKAP79/150 protein**. AKAP79/150 binds the Kv7.2 C-terminus; here, the protein forms a trimeric complex with protein kinase C (PKC). Activation of PKC leads to phosphorylation of serine residues located in helix B, which suppress Kv7.2 currents. This effect is largely prevented by removing two putative PKC phosphorylation sites in helix B (Hoshi et al., 2003)

**The SNARE protein syntaxin-1A (syx-1A)** is a plasma membrane protein that regulates neurotransmitter release; when N-terminal of syx-1A interacts with neuronal Sec1 (STXBP1), establish a core complex involved in membrane fusion and following neurotransmitters release (Misura et al., 2002)

In both Kv7.2 and Kv7.3 subunits, Syx-1A interacts with the helix A, producing two opposite effects; syx-1A appears able to reduce Kv7.2 currents by about 50% while it failed to inhibit the Kv7.3 currents. This could be due to the presence of additional binding sites for syx-1A

in the Kv7.2 channel (in particular, in the N-terminal showing a different sequence between the two subunits), which may not be present in Kv7.3 (Regev et al., 2009).

**Ankyrin-G (AnkG)** is an adaptor protein that allows localizing Kv7.2 and Kv7.3 subunits at the axon initial segment and in nodes of Ranvier, two neuronal sites crucially involved in the generation and propagation of action potentials. Ankyrin-G selectively interacts with Kv7.2 and Kv7.3 subunits, binding the distal part of the helix-D in C-terminus. (Devaux et al. 2004; Pan et al., 2006). **Nedd4-2** is a ubiquitin-protein ligase that regulates the plasma membrane expression of Kv7.2/Kv7.3 and Kv7.3/Kv7.5 channels (Ekberg et al., 2007). The protein reduces the current generated by these channels, probably by promoting their ubiquitination, internalization, and degradation. To date, it is well described that a PY domain, localized at the C-terminal domain of Kv7.1, is crucial for this process, whereas the role of the same region in Kv7.2/Kv7.3 subunits is less defined (Figure 4)

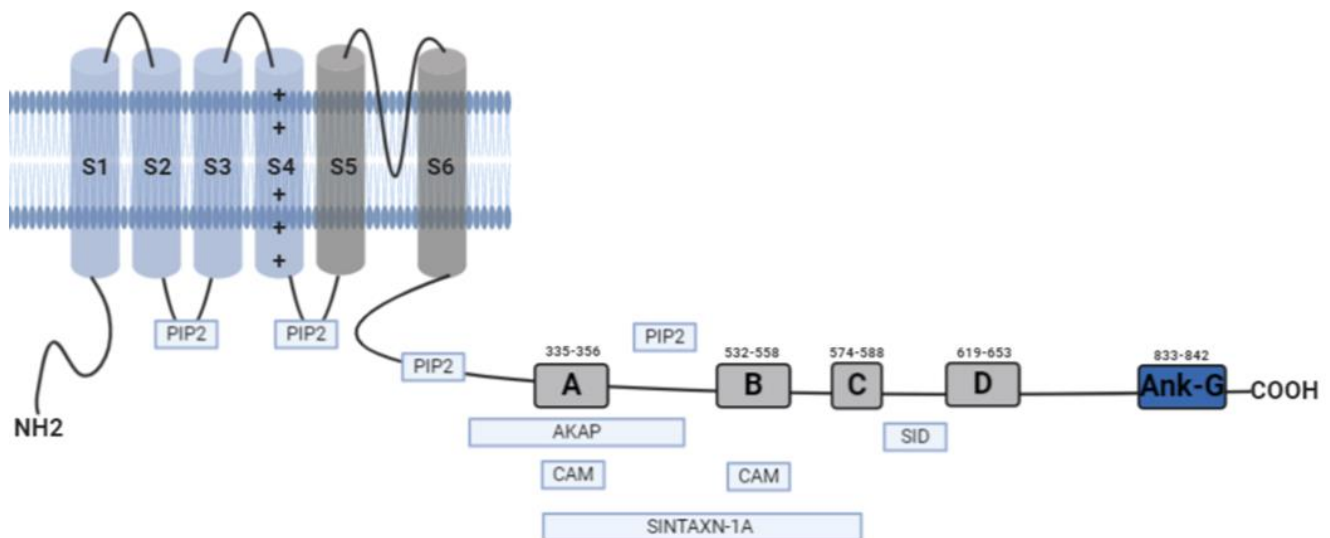


**Figure 4. Topological representation of Kv7.2 subunit.** The schematic topology of a Kv7.2 subunit formed by six transmembrane segments (S1-S6) and intracellular NH2 and COOH termini. The region encompassing S1-S4 segments forms the VSD (in blue), whereas the S5-S6 region and the intervening linker form the ion-selective pore (in gray). A long C-terminal region is characterized by 4  $\alpha$ -helix domains (from A to D). The C and D helices form the Subunit Interaction Domain (SID), which is involved in multimerization and subunit-specific heteromerization. ; CaM, calmodulin; AKAP, A-kinase-anchoring protein; PKC, protein kinase C; Ank-G, ankyrin-G; PIP2, phosphatidylinositol-(4,5)-bisphosphate.

## 1.6 Neuronal Kv7 channels; cellular, subcellular distribution

The **Kv7.2** and **Kv7.3** subunits, encoded respectively by KCNQ2 and KCNQ3 genes, are highly expressed in both the central and peripheral nervous systems. In the brain, Kv7.2, Kv7.3 have been detected in different areas, including the dentate gyrus and CA1-3 regions of the hippocampus, the subiculum, all layers of the neocortex, and in the reticular nucleus of the thalamus (Cooper et al., 2001; Tzingounis et al., 2010; Weber et al., 2006; Geiger et al., 2006). In neuronal cells, Kv7 channels are localized at key subcellular sites, including the perisomatic region, the axon initial segment (AIS), nodes of Ranvier, and synaptic terminals. According to their subcellular localization, Kv7 channels regulate several aspects of neuronal excitability (Figure 5).

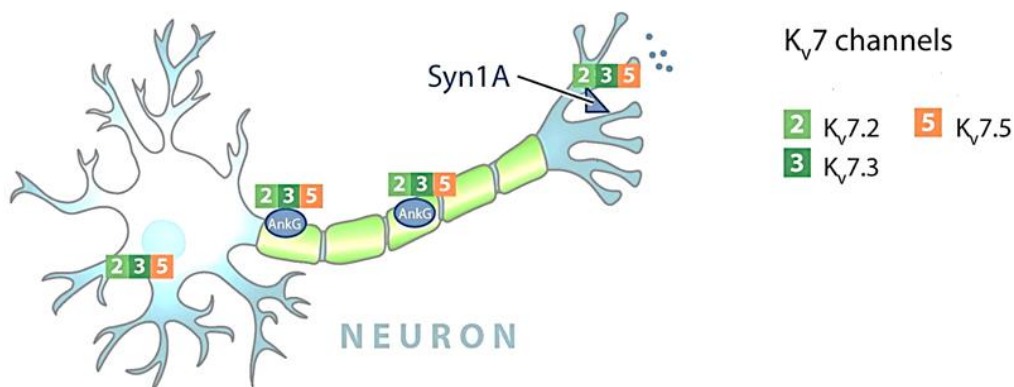


**Figure 5. Schematic representation of the distribution of Kv7 channels in the different compartments of a myelinated axon.** The Kv7 channel is found at the AIS, nodes of Ranvier and presynaptic terminals (adapted from Barrese et al., 2017)

### 1.6.1 The functional role of neuronal Kv7 channels

First isolated by Brown and Adams, using voltage-clamped frog sympathetic neurones (Brown and Adams 1980) and later recorded in mammalian brain neurons (Halliwell JV et al., 1982), that so called M-current ( $I_{KM}$ ) is a  $K^+$ -selective, non-inactivating, slowly activating/deactivating current. Despite its identification in the 1980, the molecular identity of the channels underlying the M-current remains unknown for several years and only in 1998, Wang and coll. discovered that Kv7.2 and Kv7.3 subunits represented the molecular basis of the M-current ( $I_{KM}$ ) (Wang et al., 1998). Although also Kv7.5 contributes has been suggested to contribute (Schroeder BC et al., 2000. Lerche C et al., 2000).

In the axon initial segment (AIS) and in unmyelinated portions of the axons, the nodes of Ranvier, Kv7.2/7.3 channels are involved in the control of the resting membrane potential. Here, they increase the action potential threshold but also promote the recovery of inactivated voltage-gated  $Na^+$  channels (Nav) (Battefeld et al., 2014).

The action potential is a transient change in the membrane potential, induced by the flow of ions inside/outside the cell; as shown in Figure 6A, it is characterized by a gradual depolarization versus threshold values, a rapid rising phase, an overshoot, and a repolarization phase. The repolarization phase is followed by a brief afterhyperpolarization (AHP), a latter phase resulting in  $K^+$  channels remaining open. AHP is further divided into three phases: I) a fast one, namely fAHP, lasting 1-5 ms, largely mediated by  $Ca^{2+}$  - and voltage-dependent BK channels; II) a medium one called mAHP, lasting 50-200 ms, mediated by Kv7 and HCN channels; III) and a slow one the sAHP, lasting from about 0.5 s to several seconds, mediated by Kv7 and SK  $Ca^{2+}$  channels. The M-current contributes to the medium (mAHP), and the slow components (sAHP) of the afterhyperpolarization current determine the refractory period and the discharge frequency on neurons (Tzingounis et

Nicoll, 2008). Therefore,  $I_{KM}$  contributes to spike-frequency adaptation by reduces the frequency of neuronal firing in response to sustained stimuli. When  $I_{KM}$  is inhibited (e.g., by channel blockers like linopirdine or XE991), the neuron remains depolarized for a long period, during which it may generate multiple spikes (Yue and Yaari, 2004) (Figure 6 B-C). Finally, Kv7 channels are express in the presynaptic terminal and can modulate the release of the neurotransmitter. In 2003 Martire and co-workers, have demonstrated that activation of presynaptic  $I_{KM}$  may hyperpolarize hippocampal nerve endings, reducing  $Ca^{2+}$  influx through voltage-gated  $Ca^2$  channels resulting in a reduction of norepinephrine GABA and D-aspartate release (Martire et al., 2004). The same authors in 2007 described the involvement of Kv7.2 subunits in dopamine release from rat striatal synaptosome, obtaining that [3H] dopamine release is inhibited by the  $I_{KM}$  activator retigabine while  $I_{KM}$  blockers TEA and XE991 enhanced [3H] dopamine release and prevented retigabine induced inhibition (Martire et al., 2007)

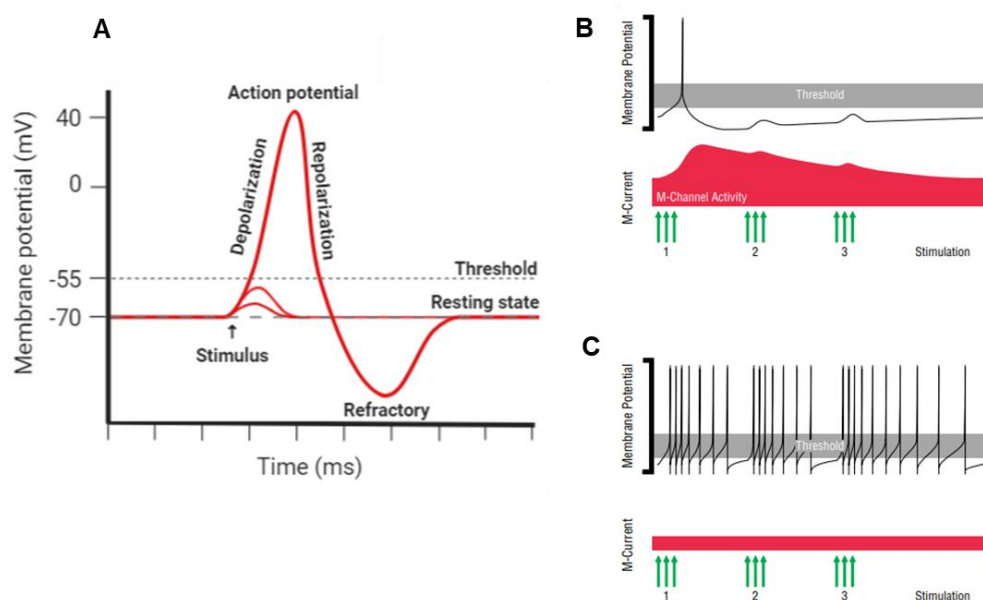


**Figure 6. Role of neuronal M-current in controlling excitability.** A) Representation of an action potential. B) Excitatory inputs (green arrows), cause membrane depolarization and a single action potential. Afterward, increased activation of M-channels hyperpolarizes the membrane potential, preventing spiking in response to recurrent excitation. C) When M-channel activity is reduced (for example, in the presence of mutations), excitatory inputs lead to multiple action potentials (adapted from Cooper and Jan, 2003)

### 1.6.2 M-channels regulation

The M-current (hence its definition) is suppressed upon stimulation of several receptors linked to pertussis toxin-insensitive G proteins of the Gq/11 family, like M1, M3, and M5 subtypes of muscarinic receptors, which activate the phospholipase C (PLC), causing hydrolysis of PIP2 into diacylglycerol (DAG) and inositol triphosphate (IP3), leading to the activation of PKC.

Activation of the Gq pathway produces three phenomena that negatively modulate the current M: I) As described previously, the activity of Kv7 channels is closely related to adequate levels of PIP2. Consequently, the depletion of this phospholipid caused by activation of muscarinic receptors prevents the opening of channels. II) Activation of PKC, which anchors the Kv7 complex through AKAP79/150, phosphorylates the C-terminus of the Kv7.2 subunit, which overlaps with the CaM binding site in helix b. Phosphorylation of the Kv7.2 subunit leading to dissociation of CaM and unstabilized PIP2 interaction (Kosenko et al., 2012).

III) The production of the second messenger IP3 triggers  $\text{Ca}^{2+}$  release from the endoplasmic reticulum. The  $\text{Ca}^{2+}$ /CaM complex binding sites overlap the putative binding site for PIP2, reducing the interaction of PIP2 with the channel (Gamper and Shapiro 2003). In all cases, suppression of  $I_{KM}$  inhibits the hyperpolarization of the cell membrane and increases neuronal excitability. Recently, using an *in silico* screening approach, the CP1 compound structural resembling PIP2 was found.

As reported by the authors, CP1 could substitute PIP2 and recover KCNQ1 currents that were abolished by depletion of membrane phospholipid. Like PIP2, CP1 activated KCNQ1 channels by enhancing VSD-pore coupling. Also, KCNQ3 and KCNQ2 were activated but lesser than KCNQ1 (Liu Y et al., 2020)

## 1.7 KCNQ2 and KCNQ3 channelopathies

Mutations in KCNQ2 (encoding for Kv7.2 channels) are responsible for a wide spectrum of neonatal-onset epileptic diseases, ranging from more benign forms, like *Benign Familial Neonatal Seizures* (**BFNS**), to more severe forms, like the *Neonatal onset developmental and epileptic encephalopathy* (**DEE**). Recently, mutations in the KCNQ2 gene have also been associated with non-epileptic neurodevelopmental diseases.

BFNS is characterized by multifocal seizures starting around the third day of life and disappearing within a few weeks or months; however, 10-15% of affected children show seizures later in life (Plouin et al., 1994). Seizures are generally brief, lasting one to two minutes, and the motor activity may be confined to one body part, migrate to other body regions, or generalize. The neuropsychological development is usually normal (Miceli et al., 2018). Among the benign forms, have also been described two genetic conditions similar to BFNS: The *Benign Familial Infantile Seizures* (BFIS) or *Benign Familial Neonatal-Infantile Seizures* (BFNIS) (Zhou et al. 2006, Zara et al. 2013). In BFIS, seizures start around 6 months of age, while in BFNIS, seizures display an intermediate age of onset between the neonatal and the infantile periods.

On the other hand, DEE (recently classified as early infantile epileptic encephalopathy type 7, or EIEE 7) is characterized by pharmacoresistant seizures that begin in the first week of life and remit between nine months and four years of age. Contrary to BFNS, patients show moderate to severe developmental impairment (Weckhuysen S et al., 2012). Additionally, KCNQ2 mutations have been identified in several individuals with Ohtahara syndrome (Saito H et al., 2012), the most severe and the earliest developing age-related epileptic encephalopathy, characterized by tonic seizures occurring within the first three months of life, often within the first two weeks. Psychomotor development and prognosis are generally very poor. As previously reported, severe phenotype related to KCNQ2 mutation can also be related to non-epileptic neurodevelopmental diseases. In 2017 Mulkey and colleagues



described 10 patients carrying KCNQ2-R201C/H variant showing neonatal encephalopathy without seizures, burst suppression EEG, profound developmental delay, and early mortality (Mulky et al., 2017). Like the KCNQ2 gene, mutations in the KCNQ3 gene (encoding for Kv7.3 subunit) are related to benign epilepsies with seizures starting in the neonatal (BFNS) or early infantile (benign familial infantile seizures (BFIS) period., however, KCNQ3 variants represent a relatively rare cause of BFNS, e.g., 1/33 of pedigrees, compared with 27/33 for KCNQ2. (Miceli et al., 2017). The clinical characteristics of Kv7.3-BFNS appear indistinguishable compared to Kv7.2-BFNS. Patients usually present a normal psychomotor development, although some individuals carrying the KCNQ3-related BFNS variants I317T (Soldovieri et al., 2014) and R330L (Miceli et al., 2015b) showed some degree of intellectual disability. Additionally, more severe phenotypes have been associated with KCNQ3; pathogenic variants have been described in few patients with DEE (Allen et al., 2013, Miceli et al., 2015; Grozeva et al., 2015; Ambrosino et al., 2018), ID apparently without epilepsy (Rauch et al., 2012; McRae et al., 2017), cortical visual impairment (Bosch et al., 2016) and ID and autism spectrum disorder (Sands et al., 2019).

In BFNS, KCNQ2 mutations are transmitted from affected parents following a classical autosomal dominant inheritance mode and are mostly missense, splice, nonsense, and frameshift variants as well as exon and whole-gene deletions. On the other hand, KCNQ2-related DEE mutations are all missense *de novo* pathogenic variant (except 2 variants causing an in-frame deletion of a single amino acid); however, few children with KCNQ2-DEE were born from mosaic parents (Milh et al., 2015; Kato et al., 2013; Mulky et al 2017). Mutations found in BFNS appear to be spread along the entire Kv7.2 sequence whereas DEE-associated mutations appear to be concentrated in critical channel domains, such as: the S4 domain, the pore, the proximal C-terminal segment which binds PIP2 and calmodulin, and the B helix, which also is involved in CaM-binding (Millichap et al., 2016). More recently, Goto and co-workers demonstrated that while BFNE missense mutations are frequently

localized in the VSD between the S2 and S3 segments, DEE missense variants are more frequent in S6 and its adjacent PD, as well as in the intracellular domain between S6 and helix A (Goto et al., 2020).

KCNQ2-related BFNS missense variants, causes a mild loss of channel activity (Loss-of-function, LoF), that cannot be compensated by the wild type allele (haploinsufficiency). Particularly, functional studies suggest that in most cases a decrease of  $I_{KM}$  of only 25% is sufficient to cause BFNS (Schroeder BC et al., 1998). Besides missense mutations, frameshift/deletion variants account for 36% (39/108) of BFNS-causing variants in KCNQ2 ([www.riken.org](http://www.riken.org)).

Unlike the benign form whose pathogenic mechanism is related to haploinsufficiency, pathogenic variants causing KCNQ2-DEE exert more severe functional defects on potassium current function; subunits carrying missense variants would decrease channel function more than 25%, suggesting that the so-called dominant-negative effect (DNE) could be responsible for the severe epileptic phenotype (Orhan G et al., 2014). As for KCNQ2, BFNS mutations, inherited in an autosomal dominant manner, are mostly missense and lead to loss-of-function (LoF) effect of channel activity. Despite the benign conditions, inherited LoF variants could be associated to more severe phenotypes; a patient with early-onset DEE, severe cognitive delay, with absent speech and tetraparesis carrying two Kv7.3 missense mutations (V359L and D542N) in compound heterozygosis, each inherited from an asymptomatic parent, has been described by Ambrosino et al. (2018). As previously reported, heterozygous frameshift variants in KCNQ2 are frequent causes of BFNS. In KCNQ3, two frameshift variants, the S407Ffs\*27 and F534Lfs\*15, causing LoF effect, were found in homozygosity in patients with developmental delay and neonatal seizures (Kothur et al., 2018. Lauritano et al., 2019), demonstrating that, contrary to KCNQ2, homozygous variants are compatible with life. In addition, in both families described, heterozygous carrier

parents of the KCNQ3 frameshift variant were unaffected , suggesting that KCNQ3 frameshift mutations are better tolerated than KCNQ2 frameshift variants

In addition to the LoF mechanisms, *de novo* missense variants causing gain-of-function (GoF) effects on the  $I_{KM}$ , was found in KCNQ2 patients (Miceli et al., 2015a) (Figure 7A).

*De novo* missense mutations producing a GoF effect have been described also described in KCNQ3 (Miceli et al., 2015a) (Figure 7B).

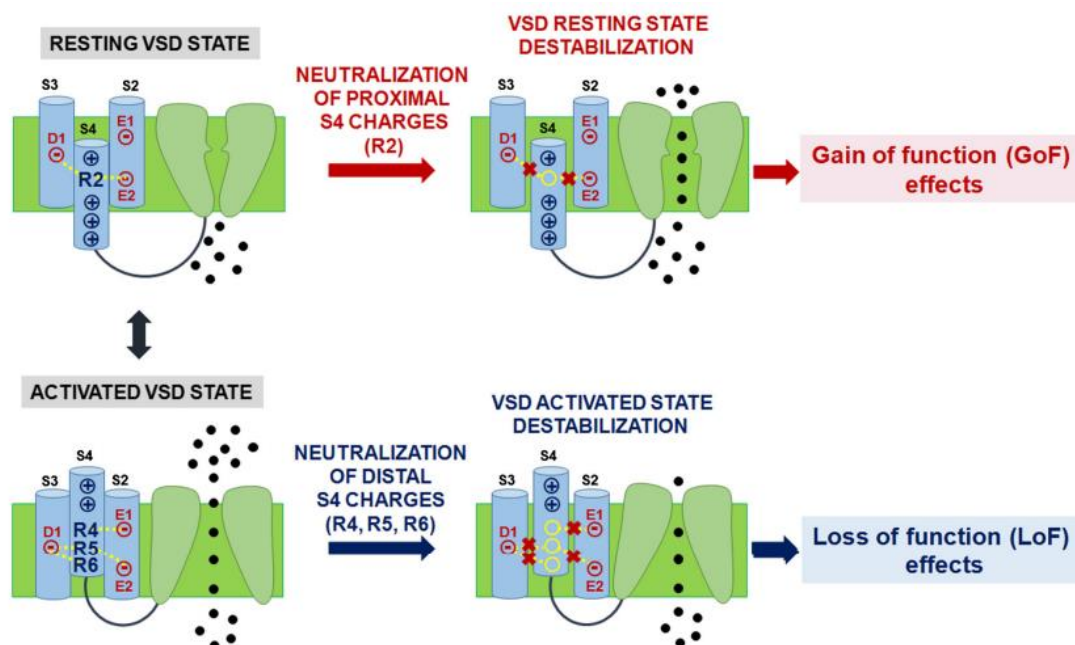
To understand the molecular basis of these two different functional defect, as reported in a recently published work of our group, multistate structural modeling has been used. Our observation demonstraed that the activated VSD configuration is stabilized by hydrogen bonds established between arginine residues (R4, R5, R6) and an internal negative amino acid cluster mostly provided by E140 in S2 and D172 in S3 whereas R2 residue, stabilized the resting states by forming an intricate network of electrostatic interactions with neighboring negatively charged residues;. Thus, neutralization of the charge at R2 preferentially destabilized the resting VSD configuration, thereby causing constitutive channel activation, possibly explaining the observed GoF effects while neutralization of the charge at R4, R5, R6 destabilizing the VSD-activated configuration and causing LoF effects (Figure 8) (Nappi et al., 2020)

a				
KCNQ2				
GENOTYPE	R213Q, T274M, G279S, A294V	M208V, D212G, R214Q, Y284C, A306T	R144Q, R198Q	R201C, R201H
	LoF		NORMAL	GoF
PATHOMECHANISM	DOMINANT-NEGATIVE	HAPLOINSUFFICIENCY	MILD	SEVERE
CLINICAL PHENOTYPE	Neonatal-onset DEE	Self-limiting BFNS	Infantile spasms, global ID without neonatal seizures	Neonatal-onset DEE, global ID, high mortality

b				
KCNQ3				
GENOTYPE	R330L, V359L/D542N	R330C, G310V	R227Q	R230C/H/S
	LoF		NORMAL	GoF
PATHOMECHANISM	SEVERE	HAPLOINSUFFICIENCY	MILD	SEVERE
CLINICAL PHENOTYPE	Epilepsy and neurocognitive deficits	Self-limiting BFNS	ASD and sleep-activated spikes	ASD, and multifocal status epilepticus during sleep

**Figure 7. Genotype-phenotype correlations and potential pathogenetic mechanisms for KCNQ2 (panel a) and KCNQ3 (panel b).** DEE, developmental epileptic encephalopathy; ID, intellectual disability; BFNS, benign familial neonatal seizures; ASD, autism spectrum disorders (from Nappi et al., 2020)



**Figure 8. Functional consequences of the neutralization of arginines (R) in the proximal (R2) and distal (R4, R5, R6) portions of the S4 transmembrane segments on VSD movement** (from Nappi et al., 2020)

## 1.8 Animal models of KCNQ dysfunction

To better understand the pathophysiological role and to confirm the genotype-phenotype correlation, several mice models of KCNQ2 and KCNQ3 gene dysfunction have been generated.

The first animal model was developed by Watanabe and colleagues in 2000; this knock-out (KO) mouse was characterized by a deletion of 3 exons in the KCNQ2. Interestingly, while homozygous (KCNQ2<sup>-/-</sup>) mice died within the first day of life, heterozygous (KCNQ2<sup>+/-</sup>) mice showed an increased sensitivity to pentylenetetrazole (PTZ) stimuli (Watanabe et al, 2000). More recently, this animal model has been used to evaluate the role of KCNQ2 gene in autism-associated behaviors, considering that mutations in neuronal KCNQ genes are not only responsible for BFNS or DEE, but can be associated to neurodevelopmental disorders (NDDs), a collection of disorders that include autism spectrum disorder (ASD), intellectual disability, and developmental delay. As reported from Kim and collaborators, compared to KCNQ2<sup>+/+</sup> (WT) littermates, heterozygous mice display abnormalities in multiple behaviors including circadian-dependent activity; males and females displayed hyperactivity during the light phase, enhanced exploratory behaviors, and repetitive grooming but decreased sociability. Moreover, while males displayed enhanced compulsive-like behavior and social dominance, the female did not. Increased seizure susceptibility and behavioral abnormalities were observed, suggesting that reduced Kv7 current may contribute to ASD-associated behaviors in a gender-dependent manner (Kim EC et al., 2019).

Similar to the KCNQ2<sup>+/-</sup> KO mice, *stz1* mice, characterized by a large genomic deletion encompassing the KCNQ2 gene, displayed an increased sensitivity to the proconvulsant PTZ together with morphological abnormalities in the hippocampal region (Yang 2003). Conversely to KCNQ2<sup>-/-</sup> mice, homozygous KCNQ3 KO mice showed no seizures and survived until adulthood, further confirming the distinct functional role of KCNQ2 and KCNQ3 genes. (Tzingounis et al, 2008).

Because of the higher mortality of KO KCNQ2 mice, conditional strategy has been used. In fact, while in constitutive knockout mice, the gene deletion occurs throughout the nervous system, in conditional knockout mice deletion occur in a restricted area. Conditional KO mice have been developed by Soh and colleagues to evaluate the effects of the deletion of KCNQ2 or KCNQ3 in two specific populations of neurons: the cortical pyramidal neurons (Soh et al, 2014) and interneurons (Soh et al, 2018). Deletion of KCNQ2 produced increased excitability (possibly due to reduced mAHP) in pyramidal neurons and premature death in mice. Conversely, deletion of KCNQ3 gene in the same neuronal population neither increases excitability nor impairs the survival of mice. (Soh et al, 2014). Silencing of KCNQ2 and KCNQ3 in interneurons selectively increased the firing of parvalbumin-positive interneurons which in turn led to homeostatic potentiation of fast excitatory synaptic activity. Consequently, mice with decreased KCNQ2 in parvalbumin neurons showed a reduced latency to onset of seizures induced by picrotoxin (Soh et al, 2018).

Several animal models were generated to reproduce mutations found in patients. Using the Tet-off strategy, Peters and colleagues generated a knock-in mice expressing the mutant G279S in KCNQ2, identified in a patient with EOEE (Sharawat et al. 2018; Indian J Ped). Dominant-negative suppression of  $I_{KM}$  in this model caused spontaneous seizures, behavioral hyperactivity, and significant hippocampal alteration suggesting a crucial role of the M-current for the development of normal hippocampal morphology (Peters et al, 2005). To reproduce the human BFNS phenotype, Singh and colleagues obtained two knock-in mice models by introducing two missense mutations found in BFNS the KCNQ2 A306T and KCNQ3 G311V (Singh et al, 2008). As reported by the author, both heterozygous knock-in mice appeared more susceptible to seizures when compared with wild-type littermates while homozygous mutant mice showed early-onset spontaneous generalized tonic-clonic seizures and higher mortality. Nevertheless, no significant morphological alteration, such as hippocampal mossy fibers sprouting or neuronal loss, was found in homozygous mice, thus

paralleling the normal morphological developmental exhibited by most BFNE patients (Singh et al., 2008). Similar characteristics were exhibited in two other transgenic mice where BFNS-causing mutations (Y284C, A306T;) were introduced using the kick-in strategy (Tomonoh et al, 2014).

Recently, Milh and colleagues have developed the first knock-in mouse carrying a recurrent variant in KCNQ2 (T274M), known to cause DEE and able to induce a dominant-negative effect, with a 70%–80% reduction of the current (Orhan G et al., 2014). The knock-in mouse *Kcnq2*<sup>Thr274Met/+</sup> faithfully reproduces what is expected based on the human phenotype: no morphological brain alterations, no neurosensory alterations before the onset of seizures occurring at P20 followed by a high rate of unexpected death in epilepsy, seizures only exceptionally observed after P100, and important cognitive impairment (Milh et al., 2020).

## 1.9 Pharmacology of Kv7 channels

Given their prominent role in human physiology and pathology, it is not surprising that Kv7 channels represent attractive pharmacological targets for several neuropsychiatric conditions. Compounds acting on neuronal Kv7 channels include both *activators* and *blockers*. Historically, *blockers* were developed for treatment of learning and memory disorder while application of *activators* range from the anti-nociceptive and anticonvulsant use to the treatment of migraine, anxiety (Munro, et al., 2007; Korsgaard et al., 2005), mania (Dencker et al., 2008), ADHD (Hansen, et al., 2008) addiction to psychostimulants (Hansen et al., 2007) and depression (Friedman et al., 2016) (Figure 9).

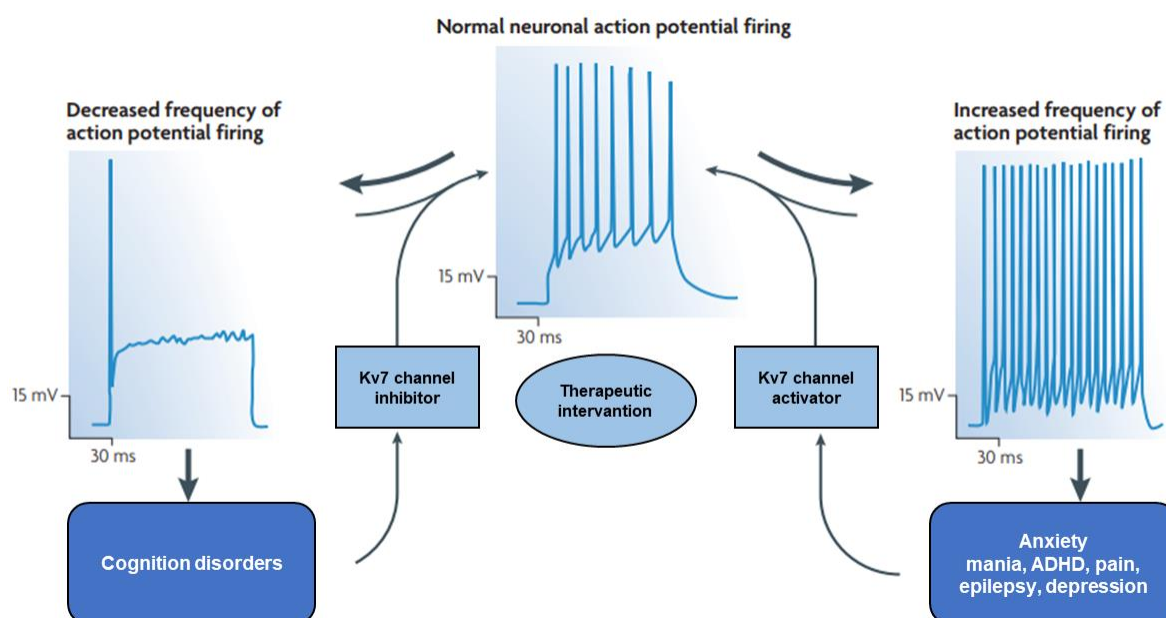


**Figure 9.** Effects of Kv7 channel inhibitors and activators on pathologically altered neuronal activity (adapted from Wulff et al., 2009).



### 1.9.1 I<sub>KM</sub> blockers

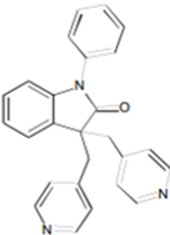
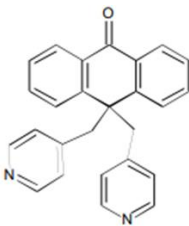
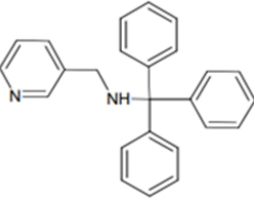
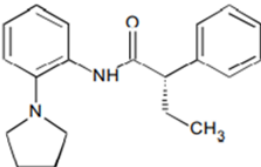
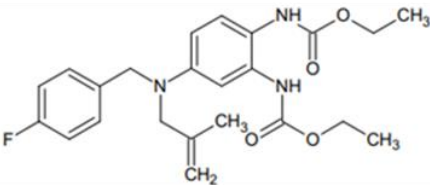
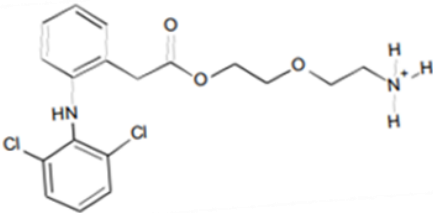
The first selective Kv7 blocker has been the phenyl indolinone derivative linopirdine (*for all structure molecules see Table 1*), synthesized in 1980s (Aiken et al., 1995). Because of its ability to increase the performance in learning and memory tests, in several animal models (Brioni et al., 1993) it has been proposed for the treatment of neurodegenerative conditions like Alzheimer's disease. However, clinical trials on Alzheimer's patients did not show a clear effectiveness of this compounds (Rockwood et al., 1997).

Unfortunately, linopirdine is a non-selective Kv7 blocker, being active also on cardiac Kv7.1 channels, although with a lower potency when this channel co-assembles with KCNE1 accessory subunits. Functional analogs of linopirdine with an anthraquinone structure, the **XE-991** showing an increased potency in blocking Kv7 currents but, like linopirdine, also XE991 is unable to discriminate among Kv7 subunits (Wang et al., 2000).

Differently from non-selective Kv7 blockers linopirdine and its derivatives, 3-(triphenylmethylaminomethyl) pyridine **UCL2077** inhibits Kv7 channels in a subtype-selective manner, acting mainly on Kv7.1 and Kv7.2 channels. Moreover, this compound increases Kv7.3 currents at negative membrane potentials, while inhibits them at more depolarized values (Soh and Tzingounis, 2010). Another potent Kv7 inhibitor recently described is **ML252**. This molecule, unlike other Kv7 channel blockers (XE991, linopirdine), exerts an inhibitory action at very low concentrations, proving to be very potent. Furthermore, it appears to be more selective than other inhibitors in blocking specifically Kv7.2 isoforms: in fact, the inhibitory action on Kv7.2 currents ( $IC_{50}=69$  nM) is about 40 times greater than that shown on Kv7.1 cardiac isoform ( $IC_{50}=2.92$   $\mu$ M). The ML252 shows reduced selectivity for Kv7.2/Kv7.3 heteromeric channels ( $IC_{50}=0.12$   $\mu$ M) or Kv7.4 channels ( $IC_{50}=0.20$   $\mu$ M) (Cheung et al., 2012). Interestingly, SAR studies revealed that small structural changes of ML-252 (substitution of the ethyl group with a hydrogen) are sufficient to cause a functional switch of its activity from an antagonist to an agonist.

Small structural modifications in the Kv7 activator retigabine generate compounds (**HN38**) 7-times more potent than XE991 in inhibiting Kv7.2 channels (Hu et al., 2013). In addition another blocker, the fenamets **NH17** has been described as a Kv7.2 channel inhibitor, although its subtype selectivity for other Kv7 family members is unknown (Peretz et al., 2017).

Table 1. Kv7 channel inhibitors.

Compound Name	Structure
Linopirdine	
XE991	
UCL-2077	
ML252	
HN38 (Retigabine derivative)	
NH17 (Fenamate)	

## 1.9.2 I<sub>KM</sub> Activator

### 1.9.2.1 Flupirtine, Retigabine and Derivatives

Developed between the 1970s and the 1990s by the Chemiewerk Homburg, Frankfurt am Main, Germany with the purpose to synthesize a novel non-opioid centrally acting analgesic drug, **flupirtine** (trade name Katadolon) represent the first neuronal Kv7 activator.

The analgesic action of flupirtine has been initially ascribed to its ability to act as an antagonist of N-methyl-D-aspartate (NMDA) receptors or an agonist of  $\gamma$ -amino-butyric acid (GABA<sub>A</sub>) receptors (Szelenyi et al., 2013), but further studies have demonstrated that flupirtine enhanced the activity of I<sub>KM</sub>, acting on homomeric Kv7.2 channels at concentrations close to those achieved during standard therapy with this drug (2-6  $\mu$ M) (Martire et al., 2004). Because of its severe liver toxicity, to date, the clinical use of flupirtine as non-opioid analgesic, is limited to short-term pain management as recommended by European Medicines Agency:

([http://www.ema.europa.eu/ema/index.jsp?curl=pages/medicines/human/referrals/Flupirtinecontaining\\_medicines/human\\_referral\\_prac\\_000019.jsp&mid=WC0b01ac05805c516f](http://www.ema.europa.eu/ema/index.jsp?curl=pages/medicines/human/referrals/Flupirtinecontaining_medicines/human_referral_prac_000019.jsp&mid=WC0b01ac05805c516f)). In addition to analgesia, flupirtine displays neuroprotective effects (Boscia et al., 2006) and anticonvulsant activity, in pentylenetetrazol-induced seizures (PTZ) mice models and in patients with pharmaco-resistant epilepsy. However, the pharmacologically active dose in those patients is ten-times higher than that producing analgesia (Rostock et al., 1996).

More recent studies have demonstrated that flupirtine, unlike phenobarbital or diazepam, appears more effective in preventing and suppressing seizures in kainic acid model of neonatal seizures (Raol et al., 2009)

To separate the analgesic action from the anticonvulsant activity, molecular modeling studies have been carried out. Analyses of pharmacophoric region suggested that the phenyl ring and the basic nitrogen atom in the pyridine put at a specific distance from this

ring, is essential for the analgesic activity. The absence of this basic nitrogen atom enhanced the antiepileptic activity, reducing at the same time analgesic activity (Figure 10).

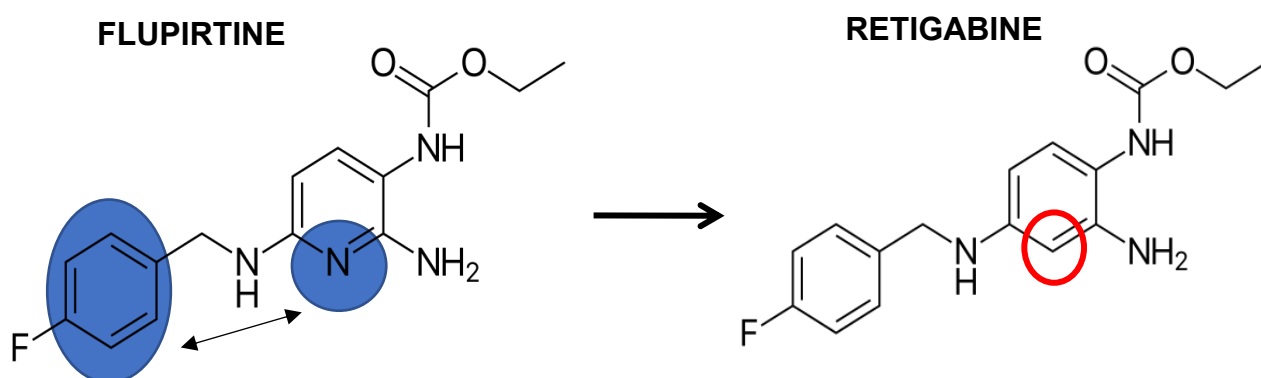


**Figure 10. Pharmacophore modification of flupirtine and development of retigabine.**

Based on these observations a synthesis program began and resulted in the development of several desazaflupirtine derivatives. Among this new class of anticonvulsants, the most potent obtained has been the retigabine. **Retigabine** (trade name Trobalt in Europe or Potiga in the USA) represent the first approved anticonvulsant drug acting on Kv7 potassium channel. The principal effect is a hyperpolarizing shift in channel activation, together with an acceleration in channel activation and a slowing down of its deactivation (Main et al., 2000). Anyway, retigabine is a nonselective Kv7 channel opener and its effects on voltage-sensitivity depend on the Kv7 family subtype. For instance, the cardiac Kv7.1 channel is completely insensitive, while on Kv7.3 homomers the effect on voltage sensitivity is maximal (-43mV), intermediate for Kv7.2/3 heteromers (-30 mV) and Kv7.2 homomers (-24 mV) and very small for Kv7.4 homomers (Tatulian et al., 2001) (Table 1). In Kv7.5 homomers retigabine does not change voltage sensitivity, but increases current amplitude (Dupuis et al., 2002). Finally, on Kv7.2/3 heteromers retigabine increases the single channel open probability by stabilizing the open conformation, without any significant change in channel conductance (Tatulian and Brown 2003).

**Table 2. Potency of retigabine against KCNQ2/3, KCNQ1, KCNQ2, KCNQ3, and KCNQ4. (From Tatulian et al 2001)**

	Maximum shift in $V_{1/2}$ (mV)	Retigabine $EC_{50}$ (M)
<b>KCNQ2/3</b>	-30.4	$1.9 \pm 0.2$ (n=5)
<b>KCNQ1</b>	-0.7	$100.1 \pm 6.5$ (n=5)
<b>KCNQ2</b>	-24.2	$2.5 \pm 0.6$ (n=5)
<b>KCNQ3</b>	-42.8	$0.6 \pm 0.3$ (n=5)
<b>KCNQ4</b>	-24.6	$5.2 \pm 0.9$ (n=5)

Anticonvulsant activity of retigabine has been also demonstrated in a broad spectrum of animal model. In 1996 Rostock and collaborators demonstrated that retigabine was effective in reducing seizure induced electrically (MES) or chemically by pentylenetetrazole (PTZ), picrotoxin and N-methyl-D-aspartate (NMDA). The drug has been also effective in genetic animal model like the DBA/2 mouse in which showed an additive effect when co-administered diazepam, phenobarbital, phenytoin, and valproate (Rostock et al., 1996; de Sarro et al 2001) or epilepsy-prone rats (GEPR-3 and GEPR-9) (Dailey et al., 1995). Moreover, in the amygdala kindling model, retigabine was able to reduce seizure severity and duration, total duration of behavioral changes, and after discharge duration showing higher potency compare to valproate (Tober et al., 1996). The drug also exhibited anticonvulsant activity in two pharmacoresistant epilepsy models; lamotrigine-resistant kindled rats (Postma et al., 2000) and in the 6 Hz psychomotor mouse model (Barton et al., 2001). More recently, retigabine has been test in two heterozygous knock-in mice carrying BFNS causing mutations Y284C, A306T in KCNQ2 (KCNQ2<sup>Y284C/+</sup> and KCNQ2<sup>A306T/+</sup>. Here, after intraperitoneal injection of kainic acid, retigabine mitigated induced seizure activities in both mice models, more significantly than phenobarbital (Ihara et al., 2016).

Retigabine recognizes an intracellular hydrophobic pocket located between the segments S5 and S6 in the pore domain (Main et al 2000). Within this cavity, a residue of tryptophan (W236 in Kv7.2 and W265 in Kv7.3), present at the end of the S5 helix, was found to be crucial for the retigabine effect. Beside this residue, also other amino acids are involved in the binding of retigabine, like L243 in S5, L275 in the pore, L299/ and Gly301 in the S6 (according to Kv7.2 sequence); however, none of them seems to be critical as the tryptophan. The key-role of this residue was confirmed by site-specific mutagenesis experiments; substitution of this residue with a leucine, resulted in a completely loss ability of retigabine to activate Kv7.2 currents (Schenzer et al., 2005; Wuttke et al., 2005).

In 2009 Lange and co-authors, hypothesized a generic hydrophobic interaction between retigabine and the conserved tryptophan residue therefore the fluorophenyl ring of retigabine was in either the vicinity of the aromatic side chain of tryptophan (Lange et al., 2009) (Figure). More recently, Kim and collaborators, using unnatural amino-acid, demonstrated that an H-bond interaction occur between the carbamate group of retigabine and the tryptophan residue. In fact, repositioning of the indole nitrogen atom prevents the formation of the H-bond suppressing the effects of retigabine whereas, the introduction of a W analogue (F3-W), with altered electrostatics but left intact or enhanced H-bonding ability, enhances retigabine potency. This evidence suggests a “flip” conformation compared to the original proposed by Lange (Kim et al., 2015) (Figure 11).

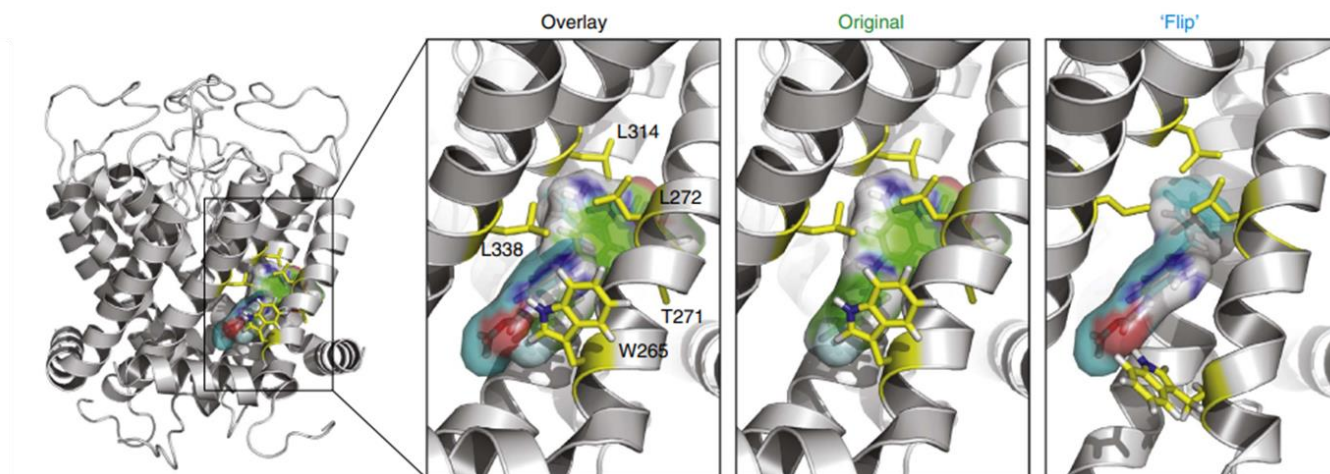


**Figure 11. Retigabine binding poses.** Two orientations are shown with the carbamate group in either the vicinity of Leu314 ('original' model) or Trp265 ('flip' model). The two binding models are superimposed in the 'overlay' (from Kim et al., 2015)

The hypothesis that retigabine forms a direct hydrogen bond with indole ring of tryptophan was recently validated by the published cryo-electron microscopy (cryo-EM) structures of the human KCNQ2 and KCNQ4 in complex with retigabine (Li X et al., 2020; Li T et al., 2020). Interestingly, in these models, further interaction sites were described; in both cases an H-bond interaction occurred between the aniline group of retigabine and the side chain of serine. To solidify the observations from the structural analysis, electrophysiological experiments were performed by the authors, obtaining that in Kv7.2, Ser303A mutation, decreased the potentiation activity of retigabine on Kv7.2 by attenuating the left-shift of the G-V curves ( $\Delta V_{1/2}$ ) (Li X et al., 2020) while in Kv7.4 the mutant Ser309H (Histidine) completely abrogated retigabine's ability to activate the channel (Li T et al., 2020). On the other hand, in KCNQ4<sub>EM</sub> a pi-stacking contact was observed between fluorophenyl group of retigabine and the aromatic ring of F246; mutation of F246 to alanine partially abrogated the retigabine effect (F240 on Kv7.2) (Li T et al., 2020) (Figure 12). Nevertheless, the precise structural basis for the activation mode remains enigmatic. Alignment of the apo structure of KCNQ2 (without the ligand) and KCNQ2-retigabine, revealed that retigabine binding causes



conformational changes mainly in the PD. By contrast, the VSD in KCNQ2-retigabine structure remained almost unchanged but the high B-factor, which reflect the fluctuation of atoms about their average positions and provide important information about protein dynamics, indicated that it displays increased mobility upon retigabine binding. According KCNQ4<sub>EM</sub>, alignment of the apo structure of KCNQ4 and KCNQ4-retigabine revealed displacement of residues that are involved in ligand binding, as well as the movement of S5. This last, was transduced to the whole VSD through the S4-S5 linker. These conformational changes caused by the binding of retigabine provide a possible explanation for the activation mechanism on KCNQ channels, suggesting that retigabine acted as an allosteric modulator.

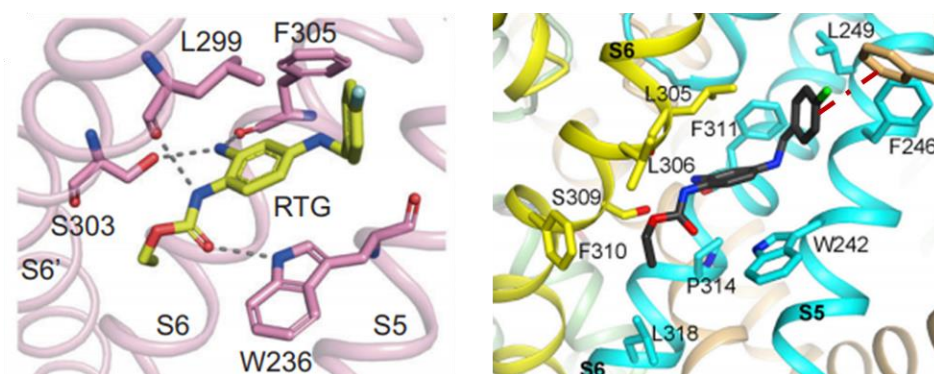
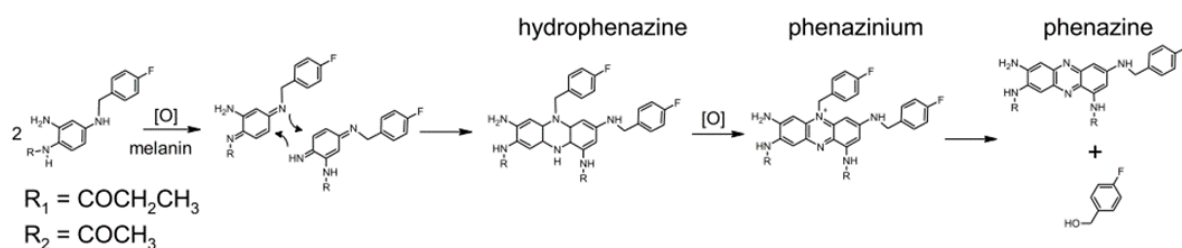


**Figure 12. Localization of retigabine in KCNQ2 (right) and KCNQ4 (left). From Li X et al., 2020; Li T et al., 2020**

Retigabine has been approved in 2011 for clinical use as adjunctive treatment of partial-onset seizures in adults who responded inadequately to alternative treatments. The drug has also shown to be effective in the treatment of KCNQ2 LoF mutations, representing a valid personalized therapy approach (Millichap et al.,2016). Unfortunately, in 2017, GlaxoSmithKline (GSK) announced the permanent discontinuation and market withdrawal because of its unfavourable risk/benefit ratio due to: I) *poor selectivity for Kv7 subtypes*. Indeed, activation of Kv7.4 and Kv7.5 channels expressed in genitourinary smooth muscle caused urinary retention. Recently, this hypothesis has been questioned by Tykocki and colleagues which suggest that urological side effects of retigabine are due to activation of Kv7 channels in sensory nerves which decreases sensory outflow in the mouse urinary bladder (Tykocki et al 2019). II) *Short half-life*. The rapid metabolism by phase-II enzymes (acetylation and N-glucuronidation), leading to the requirement of a three-times-a-day dosing regimen (Barrese et al., 2010). III) *Poor brain penetration*. Due to the limited lipophilicity ( $\log P = 3.08$ ) (Zhou et al.,2015) IV) *Chemical instability*. In 2013, the Food and Drug Administration (FDA) issued an alert that retigabine could induce retinal and mucocutaneous blue-gray discoloration in patients treated for at least four years. A proposed mechanism for formation of the phenazinium dimers is outlined in Scheme 1. Dimer formation can be rationalized through a concerted or stepwise conjugate addition pathway to form the two new C–N bonds of the hydrophenazine ring following initial oxidation of RTG to the diimide quinine. The final step would involve oxidation to aromatize the hydrophenazine ring to the phenazinium cationic species.



**Scheme 1. Proposed Mechanism for the Formation of Phenazinium Dimers**

In animal models, considering pigmented (Long Evans) and albino (Wistar Han) rats, dimers have been detected only the eye tissues from the pigmented rats while they were absent non-melanin containing ocular tissues from the albino rats, demonstrating a high affinity of these by products to tissue containing melanin (Groseclose and Castellino 2019).

For these reasons, several companies and academic groups are pursuing the synthesis of novel retigabine derivatives with improved physico-chemical, pharmacokinetic, or pharmacodynamic properties.

In 2015 Kalappa and colleagues, synthesized the fluoroanilinic retigabine derivative **SF0034** (for all structure molecules see Table 3), obtained by introducing a fluorine atom at the 3-position of the aniline ring of retigabine. The compound appeared 5-times more potent than retigabine on Kv7.2/Kv7.3 channels showing an  $\text{EC}_{50}$  of  $1.3 \pm 0.3 \mu\text{M}$  and  $6.5 \pm 1.5 \mu\text{M}$ , respectively.

Moreover, SF0034 showed reduced affinity for the channels associated with urinary retention side effect, such as Kv7.4/Kv7.5 and more chemical stability compared to retigabine. In fact, incorporation of an electron-withdrawing atom on the aniline ring of retigabine reduce the oxidation and the consequent dimers formation. Considering *in vivo* model, in the MES and corneal kindled seizure models SF0034 was significantly more potent than retigabine (Kalappa et al., 2015)

Considering the structure of SF0034, in 2016 by Kumar and collaborators synthesized the **RL648-81**, characterized by a CF<sub>3</sub>-group at the 4-position of the benzylamine moiety,

combined with the fluorine atom on the aniline ring. Compared to SF0034, RL648-81 has been reported to be 3- times more potent in activating Kv7.2/Kv7.3 channels with an EC<sub>50</sub> of 0.6±0.02 µM and 0.19±0.02 µM, respectively. As well as SF0034, RL648-81 appears to preferentially target Kv7.2/Kv7.3 channels over Kv7.4/Kv7.5 channels, thus obtaining a compound more potent, selective, and stable than retigabine.

Starting from the RL648-81 as new lead compound, Liu and co-authors synthesized 19 newly analogues. Several molecules exhibited an improved selectivity on Kv7.2/Kv7.3 over the other tested channels (e.g., Kv7.3/Kv7.5, Kv7.4, and Kv7.4/7.5) specifically, **RL-36** and **RL-12** resulted more potent on Kv7.2/3 with EC<sub>50</sub>s of 1 µM compared to Kv7.3/5, Kv7.4 and Kv7.4/5 (EC<sub>50</sub>s >10 µM). The authors also identified an analogue of RL648-81, RL-56, remarkably potent on Kv7.2/3 (EC<sub>50</sub> 0.11±0.02 µM) compared to lead compound.

Similarly, to retigabine, conserved residue W236 is necessary for SF0034, and RL648\_81 activity. In both cases, gating effect on KCNQ2 channels are abolished upon substitution of W236 to L (leucine) suggesting that these analogues share the same binding site.

As reported previously, one of the limits of retigabine is our poor brain penetration, lead to the limited lipophilicity. To overcome them, by introducing a propargyl group at the N position of the retigabine linker, the so-called **P-retigabine** has been developed. The compound showed an increased brain-to-plasma ratio equal to 2.30 versus 0.16 for retigabine, while electrophysiological experiment demonstrated that P-retigabine was more potent than retigabine on Kv7.2. In *in vivo* models, P-retigabine exhibits an improved antiepileptic activity anticonvulsant less toxicity when compared to retigabine (Zhou et al., 2015).

Based on P-retigabine structure, the N-3 tertiary butyl substituted compound has been synthesized (Wang et al 2019). The so-called **compound 10g**, exhibited a highly selectivity to Kv7.4 and Kv7.5 channels without potentiating the other subtypes of the family. Particularly, compound 10g showed EC<sub>50</sub> values of 0.78 and 1.68 µM, on Kv7.4 and Kv7.5 respectively, while the EC<sub>50</sub> on Kv7.2 was >30 µM. Mainly, the compound increased current

the current amplitude, with no effect on the voltage-dependent activation curves probably because, according to authors, G-V shift should be sensitive to N-3 structure alterations (Wang et al 2019).

To obtain more stable compounds another strategy has been to replace the secondary amine linker by a sulfur atom. With this approach Bock and colleagues have produced a series flupirtine/retigabine derivatives which showed a strong less oxidative behaviour and a pharmacological activity retained or even increased. For example, flupirtine analog **compound 48**, showed an enhanced potency on Kv7.2/Kv7.3 ( $EC_{50}$  of 1.4 nM), improved toxicity/activity ratio and the same efficacy as retigabine while **compound 36** showed the same potency and efficacy as flupirtine but less toxicity.

Another flupirtine/retigabine chemical analogue is NS15370, a potent Kv7.2-Kv7.5 channels activator, showing an  $EC_{50}$ s between 40 and 150 nM. NS15370 is effective in rodent models of partial epilepsy the 6 Hz seizures and rat amygdala kindling providing full protection against discharges (Dalby-Brown et al., 2013).

To remove the aniline ring of the retigabine, responsible for dimers formation, a series of dimethoxy-pyrimidines have been synthesized by Davoren and colleagues. Among them the lead compound **PF-05020182**, in which the aniline structure and carbamate at the 5-position have been replaced with a 4,6-dimethoxypyrimidine and an amide respectively, showed: potent Kv7.2/7.3 channel opener activity, no effect over the cardiac Kv7.1/KCNE1 channels and anticonvulsant activity in the maximal electroshock (MES) model (Davoren et al., 2015).

Based on the structure of retigabine and PF-05020182 using hybridization drug design strategy, a novel series of substituted piperidine derivatives were obtained by introducing in RTG the amide group instead of the carbamate group and two methyl groups into the core phenyl scaffold. Between these, **compound 11** displayed a better activity than RTG on

Kv7.2, with an EC<sub>50</sub> of 0.22 µM compared to 0.35 µM for the control retigabine and a good PK profiles in rat (Yang S et al., 2018).

Piperidine derivatives were subsequently optimized by the authors who synthesized a novel series of N-phenylbutanamide derivatives. Several molecules were found to be potent Kv7 openers in Rb<sup>+</sup> flow test, for **compound 1** the calculated EC<sub>50</sub> was 0.02 microM. Subsequently tested by patch-clamp, compound 1 a strong leftward shift a of about -66.21 ± 5.55 mV compared -40.00 ± 2.80mV of retigabine. A significant anti-convulsant activity in MES model with no adverse effects and good brain permeability was also exhibit (Yang S et al., 2018).

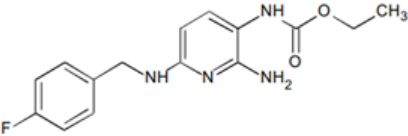
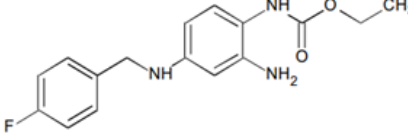
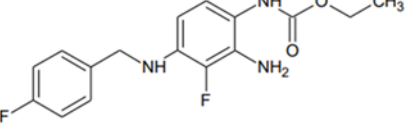
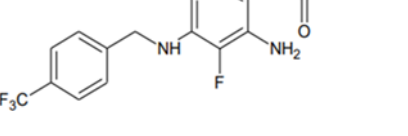
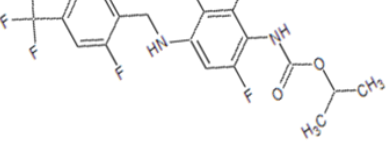
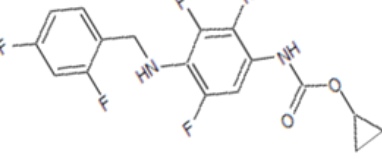
More recently, several conformationally restricted analogues have been synthesized by Ostacolo and collaborators displaying higher potency and improved chemical stability.

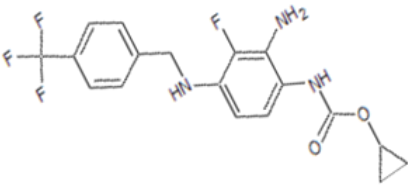
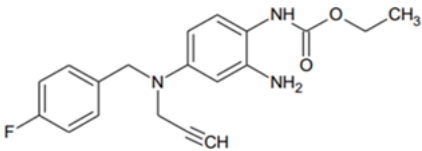
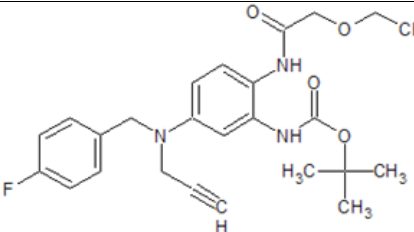
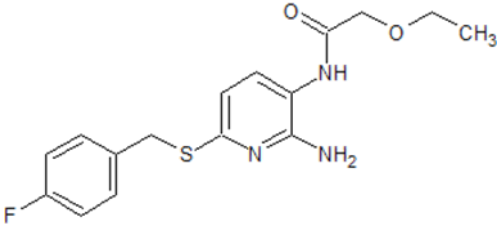
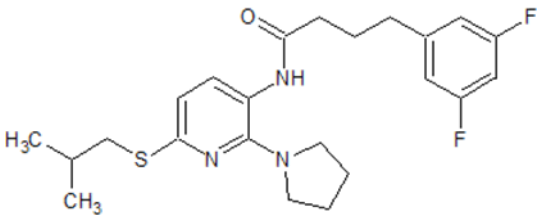
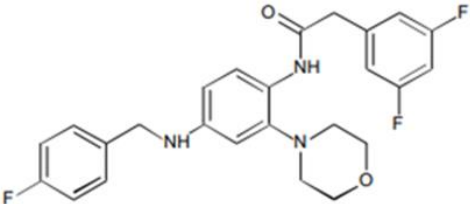
Among 42 tested compounds, the two selected compounds 23a and 24a were able to increase Kv7.2 currents more than retigabine at -40 mV and at 0 mV. Compared to the reference compound, **compounds 23a** and **24a** exhibited slow ON/OFF kinetics due to their increased hydrophobicity, a very important aspect since, as report previously, one limit of retigabine is its poor brain penetration, a pharmacokinetic drawback that might be improved by the increased hydrophobicity. Additionally, compared to retigabine (EC<sub>50</sub> 0.93 ± 0.43 µM) compound 23a showed higher potency on Kv7.2 channels with an EC<sub>50</sub> of 0.08 ± 0.04 µM whereas no change in potency was observed for 24a (EC<sub>50</sub> 0.63 ± 0.07 µM). Furthermore, both derivatives showed higher potency in activating heteromeric Kv7.2/Kv7.3 and homomeric Kv7.4 channels.

Actually, Xenon Pharma has developed the **XEN1101**, a Kv7 potassium channel modulator, chemically designed to improve potency, selectivity, pharmacokinetics, and chemical stability of retigabine. Nowadays Xenon has initiated a Phase 2b clinical trial with XEN1101. Moreover, Xenon has initiated a Phase 3 randomized, double-blind, placebo-controlled,

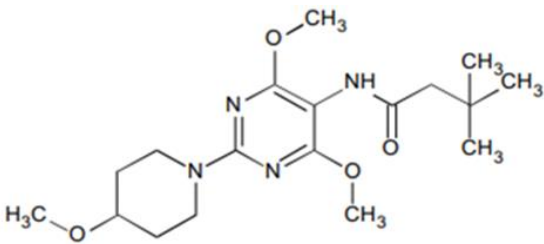
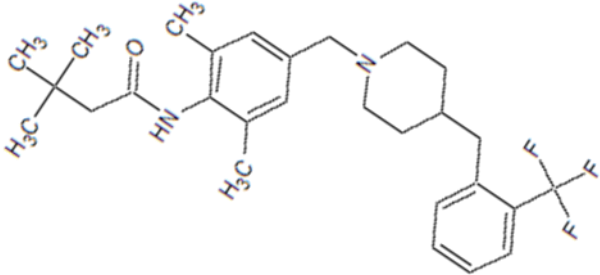
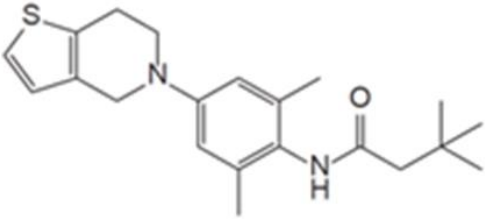
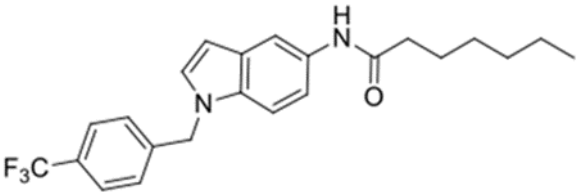
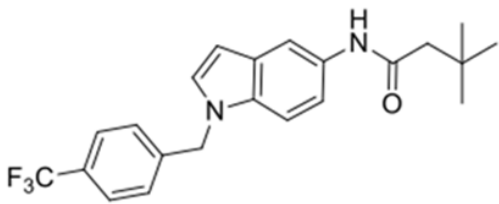
parallel group, multicenter clinical trial, called the “EPIK” study, evaluating the efficacy, safety, and tolerability of **XEN496**, a pediatric formulation of retigabine, administered as adjunctive treatment in approximately 40 pediatric patients aged one month to less than 6 years with KCNQ2-DEE.

**Table 3. Flupirtine, Retigabine and Derivatives**

Compound Name	Structure
Flupirtine	
Retigabine	
SF0034	
RL648_81	
RL_12	
RL_36	

<p><b>RL_56</b></p>	
<p><b>P-Retigabine</b></p>	
<p><b>Compound 10</b> (P-ret analogue)</p>	
<p><b>Compound 48</b> (Flupirtine analogue)</p>	
<p><b>Compound 36</b> (Flupirtine analog)</p>	
<p><b>NS15370</b></p>	



<p><b>PF-05020182</b></p>	
<p><b>Compound 11</b> (PF-05020182 analogue)</p>	
<p><b>Compound 11</b> (PF-05020182 analogue)</p>	
<p><b>Compound 23a</b> (retigabine analogue)</p>	
<p><b>Compound 24a</b> (retigabine analogue)</p>	

### 1.9.2.2 Acrylamide

Besides flurpitine and retigabine, other molecules are potent activators of Kv7 channels, like compounds belonging to the class of the acrylamide. Developed by the Bristol-Myers Squibb Pharmaceutical Research Institute the fluoro-oxindoles **BMS- 204352** (*for all structure molecules see Table 4*) represent the first acrylamide synthesized. Originally described as an agonist of calcium-activated potassium channels (BK channels) indicated for the treatment of ischemic stroke (Gribkoff et al., 2000), BMS- 204352 was also active on Kv7.4 channels, able to produce a leftward shift of the activation curve and an increase in the maximal current, with an EC<sub>50</sub> of 2.4  $\mu$ M compared to 1.4  $\mu$ M for the control retigabine (Schroder et al., 2001).

Later, the Bristol-Myers Squibb, synthesized the so called **(S)-1** compound, a Kv7.2 opener with excellent oral bioavailability, showing positive effect in a cortical spreading depression model of migraine (Wu et al., 2003) (S)-1 exhibited opposite effect on Kv7 channels family members; acting as a blocker of Kv7.1 and Kv7.1/KCNE1 current whereas on Kv7.4 and Kv7.5 enhanced the maximal current amplitude at all potentials, contrary to Kv7.2 and Kv7.2/ Kv7.3, in which the activation/block of was strongly voltage-dependent (Bentzen et al., 2006).

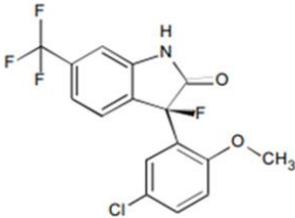
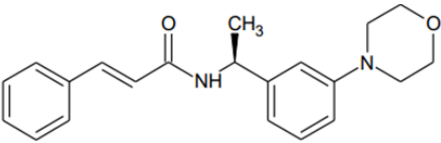
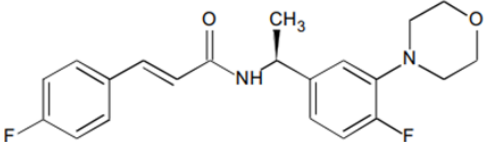
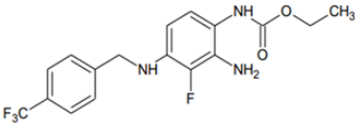
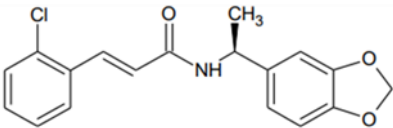
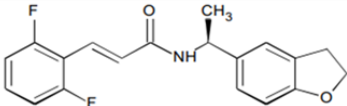
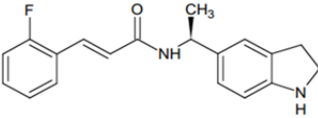
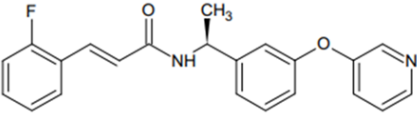
Since (S)-1 compound leading to the formation of a reactive intermediate found to be responsible for CYP3A4 metabolism-dependent inhibition (MDI), subsequent structural optimization yielded to the **BMS-568274**, a difluoro analogue which does not alter CYP3A4 metabolism, thus showing lesser potential for pharmacokinetic interactions (Wu et al., 2003). In the search for more powerful compounds, the **(S)-2** compound was developed. (S)-2 displayed a profound hyperpolarizing shift in the voltage-dependence of activation of Kv7.2 and the calculated EC<sub>50</sub> was 0.063  $\mu$ M. (S)-2 was also able to reduce spontaneous neuronal discharges in rat hippocampal slices (Wu et al., 2004).

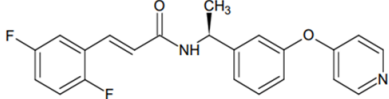
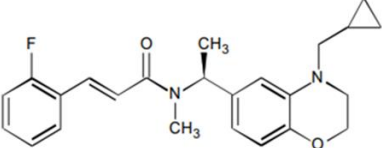
Following structure modification of (S)-2 lead to identification **(S)-3**, **(S)-4**, and **(S)-5** derivatives. Notably, (S)-3 was most potent ( $EC_{50}$   $20 \pm 1$  nM) but least efficacious, while (S)-4 and (S)-5 showed moderate potency but improved efficacy over (S)-2, (S)-3 and retigabine. Moreover, is important to underling that the (R)-enantiomers of these compounds did not show any opener activity on Kv7.2, thus suggesting a strong stereoselectivity. (Wu et al., 2004).

Recently, two biaryl ether acrylamides, **(S)-6**, and **(S)-7**, have been synthesized: the (S)-6 derivative, in particular, is a strong Kv7.2 and shown significant efficacy in the treatment of neuropathic pain (Wu et al., 2013).

Finally, a more recent analogue of acrylamide (S)-2, called **SMB-1**, shows a unique profile of action on Kv7 channels; inhibiting Kv7.2 and activating Kv7.4 channels (Blom et al., 2014). According to acrylamides binding site, (S)-1 and SMB-1 binds within the same pocket as retigabine; in both case the activity on Kv7.4 was critically dependent on the tryptophan residue in S5 (Bentzen et al., 2006).

Table 4. Acrylamides structures

Compound Name	Structure
BMS- 204352	
S)-1	
BMS-568274	
(S)-2	
(S)-3	
(S)-4	
(S)-5	
(S)-6	

<b>(S)-7</b>	
<b>SBM-1</b>	

### 1.9.2.3 Benzamides

Belonging the class of benzamides the compound **ICA-27243** (*for all structure molecules see Table 5*), represent the first benzamide described. Described as a strong Kv7.2/3 activator ( $EC_{50} = 0.4 \mu M$ ), ICA-27243 caused a hyperpolarizing shift in the voltage-dependence of activation of about -19 mV at 10  $\mu M$ . By contrast, it was less active on Kv7.4 and Kv7.3/5 channels with an  $EC_{50}$ s of 9.7  $\mu M$  and >30  $\mu M$ , respectively. No effect on GABA-activated chloride channels, Nav 1.2 Voltage-Dependent Sodium Channels, or voltage-gated calcium channels have been reported. In addition, ICA-27243 suppresses seizure-like activity in an *ex vivo* hippocampal slice model and exhibits anticonvulsant activity in a broad spectrum of seizure animal models such as maximal electroshock (MES), pentylenetetrazole (PTZ)-induced seizures, amygdala kindling model of partial seizures and in the 6-Hz model of psychomotor seizures (Wickenden et al., 2008; Roeffols et al., 2008). For these reasons, **ICA-27243** represented a good antiepileptic candidate, even though toxicity studies showed that repetitive dosages of the drug-induced non hemolytic anemia in animal models.

Therefore, novel N-pyridyl benzamides derivatives were synthesized, like the **ICA-069673**, an orally active compound effective in several animal models of epilepsy, with good pharmacokinetic properties and higher selectivity on Kv7.2/3 over Kv7.3/5 (Amato et al., 2011).

Another compound belonging to the class of benzamides is ICA-110381 which predominantly activates Kv7.2 causing a hyperpolarizing shift in channel activation and a slowing of channel deactivation. **ICA-110381** showed anticonvulsant activity in the amygdala kindling model by reducing seizure severity and duration (Boehlen et al., 2013). High-throughput screening of the ChemBridge Diverset<sup>TM</sup> library composed by 20,000 compounds allowed the identification of the benzamide **ztz240**, structurally similar to ICA-27243. On Kv7.2 10 $\mu M$  ztz240, produced a significant increase in outward current amplitude,

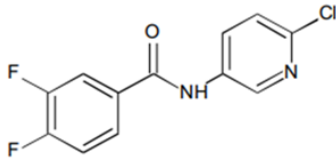
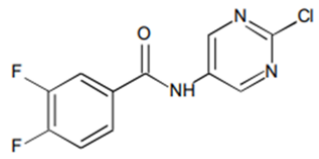
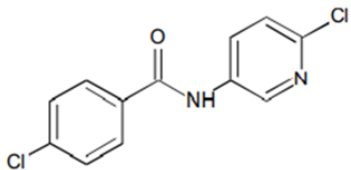
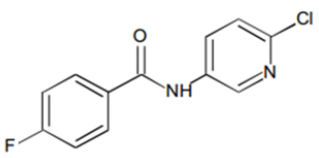
a slowing in deactivation kinetics, and a marked left-shift on the voltage activation curve ( $V_{1/2} -58.7 \pm 7.7 \text{ mV}$ ). On the other hand, ztz240 (10  $\mu\text{M}$ ) potentiates Kv7.4 and Kv7.5 more than Kv7.2, in terms of current amplitude whereas, the left shift of activation was smaller. Finally, Kv7.3 and Kv7.1 were insensitive to the compound (Gao et al., 2010)

Compared to retigabine and acrylamides, the compounds belonging to the class of benzamides show a different binding site. While retigabine binds in a hydrophobic pocket in the pore domain (PD), benzamides bind to the voltage-sensing domain (VSD) (Padilla et al., 2009); when tested on Kv7.2 W236L, the mutant was sensitive both to ICA compounds and ztz240 (Padilla et al., 2009; Gao et al., 2010; Boehlen et al., 2013). Recently it has been demonstrated that these compounds not only differ for the binding site but also for the subunit stoichiometry needed to evoke their effects, indeed, while for retigabine a single subunit is sufficient to produce the near-maximal effect (Yau et al., 2018), all four subunits are required for maximal sensitivity to ICA-069673 and even a single insensitive subunit leads to significantly diminished effects (Wang et al., 2018).

To understand which residues in VDS are involved in the binding of these compounds mutagenesis experiments were conducted. Considering the ztz240, the phenylalanine in position 137 (highly conserved in the family of Kv channels) was found to be critical for the activity of the compound, and when mutated with an alanine (F137A) dramatically reduced the effect of ztz240 on Kv7.2. Also, other residues seemed important like E130, I134, G138, R207 (Li P et al., 2013). Regarding ICA-069673, Wang and co-workers in 2016 demonstrated that the two residues F168 and A181 in the S3 segment appear essential for its activity (Wang et al., 2016). More recently, cryo-electron microscopy (cryo-EM) structures of the human KCNQ2 in complex with ztz240 has been obtained (Li X et al., 2020), confirming that the binding site is located between the S3 and S4 segments in the VSD and residues F137, I171, D172, R207, R210 are involved in ztz240 binding. Indeed,

electrophysiology experiments performed on F137A, D172A, and R210Q mutants, in presence of 5  $\mu$ M ztz240, revealed a reduced increase of outward current amplitude ratio and prevented or attenuated the left-shift of the curve. Furthermore, R207Q attenuated the left-shift of the curve without changing the outward current amplitude whereas mutation I171A decreased the outward current amplitude with no effect on the voltage activation. It is important to note that residues involved in the interactions with the ztz240 are less conserved in Kv7.1 or Kv7.3. This could explain the lesser sensitivity of these two Kv7 family subtypes to ztz240 (Li X et al., 2020)

**Table 5. Benzamides structure**

Compound Name	Structure
ICA-27243	
ICA-069673	
ICA-110381	
ztz240	



#### 1.9.2.4 Fenamates

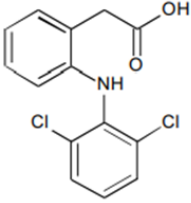
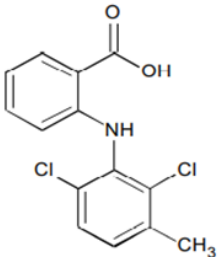
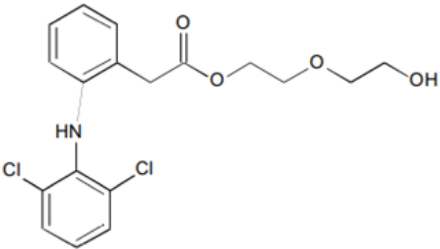
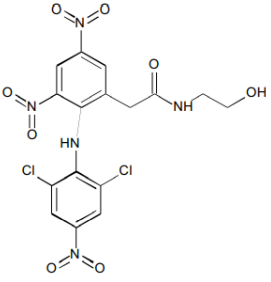
Belonging to the family of **fenamates**, **meclofenamic** (*for all structure molecules see Table 6*) acid and diclofenac, two well-known nonsteroidal anti-inflammatory drugs acting as non-selective inhibitors of the COX-1 and COX-2 cyclooxygenases, activate Kv7 potassium channel. Mainly these two compounds activate Kv7.2/3 channels, by causing a leftward shift in the voltage-dependent gating of the channel and slowing the deactivation kinetics while no effects are elicited on cardiac Kv7.1 channel (Peretz et al., 2005). Moreover, diclofenac also exhibits anticonvulsant activity in MES model.

To separate the  $I_{KM}$ -opening property from COX inhibition activity, several derivatives have been developed. Among them, the diclofenac derivative **NH6** was obtained by adding a diethylene glycol tail to the carboxylic acid group of the molecule. On Kv7.2/3 channels, NH6 caused a hyperpolarizing shift of the voltage activation curve and markedly slowing of the deactivation kinetics whereas it did not affect homomeric Kv7.1 and heteromeric Kv7.1/KCNE1 currents. In cortical, hippocampal, and dorsal root ganglion (DRG) neurons the compounds strongly reduced the number of evoked and spontaneous action potentials while in hippocampal slices it decreased somatically evoked spike afterdepolarization of CA1 pyramidal neurons. By activating M-channels, NH6 decreased the frequency of miniature excitatory (mEPSC) and inhibitory (mIPSC) postsynaptic currents with no modification in their amplitude and waveform (Peretz et al., 2007).

The second derivative of diclofenac called **NH29** was able to increase Kv7.2 currents, produced a hyperpolarizing shift in the gating of the channel, and significantly enhanced both activation and deactivation kinetics of Kv7.2 channels, whereas like the other members of the family it failed to activate homomeric Kv7.1. In DRG neurons and primary cultures of hippocampal neurons **NH29** reduced the number of evoked spikes and depressed synaptic transmission, respectively. NH29 was active in retigabine-insensitive Kv7.2 W236L channels suggesting that did not interact with the RTG binding site on Kv7.2. Docking

studies have demonstrated that NH29 binds a pocket in the VSD formed by K120 in the S1-S2 loop, Y127 and E130 in helix S2, and L200 and R207 in S4. Here, the nitro group of one aromatic ring of NH29 forms a hydrogen bond with the guanidinium group of R207 and the carboxylate of E130 (Peretz et al., 2007).

**Table 6. Fenamates structure**

Compound Name	Structure
<b>Diclofenac</b>	
<b>Meclofenamic acid</b>	
<b>NH6</b>	
<b>NH29</b>	

### 1.9.2.5 Other chemotypes of neuronal Kv7 activators

In 2011 Yu and co-workers screening the NIH Molecular Libraries Small Molecule Repository (MLSMR) containing 300 000 molecules, identified the compound **ML213** (*for all structure molecules see Table 7*). As reported by the authors, the molecule activated preferentially Kv7.2 and Kv7.4 channels, producing a leftward shift in their activation curves and showing an EC<sub>50</sub> of 230 nM on Kv7.2 and 510 nM on Kv7.4. Subsequent studies performed in A7r5 vascular smooth muscle cell line, have shown that ML213, was a potent and effective activator of homomeric Kv7.5 and heteromeric Kv7.4/7.5 channels and was able to increase the maximum conductance, to negatively shift of their activation curves and to decrease the current deactivation rates. Substitution of the tryptophan residue at position 235 of Kv7.5 and 242 of Kv7.4 to leucine (W235L/W242L), abolished the effects of ML213 on Kv7.5 and Kv7.4 demonstrating that the compound recognized the same binding site of retigabine (Brueggemann et al., 2014).

**Zinc Pyrithione** (ZnPy), a compound used for the treatment of psoriasis and dandruff control, has been demonstrated to be a potent activator of Kv7 channels, except for Kv7.3 and Kv7.1/KCNE1 subunits. This molecule produced an increase in open probability, a leftward shift in the activation process and a reduction in the deactivation rate (Xiong et al., 2007). The binding site is located within the pore, but unlike retigabine ZnPy is active in retigabine-insensitive Kv7.2 W236L channels suggesting that this residue is not essential for the activity. Moreover, mutagenesis studies based on Kv7.2 channels have revealed that residues L249 in S5, L275 between S5 and the pore region, and A306 in segment S6 play an important role (Xiong et al., 2008).

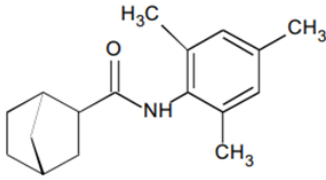
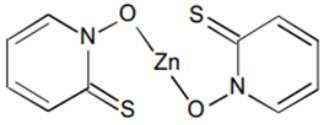
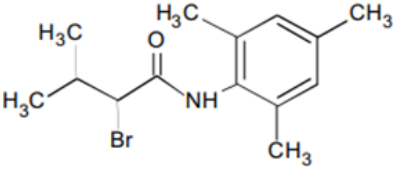
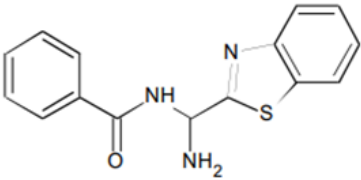
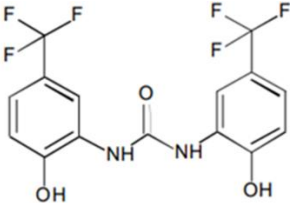
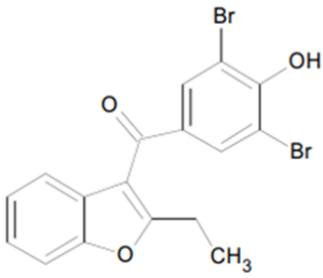
High-throughput screening of a library of 80,000 compounds enabled the identification of two novel Kv7.2 activators, the amide **ZG1732** and the benzothiophene **ZG2083**. The two selected compounds increased the outward Kv7.2 currents and left shifted the activation

curve, showing an EC<sub>50</sub> of 1.04±0.18 µmol/L for ZG1732 and 1.37±0.06 µmol/L for ZG2083 (Yue et al., 2016)

The compound **NS1643**, reported as an opener of Kv11 channels, is also a Kv7 channel activator; in fact, NS1643 potentiated homomeric Kv7.2, Kv7.4, and heteromeric Kv7.2/3, but not cardiac Kv7.1 channel. When tested on Kv7.2 channels, NS1643 left shifted the activation curve and slowed deactivation. Analysis of the dose-response curve of NS1643 revealed an EC<sub>50</sub> value of 2.4 µM (Li et al., 2014).

**Benzbromarone** (BBR), an inhibitor of urate transporters, has been recently demonstrated to activate Kv7 channels. BBR shows promising antinociceptive effects, consistently attenuating bradikinin-, formalin-, or monosodium urate-induced inflammatory pain in rat and mouse models (Zheng et al., 2015)

**Table 7. Structure of other chemotypes of neuronal Kv7 activators**

Compound Name	Structure
<b>ML213</b>	
<b>ZnPy</b>	
<b>ZG1732</b>	
<b>ZG2083</b>	
<b>NS1643</b>	
<b>Benzbromarone</b>	

#### 1.9.2.6 Gaba, gabapentinoids, and ketogenic diet

The hypothesis that endogenous ligand, with similar chemical properties to retigabine, were able to bind the conserved tryptophane residue in S5 of Kv7 channels was pursued for the first time by Manville and colleagues. The authors found that the primary inhibitory neurotransmitter **GABA**, containing a negative electrostatic surface potential centered on a carbonyl group (like retigabine), interacted with Kv7.2–5 tryptophane; electrophysiological recordings showed that Kv7.3, Kv7.5 and Kv7.2/3 channels, were activated by GABA, which caused a negative-shifts in the voltage activation current (Manville et al., 2018b).

Because of the structural similarities with GABA, the authors, hypothesized that **gabapentin** and **pregabalin** could modulate Kv7 channels. The results obtained showed that gabapentin, but not pregabalin, was a potent activator of the heteromeric Kv7.2/3 and homomeric Kv7.3, Kv7.5 channels (Manville et al., 2018c). By contrast, Kv7.2 and Kv7.4 were insensitive. Kv7.3 and Kv7.2/3 channels exhibited similar sensitivity showing an EC<sub>50</sub> of 4.2 nM and EC<sub>50</sub> 5.3 nM, respectively, whereas Kv7.5 showed higher potency (EC<sub>50</sub> 1.9 nM) compared to Kv7.3 and Kv7.2/3. Gabapentin activation of Kv7.2/3 or homomeric Kv7.3 channels requires Kv7.3-W265 residue, the conserved tryptophan in segment S5. Pregabalin failed to activate Kv7.2/3 because of the lack of the negative electrostatic surface potential close to carbonyl group (Manville et al., 2018). More recently, gabapentin has been used for the first time as a precision treatment in a DEE-affected child carrying a *de novo* LoF in KCNQ2 (Soldovieri et al, 2020)

Two related endogenous metabolites of GABA, **β-hydroxybutyric acid (BHB)** and **γ-amino-β-hydroxybutyric acid (GABOB)** have been reported to activate Kv7.2/3. BHB, the primary ketone body generated by ketosis, directly activated Kv7.2/3 channels, showing an EC<sub>50</sub> of 0.7 μM, and exhibited an anticonvulsant activity in the PTZ seizure assay in mice. Also, GABOB activated Kv7.2/3 channels with high affinity (EC<sub>50</sub> 0.12 mM) and lower efficacy than GABA or BHB. In addition, GABOB acted as a partial agonist and competed

with GABA, retigabine and BHB for the same binding site. (Manville et al., 2020). Among nonpharmacological therapies, the ketogenic diet (KD) has been shown to be particularly effective in children with DEE caused by KCNQ2 variants (Ko et al., 2018). More recently, Miceli and co-authors have demonstrated that BHB was able to reverse channel dysfunction induced by the Kv7.3-M240R variant identified in a BFNS family (Miceli et al., 2020).

### 1.9.2.7 Traditional medicine

In recent years, several plant compounds have proven effective in activating Kv7 potassium channels. Two components of *M. oppositifolius* leaf extract, **mallotoxin (MTX)** and **isovaleric acid (IVA)** have been reported to be potent activator of Kv7.2 channels, synergistically activate Kv7.2/3 and protect against tonic seizures and associated mortality in PTZ mouse model. MTX and IVA anchor the same binding pocket of retigabine, but mutagenesis results indicate a differential requirement of W236/W265. The presence of these residues was not required for MTX binding, by contrast, was essential for IVA on activating Kv7.2/3. Retigabine might synergize with MTX and/or IVA, converting Kv7.2/3 it into a voltage-independent channel (Manville RW et al., 2018a). The compound **E-2-dodecenal** contained in methanolic cilantro leaf extracts (*Coriandrum sativum*) activated preferentially Kv7.2 and Kv7.5 while lesser effects were produced on Kv7.1 and Kv7.4 and no effect on Kv7.3. Finally, Kv7.2/3 channels were highly sensitive ( $EC_{50}$  of 60 nM). Consistent with docking studies, mutagenesis experiments confirmed that Kv7.2–W236 residue in S5 and Kv7.2–R213 in the S4–S5 were both required for E-2-dodecenal effects in Kv7.2/3 channels (Manville et al., 2019a). Additionally, E-2-dodecenal showed anticonvulsant activity in PTZ model. **Aloperine**, extracted from the *Sophora flavescens* specifically activated Kv7.5 channel with an  $EC_{50}$  of 390 nM and required Kv7.5–R212 residue for both binding and activation. In the vasculature, channels formed by Kv7.5 alone or complex with Kv7.4 are a potential target for blood pressure control medications (Manville et al., 2019b).



### 1.10 Precision medicine in Epilepsy

Thank to advances in the identification of the underlying causes of epilepsies, new scenarios in the therapeutic management of patients were born, no longer based on the treatment of epilepsy types or syndromes, but on a precision approach that ideally should be targeted towards the precise molecular pathogenesis of disease. To date, several are the examples of precision medicine currently established or investigated for the treatment of rare genetic epilepsies.

About 25% of epilepsy-causing genes encode for ligand and voltage-gated ion channels (Oyrer et al., 2018). As reported previously, retigabine has been demonstrated to be effective in patients showing KCNQ2 encephalopathy associated with loss-of-function (LoF) mutations (Millichap JJ et al., 2016), and gabapentin (as a substitute for retigabine) has been proposed as a precision therapy for developmental epileptic encephalopathies (DEEs) caused by KCNQ2 LoF variants. (Soldovieri et al., 2020). Potassium channel modulators have been suggested for the treatment of early-onset epilepsies caused KCNT1/KCNT2 defects; quinidine exhibits an inhibitory effect on KCNT1 potassium channel and functional studies carried out by Dilella et al. 2018 demonstrated that the blocker reverses *in vitro* the dysfunction of KCNT1 GoF mutations found in patients Epilepsy of Infancy with Migrating Focal Seizures (EIMFS). Quinidine treatment has been also proposed as a personalized approach for de novo GoF variants in KCNT2 causing developmental and epileptic encephalopathy (DEE) (Ambrosino et al., 2018). Use of sodium channel blockers has been suggested in patients with early infantile epileptic encephalopathy (EIEE) showing gain-of-function (GoF) mutations in SCN2A (Dilella et al., 2017). Pathogenic GoF variants of GRIN2A, encoding for NMDA receptor subunit 2A, are associated with severe developmental and epileptic encephalopathy; here personalized therapy with NMDAR antagonist memantine have been suggest (Pierson et al., 2014). 4-aminopyridine, a Kv1 channels inhibitor, could be considered a potential treatment strategy for patients carrying

GoF variants in KCNA2 gene, encoding the voltage-gated potassium channel KV1.2, presenting epileptic encephalopathy (Syrbe et al., 2015) or progressive myoclonus epilepsy (PME) (Canafoglia et al., 2019). Finally, considering its ability to act as a blocker of Kv3.1 (Choi et al., 2001) potassium channel, the antidepressant fluoxetine could be proposed for patients carrying KCNC1 GoF mutations, whereas the antidiabetic metformin could be a candidate drug for patients showing Kv2.1 (encoded by KCNB1 gene) mutations causing LoF effects.

Substitutive therapies are proposed to treat epilepsy caused by metabolic disorders; pyridoxin-dependent epilepsy, due to mutations in several genes (e.g ALDH7A1 encoding for the aldehyde dehydrogenase) is characterized by seizures resistant to the conventional anti-epileptic drugs but are responsive to pyridoxine (vitamin B) (Yeghiazaryan et al., 2011; 2012). Ketogenic diet has been suggested for patients carrying mutations in SLC2A1 gene, encoding the glucose transporter GLUT1, showing a deficient glucose transport through the blood-brain barrier. The principle is to provide ketone bodies to the brain as an energy source alternative to glucose (Kass et al., 2016; Daci et al., 2018)

Therapies that modify signalling pathways are indicated to treat epilepsies related to mTOR pathway dysfunction, also known as mTORopathies. Mutations in the GATOR1 complex genes DEPDC5, NPRL2, and NPRL3, which act as a negative regulator of the mechanistic target of rapamycin (mTOR) complex 1 (mTORC1) pathway, are responsible to focal epilepsy with or without focal cortical dysplasia (FCD) (Weckhuysen et al., 2016). While hyperactivation of mTOR signalling, consequent of loss-of-function of genes encoding for tuberous sclerosis complex (TSC) 1 and 2, is linked to cortical malformations and epilepsy (Citraro et al., 2016). In both cases, use of mTOR inhibitors, such as rapamycin and rapamycin derivatives (e.g., everolimus, temsirolimus and ridaforolimus) have been proposed (Vawter-Lee et al., 2019; Franz et al., 2018).

Despite the described efforts, precision therapy approaches in DEEs remain particularly challenging and identification of gene variants responsible for specific epilepsy syndrome as well as the understanding of the pathogenetic mechanisms of specific genomic variants remains crucial.

### 1.11 *In vitro* and *in silico* techniques in drug discovery

Starting a research program to discover a new drug is a big challenge. The identification and subsequent development of new molecules require considerable resources (in both human and economic terms) and time (10–15 years on average).

One of the most important steps in drug discovery process is the identification of a biological target (e.g., an enzyme or a receptor); strong experimental evidence must demonstrate that I) the target plays a crucial role in the pathogenetic mechanism and II) actions taken on it significantly modify the mechanisms of the disease. Once the target has been identified, it is necessary to define the most appropriate assay to be used for the selection of the active compounds. One of the *in vitro* technologies developed in the 1990s that has become very popular in all the laboratories worldwide is the high-throughput screening (HTS), a series of highly automated systems that enable a rapid evaluation of thousands of chemical compounds in biologic assays based on several screening methods. Evaluation of molecule collection using these automated systems increases the chance to find active compounds, the so-called “*hits*” compounds. These represent the basic structures on which pharmaceutical chemists and biologists will focus their efforts with the aim to identify the prototype molecule, the “*lead*” compound.

Consider as biological target the ion channels, HTS methodologies can be divided into non-electrophysiological and electrophysiological techniques. Starting from historical assay, among the non-electrophysiological methods, **Ligand binding assays** was extensively used, in the past, to screen channel modulators. This assay requires previous knowledge of I) target binding sites and II) a radio-labeled ligand. It is useful to determine the affinity of a given compound (without distinguishing between an agonist or an antagonist) but not its ability to alter the functionality of ion channels. Because of its intrinsic limits, ligand binding

assays have been replaced by **Flux-based assay**, even if radiolabelled dofetilide is still today regularly used to investigate potential modulators of Kv11.1 (Finlayson et al., 2001) Flux-based assay has been successfully applied to detect the functional change of ion channel activity. For this purpose, radioactive isotopes like  $^{22}\text{Na}^+$ ,  $^{45}\text{Ca}^{2+}$  and  $^{86}\text{Rb}^+$  have been used to trace the cellular influx or efflux of specific ions, such as  $\text{Na}^+$ ,  $\text{Ca}^{2+}$ , and  $\text{K}^+$  channels, respectively. However, the inconvenience and cost associated with the handling of radioactive materials, radioactive flux-based assay have been substituted by **non radioactive fluorescence-based assay** or considering the radioactive  $\text{Rb}^+$ , this has been replaced by unlabelled  $\text{Rb}^+$  detected by atomic absorption spectroscopy (Wang et al., 2004)

Fluorescence-based methods can measure the membrane-potential dependent- or ion concentration-dependent changes of fluorescence signals by using voltage-sensitive dye or ion-specific fluorescent probes, respectively. Ion-specific fluorescent reporters commonly used are fura-2, fluo-3, fluo-4, for calcium channels, Fluxor and PBFI for potassium and SBFI indicators for sodium. When the concentration of the specific ion increases, a binding event occurs between the dye and the ion, leading to an increase in fluorescence or a change in spectral properties of the dye. On the other hand, fluorescent reports of membrane potential are lipophilic compounds containing a delocalized charge (oxonols) that respond to variation in membrane potential with changes in intramolecular charge distribution or by plasma membrane association/dissociation, which causes a change in their fluorescent emission. To date, these are being overcome by genetically encoded indicators (e.g GECIs) (Wu et al., 2019).

Electrophysiological techniques range from the classical patch-clamp to multielectrode arrays (MEA). Conventional patch-clamp represents the gold standard to directly record ion channel activity but suffers from low throughput and is labor-intensive, requiring highly skilled and trained personnel. To overcome these limits, **Automated electrophysiological**

**assays** have been developed and to date, many automated platforms are commercially available (PatchXpress, IonFlux, Qpatch, Patchliner, IonWorks ecc). Compared to traditional patch, glass pipettes are replaced by a planar substrate characterized by openings where the single cell is placed. This removes the physical technicalities and allows for parallel experimentation. Conversely, MEA is characterized by multi-well plate with multiple electrodes at the bottom of each well, allowing for real-time spontaneous activity measurement from hundreds of neurons simultaneously under normal culture conditions. This device is suitable, for example, to observe the reaction of iPSC-derived neurons to compounds added to the well. Recently, Hirose et al. have reported that using inhibitory and excitatory neurons differentiated from Dravet syndrome iPSCs in MEA, they identified among 13 million drugs, two AED candidate compounds that mitigated deficient electrophysiological activity in inhibitory neurons, the core pathogenic mechanism of Nav1.1 haploinsufficiency Dravet syndrome (Hirose et al., 2020)

Among the *in-silico* techniques, Docking and Molecular Dynamics methods have always played an important role in the drug discovery process; the so-called *Virtual screening*, based on the use of software for the evaluation of the action of a library of compounds on a given target of interest, represents a valid alternative to the traditional techniques of HTS which, even if based on automated assays, remains extremely laborious, expensive in terms of costs and times. Using a virtual screening approach, among a library of 100,000 molecules, Cole et al. identified six compounds that inhibited KCNT1 channel with low- and sub-micromolar potencies (Cole et al., 2020). These techniques are able not only to predict if a molecule interacts but also how the drug will interact with binding site (e.g., which type of interaction occurs between the ligand and the target), thus, helping in the definition of the relationship between chemical-physical properties and the pharmacological activity of the molecule.

In particular, MD solves Newton's equations of motion to derive atomic positions to describe how the system evolves with time. This method is used to simulate the dynamical behavior of the system in real-time, and under real conditions (considering membrane, solvent, and ions etc). During MD simulations, the integration of Newton's second law of motions generates successive configurations of the evolving system, providing trajectories that specify positions and velocities of the particles over time (De Vivo et al., 2016). Through an MD simulation, it is, therefore, possible to know at any moment the position occupied in time by each atom, thus obtaining a sequence of frames that photograph the changes in molecular geometry. The first molecule studied by MD simulations has been the bovine pancreatic trypsin inhibitor (BPTI), a small protein constituted by only 58 residues and the simulation was done for 8.8 ps in vacuum (McCammon et al., 1977). Nowadays the continuously growing computer power, permits simulations of bigger systems ( $10^4$  - $10^6$  atoms) and simulation times of ns or  $\mu$ s.

On the other hand, Molecular docking is a computational science aiming at predicting the optimal binding orientation and conformation of interacting molecules in space. Usually, to estimate the stability of the docked complexes a scoring method is used to assess the quality.

To have a reliable model of the complex ligand-receptor docking techniques are combined with MD simulations. This is because docking suffers from one main drawback: target intrinsic flexibility is either absent or limited thus, conformation of the target is not allowed to change in the binding process. Nowadays, Emil Fischer's rigid lock-and-key binding model has been superseded by the two major drug-binding paradigms the induced-fit, in which the ligand and receptor adapt to each other during the binding process and the conformational selection which assumes that biomolecules can exist in many different conformations. In this

sense, an MD trajectory is used to explore the receptor conformational space and multiple conformations of the receptor can be generated and subsequently subjected to docking.

Moreover, MD can be used as a post docking process tool, allowing to verify if the complex is stable and ligand is correctly docked. Is useful to verify if the interactions established during the docking process are stable and if additional interactions occur during the MD. Finally, running MD after docking is useful to evaluate the interaction of the solvent with the complex and if the solvent molecules affect the stability of the ligand.

The *in silico* techniques requires the knowledge of structural information of biological macromolecules; these are readily available in the Protein Data Bank (PDB). Powerful analysis equipments are nowadays available for the resolution of complex structures such as *X-ray crystallography*, *NMR spectroscopy* and *Cryo-electron microscopy* (cryo-EM), which recently, has become crucial in the high-resolution structures determination of macromolecules. Compared to X-ray crystallography, cryo-EM specimen is made by fast freezing biological samples in liquid nitrogen temperature directly from the solution, therefore maintaining the macromolecules in their soluble states in comparison with a state in the crystal packing constraint. This lends cryo-EM the advantage to reveal structures in more close-to-native state than X-ray crystallography (Wang et a.,2017). When a target structure is not available, the structure can be predicted using the *Homology modelling* technique. This method starts from the premise that two proteins with similar primary sequences will display similar folds (3D structures). The process of homology or comparative modelling of proteins consists of the following steps: I) Identification of known 3D structure(s) of a related protein that can serve as template; to select a template structure for a known protein sequence, A BLAST or FASTA search can be used to find possible candidates. II) Sequence alignment of target and template proteins; this step plays an important role in developing accurate homology models. Thus, it is necessary to evaluate the similarity between the



template sequence and the query sequence. This similarity is called *sequence identity* and is expressed in percentage values. Generally, the minimum sequence identity required to obtain a model of sufficient quality is 30%. III) Model building for the target based on the 3D structure of the template and the alignment. IV) Refining/validation/evaluation of the models (Cavasotto et al.,2009).

## 2 Aim of the work

Retigabine has been the first antiepileptic drug acting on Kv7 potassium channels, that recognizes a hydrophobic pocket in the cytoplasmatic part of S5 and S6; here, an interaction between the carbamate group of retigabine and the tryptophan residue (W236 in Kv7.2, W265 in Kv7.3) present at the intracellular end of the S5 helix, is essential for the action of retigabine (Schenzer et al., 2005; Kim et al., 2015). Even though retigabine has proven to be very effective in the treatment of many epileptic disorders, this molecule also presents some drawback such as: poor selectivity for Kv7 subtypes, short half-life, poor brain penetration and chemical instability.

The poor selectivity of retigabine results in the activation of Kv7.4 and Kv7.5 channels expressed in the genitourinary tract, and, therefore, in urinary retention. Its rapid metabolism is responsible for the very short half-life: for this reason, patients treated with retigabine require a three-times-a-day dosing regimen (Barrese et al., 2010). In addition, the low lipophilicity hampers its ability to cross the blood-brain barrier, thus resulting in a poor brain penetration (Zhou et al., 2015). Finally, retigabine is quite unstable from a chemical point of view: the metabolites generated by light-induced oxidation are responsible for the formation of retinal and mucocutaneous blue-grey discolorations, particularly at the level of lips and nails (Groseclose, and Castellino 2019). For these reasons, in 2017 the GSK manufacturing company has withdrawn the drug from the market, making it necessary the identification of novel  $I_{KM}$  modulators.

According to these premises, the aim of this work was to develop, in collaboration with the Department of Pharmacy of the University of Salerno, a library of retigabine derivatives, based on rational drug modeling, which may overcome some of the above-mentioned limitations of the reference compound. The derivatives synthesized show one or more of the following features: I) modification on the fluorophenyl moiety to increase the potency, II) substitutions on the aniline group to increase light stability and to reduce dimerization, and III) introduction

of longer chains at the methoxy group to investigate the effect of the exploration of the deep part of the hydrophobic retigabine binding site. To facilitate screening of newly synthesized derivatives, I have generated stable cell lines expressing Kv7.2/3, Kv7.4 and, Kv7.3A315T channels and used these, in a fluorescence-based assay the so called FluxOR Green Potassium Ion Channel. By means of the FluxOR assay, I have evaluated the effect of known Kv7 activator and inhibitor to assess the sensibility and the feasibility of the assay on Kv7.2/3 channels and then, I used this to evaluate the effect of 41 retigabine derivatives. In addition, we have compared the fluorescence results with electrophysiological data.

Moreover, in the present Industrial Doctoral Project, I performed molecular modelling studies concerning the binding mode of retigabine, to refine the ligand-binding site and provide a structural basis for drug optimization and design. Starting from a homology Kv7.2 structure model previously obtained, I realized such studies by combining two computational techniques such as Docking and Molecular Dynamic simulations. In agreement with my Ph.D program, computational studies were carried out at the Computational and Medicinal Chemistry Laboratory of the Angelini S.p.A, located in S.Palomba-Pomezia (Rome).

In the present work, we were able to identify new promising Kv7 channel modulators, that appear to be more potent and chemically stable. Furthermore, an additional interaction site was identified, helping to further refinement the retigabine binding site in Kv7.2/Kv7.3.

### 3. Materials and methods

#### 3.1 Site-Directed Mutagenesis

Each mutation was engineered by using the Quick-change Site-Directed Mutagenesis (Agilent Technologies). The mutations were insert in each plasmid by Polymerase Chain Reaction (PCR), using a pair of primers (forward and reverse) (Table 8), incorporating the nucleotide mutation of interest.

**Table 8. Mutations engineered in the Kv7-templates vector and nucleotide sequences of primers used for PCR.**

<b>Mutation</b>	<b>Primers</b>
<b>Kv7.2-NheI</b>	F 5'- GGGAGACCCAAGCTAGCTTGTTTC -3' R 5'-GAACAAGCTAGCTTGGGTCTCCC-3'
<b>Kv7.3-XhoI</b>	F 5'- ATGGATCCGCGGCCTCGAGGATCTGCGATCG -3' R 5'- CGATCGCAGATCCTCGAGGCCGCGGATCCAT -3'
<b>Kv7.4-NotI</b>	F 5'- GCATTAAGCGCGGCCGCTGTGGTGGTTACGC -3' R 5'- GCGTAACCACCACAGCGGCCGCGCTTAATGC -3'
<b>Kv7.4-NotI/NheI</b>	F 5'- CTATAGGGAGACCCAAGCTAGCTTGTTCTTTTGCA -3' R 5'- TGCAAAAAGAACAAGCTAGCTTGGGTCTCCCTATAG -3'
<b>Kv7.2-S303A</b>	F 5'- CAGCGCGAAGAAGGCGACACCGATGAGGG -3' R 5'- CCCTCATCGGTGTCGCCTTCTTCGCGCTG -3'

The amplification reaction was performed in a final volume of 50 µL containing the following components: 50 ng of plasmid, 125 ng primer forward, 125 ng primer reverse, 5% DMSO, 2.5U Pfu DNA Polymerase, 1X buffer Pfu, 1 µl dNTP mix. The PCR consisted of 18 cycles, with each cycle consisting of three temperature steps, that allow the denaturation of the DNA Double Helix (95°C for 30''), the annealing of the primers to the single strand of DNA (55°C for 1') and the extension of the primers (68°C for 10'). After the amplification reaction, the

volume of the reaction contained both methylated (parental) and unmethylated (neo-synthesized) DNA. Therefore, to remove the parental DNA, enzymatic digestion was performed with 1  $\mu$ l DpnI enzyme (10 U/  $\mu$ l) able to digest only methylated DNA. Afterwards, the *DpnI*-treated and untreated samples were analyzed by agarose gel electrophoresis to confirm the presence of the mutated vector.

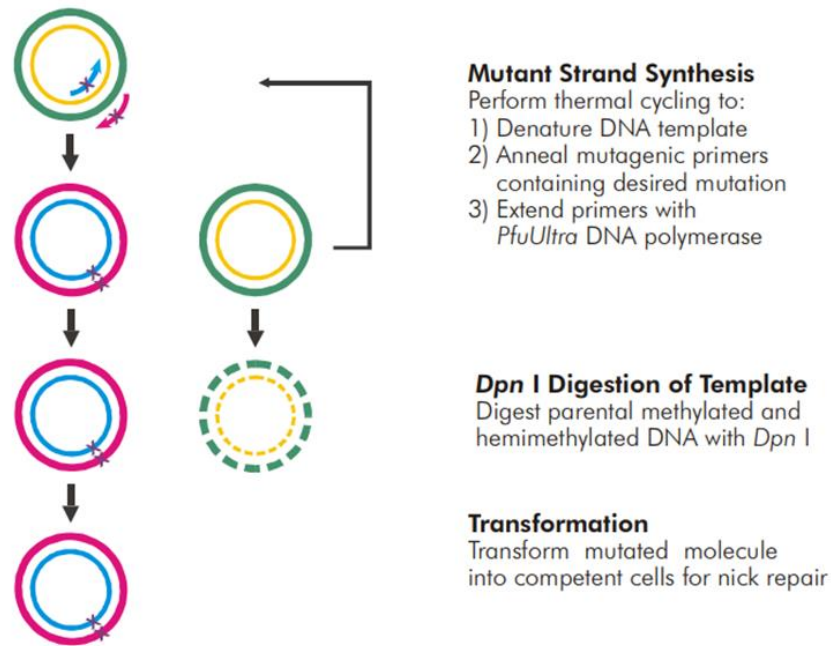


**Figure 13. Overview of the QuikChange II site-directed mutagenesis method.**

### 3.2 Bacterial transformation and plasmidic DNA preparation

Subsequently, the *DpnI*-treated sample was transformed into 100  $\mu$ l of competent *E. coli* DH5 $\alpha$  cells according to the heat-shock transformation protocol (30' at 4°C, heat shock step at 42°C for 45'' followed by 3' at 4°C), resuspended in 200  $\mu$ l SOC medium (2% tryptone, 0.5% yeast extract, 10 mM NaCl, 2.5 mM KCl, 10 mM MgCl<sub>2</sub>, 10 mM MgSO<sub>4</sub>, 20 mM glucose) and then incubated at 37°C for 45'. Afterwards, the transformed product was plated on Ampicillin-containing (50  $\mu$ m/ml) LB-Agar plates (10 g/L tryptone, 5 g/L yeast extract, 5

g/L di NaCl, agar 15 g/L) and incubated upside down at 37°C overnight. Single colonies were inoculated in 5ml of LB medium containing ampicillin (50 µg/ml) and incubated at 37°C/220 rpm overnight. DNA plasmid was extracted from bacteria cultures by using a commercially available kit (*QIAprep Spin Miniprep*, QIAGEN). Positive vectors were identified by using enzymatic digestion followed by DNA sequencing (Eurofins Genomics, Italy). To obtain DNA in large amount, one of the positive clones was amplified on a large scale and plasmidic DNA was extracted by using a commercially available kit (*Plasmid Plus Maxi*, QIAGEN). The cDNA was sequenced again, to confirm the presence of the mutation of interest and to exclude additional mutations in the entire coding sequence.

### **3.3 Cell cultures**

Chinese Hamster Ovary (CHO) cells were grown in plastic Petri dishes (100 mm, 60 mm, or 40 mm, according to the different experimental needs) in DMEM (*Dulbecco's Minimum Eagle Medium*) supplemented with 10% Fetal Bovine Serum, 1% L-glutamine (2 mM in 0.85% NaCl), 1% penicillin (50 U/mL) and 1% streptomycin (50 µg/mL) in a humidified atmosphere at 37°C with 5% CO<sub>2</sub>. Every time cells became confluent within the dishes (about every 2 days), they were split by using 1% trypsin solution and collected in novel dishes with a 1:3 dilution.

### **3.4 Generation of stable cell lines**

#### **3.4.1 PiggyBac (PB) Transposon system**

SBI's PiggyBac Transposon System consists of a PiggyBac Vector and the Super PiggyBac Transposase; the PB-CMV-MCS-EF1α-RedPuro PiggyBac cDNA Cloning and Expression Vector (Cat# PB514B-1 is characterized by the CMV promoter and the site of multiple cloning (MCS) in which, using appropriate enzymes, allows the insertion of the gene of interest. Downstream the EF1α promoter, two selection markers are expressed: an RFP reporter and the gene encoding the Puromycin N-acetyltransferase. Inverted terminal repeat

sequences (ITRs) are located on both ends of the cassette of gene expression that are recognized by the transposase, encoded by the Super PiggyBac Transposase, which efficiently integrates the ITRs and intervening DNA into the genome at TTAA sites. The Super PiggyBac Transposase is delivered to the cell via the Super PiggyBac Transposase Expression Vector, which is co-transfected with one or more PiggyBac Vectors (Figure 14-15)

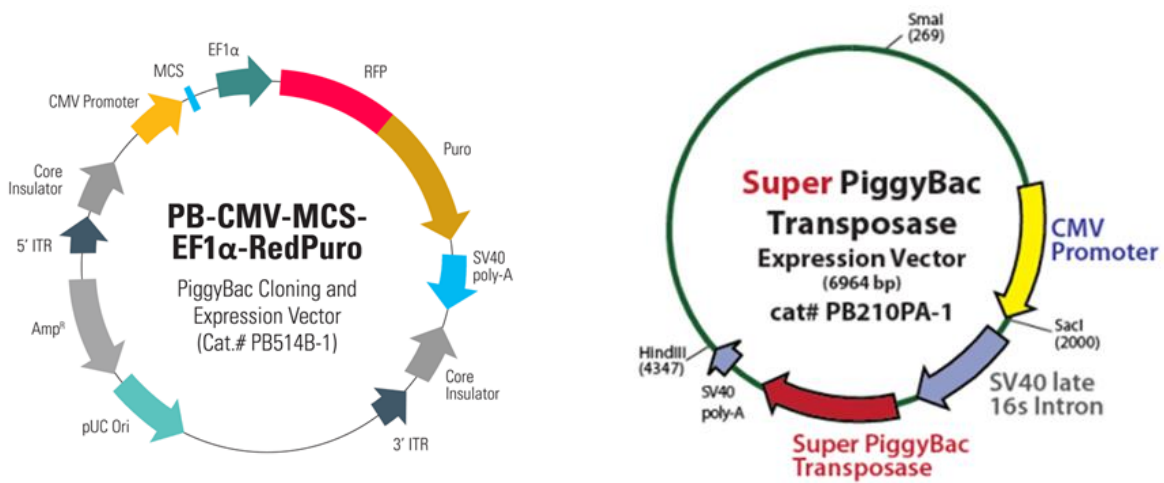
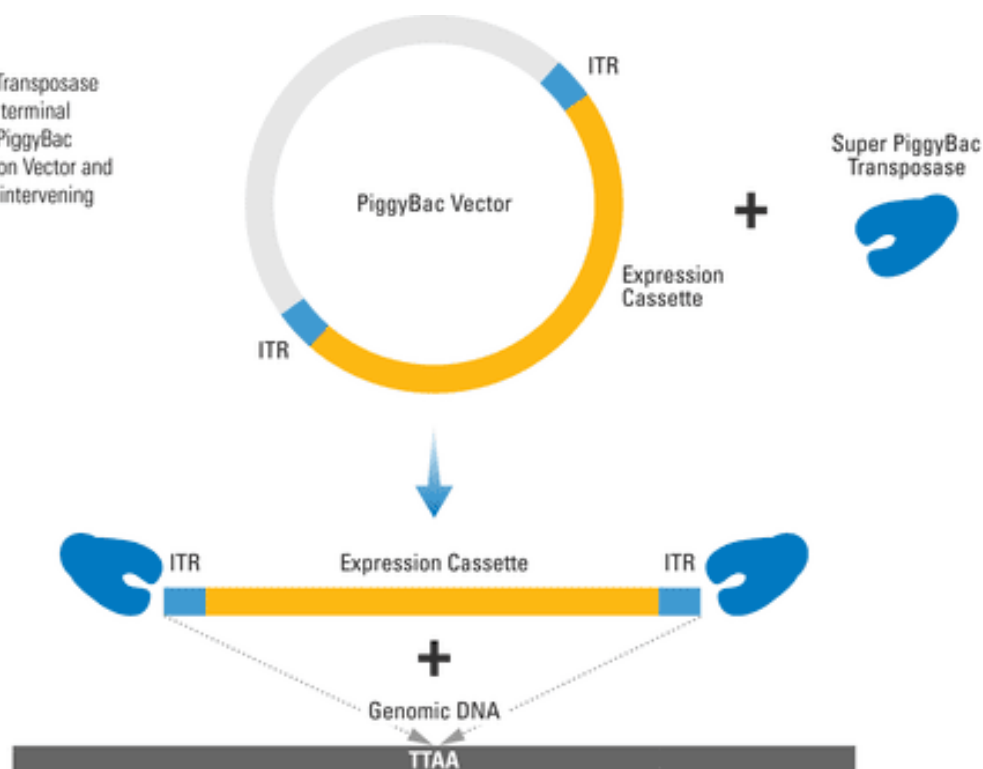


**Figure 14. Structure of the PB-CMV-MCS-EF1α-RedPuro PiggyBac Vector and the Super PiggyBac Transposase**

### Step 1

The Super PiggyBac Transposase binds to the inverted terminal repeats (ITRs) in the PiggyBac Cloning and Expression Vector and excises the ITRs and intervening DNA.



### Step 2

The Super PiggyBac Transposase inserts the ITR-Expression Cassette-ITR segment into the genome at TTAA sites.



**Figure 15 The PiggyBac Transposon System's cut-and-paste mechanism.**

### 3.4.2 Generation of PB-RedPuro- Kv7.2

The pcDNA3-KCNQ2-NheI vector was subcloned into the pB-CMV-MCS-EF1-RedPuro obtained from System Biosciences, LLC (Palo Alto, USA). Each vector was digested with 1U of NheI restriction enzyme and incubated at 37°C for 1h. Subsequently, the enzyme was inactivated incubating the mix at 65°C for 20' and then incubated with 1U of EcoRI enzyme for 1h. After the double digestion, in order to remove phosphate groups and prevent a possible closure, the pB-CMV-MCS-EF1-RedPuro vector was treated with 1U of CIP (Calf Intestinal Phosphatase) at 37°C for 1h. Subsequently, pcDNA3-KCNQ2-NheI and the pB-CMV-MCS-EF1-RedPuro vectors were analyzed by Agarose gel electrophoresis. The band



corresponding to the KCNQ2 cDNA and the band corresponding to the pB-CMV-MCS-EF1-RedPuro backbone were extracted from the gel using the GEL EXTRACTION KIT according to the manufacturer protocol.

Finally, 8µL of KCNQ2 fragment was inserted by ligation into 4µl of pB-CMV-MCS-EF1-RedPuro using 1U of T4 Ligase and incubated at 16°C overnight to obtain the final PB-RedPuro- Kv7.2 vector. The ligation product was transformed into One Shot® TOP10 Chemically Competent E. coli from Invitrogen and the right-ligated vector was selected as previously mentioned. All the sequences were validated by DNA sequencing.

### **3.4.3 Generation of PB-RedPuro- Kv7.3**

The pcDNA<sub>3</sub>-KCNQ3-XhoI vector was subcloned into the pB-CMV-MCS-EF1-RedPuro obtained from System Biosciences, LLC (Palo Alto, USA). Each vector was digested with 1U of NheI restriction enzyme and incubated at 37°C for 1h. Subsequently, the enzyme was inactivated incubating the mix at 65°C for 20' and then incubated with 1U of BamHI enzyme for 1h. After the double digestion, in order to remove phosphate groups and prevent a possible closure, the pB-CMV-MCS-EF1-RedPuro vector was treated with 1U of CIP (Calf Intestinal Phosphatase) at 37°C for 1h. Subsequently the pcDNA<sub>3</sub>-KCNQ3-XhoI and the pB-CMV-MCS-EF1-RedPuro vectors were analyzed by Agarose gel electrophoresis. The band corresponding to the KCNQ2 cDNA and the band corresponding to the pB-CMV-MCS-EF1-RedPuro backbone were extracted from the gel using the GEL EXTRACTION KIT according to the manufacturer protocol.

Finally, 6 µl of KCNQ3 fragment was inserted by ligation into 4 µl pB-CMV-MCS-EF1-RedPuro using 1U of T4 Ligase and incubated at 16°C overnight to obtain the final PB-RedPuro- Kv7.3 vector. The ligation product was transformed into One Shot® TOP10

Chemically Competent *E. coli* from Invitrogen and the right-ligated vector was selected as previously mentioned. All the sequences were validated by DNA sequencing.

### **3.4.3 Generation of PB-RedPuro- Kv7.3 A315T**

The pcDNA3-KCNQ3 A315T vector was subcloned into the PB-RedPuro-Kv7.3 vector, previously obtained. Each vector was digested with 1U of KpnI restriction enzyme and incubated at 37°C for 1h. The pcDNA3-KCNQ3 A315T and the pB-RFPpuro- Kv7.3 vector were analyzed by Agarose gel electrophoresis and the band corresponding to the KCNQ3 A315TcDNA and the band corresponding to the pB-RFPpuro- Kv7.3 vector were extracted from the gel using the GEL EXTRACTION KIT according to the manufacturer protocol. Subsequently, each extract product was digested with 1U of NotI restriction enzyme and incubated at 37°C for 1h. The pcDNA3-KCNQ3 A315T and the pB-RFPpuro- Kv7.3 vector were analyzed by Agarose gel electrophoresis. The band corresponding to the pcDNA3-KCNQ3 A315T and the band corresponding to the pB-CMV-MCS-EF1-RedPuro backbone were extracted from the gel using the GEL EXTRACTION KIT according to the manufacturer protocol.

Finally, 5 µl of KCNQ3 A315T fragment was inserted by ligation into 4 µl pB-CMV-MCS-EF1-RedPuro using 1U of T4 Ligase and incubated at 16°C overnight to obtain the final PB-RedPuro- Kv7.4 vector. The ligation product was transformed into One Shot® TOP10 Chemically Competent *E. coli* from Invitrogen and the right-ligated vector was selected as previously mentioned. All the sequences were validated by DNA sequencing.

### 3.4.3 Generation of PB-RedPuro- Kv7.4

The pcDNA<sub>3</sub>-KCNQ4-NotI-NheI vector was subcloned into the pB-CMV-MCS-EF1-RedPuro obtained from System Biosciences, LLC (Palo Alto, USA). Each vector was digested with 1U of NheI restriction enzyme and incubated at 37°C for 1h. Subsequently, the enzyme was inactivated incubating the mix at 65°C for 20' and then incubated with 1U of NotI enzyme for 1h. After the double digestion, in order to remove phosphate groups and prevent a possible closure, the pB-CMV-MCS-EF1-RedPuro vector was treated with 1U of CIP (Calf Intestinal Phosphatase) at 37°C for 1h. Subsequently the pcDNA<sub>3</sub>-KCNQ4-NotI-NheI and the pB-CMV-MCS-EF1-RedPuro vectors were analyzed by Agarose gel electrophoresis. The band corresponding to the KCNQ2 cDNA and the band corresponding to the pB-CMV-MCS-EF1-RedPuro backbone were extracted from the gel using the GEL EXTRACTION KIT according to the manufacturer protocol.

Finally, 6 µl of KCNQ4 fragment was inserted by ligation into 3 µl pB-CMV-MCS-EF1-RedPuro using 1U of T4 Ligase and incubated at 16°C overnight to obtain the final PB-RedPuro- Kv7.4 vector. The ligation product was transformed into One Shot® TOP10 Chemically Competent E. coli from Invitrogen and the right-ligated vector was selected as previously mentioned. All the sequences were validated by DNA sequencing.

### 3.5 Cell cultures and stable transfection with Lipofectamine

Chinese hamster ovary (CHO) cell line was used to create the stably transfected cell line expressing the pB-RedPuro-Kv7 vector. CHO cells were plated into 60mm cell plate and transfected at a confluence of 80%. The transfection mix containing 3 µg of pB-RedPuro-Kv7 vector, 1 µg of Super PiggyBac Transposase Expression Vector (System Biosciences, Palo Alto, USA), 20 µl of Lipofectamine (ThermoFisher, Italy) and 500 µl of DMEM (*Dulbecco's Minimum Eagle Medium*) was incubated for 15 minutes according to the manufacturer protocol. The mix was added to the CHO cell plate and incubated at 37°C for 24h. The

conditioned medium was replaced with fresh growing medium treated with 4ug/ul of Puromycin. After 7 days only the cells that had correctly internalized the expression vector and expressed the antibiotic resistance was detectable in the cell plate. Subsequently, for 3 to 8 small cell aggregates were isolated and amplified separately to obtain different stably transfected clones.

### **3.6 Whole-cell electrophysiology**

#### **3.6.1 CHO cells preparation and electrophysiology**

For electrophysiological experiments, CHO cells were seeded on glass coverslips, heat-sterilized and pre-coated with poly L-lysine, in 35 mm dishes. After 24h, CHO cells were transfected using Lipofectamine 2000, according to the manufacturer protocol (ThermoFisher, Italy). In each transfection mixture, a plasmid encoding for an Enhanced Green Fluorescent Protein (pEGFP; *Clontech*, Palo Alto, CA) was used as transfection marker (3 µg of plasmids encoding for Kv7 cDNA + 1 µg di pEGFP).

Macroscopic currents were recorded, after 1 day, using patch-clamp technique in the whole-cell configuration with glass micropipettes of 3–5 MΩ resistance. No compensation was performed for pipette resistance and cell capacitance. During patch clamp recordings, cells were perfused with an extracellular solution containing (in mM): 138 NaCl, 5.4 KCl, 2 CaCl<sub>2</sub>, 1 MgCl<sub>2</sub>, 10 glucose, 10 HEPES, pH 7.4 (adjusted with NaOH). The pipettes used for recordings were filled with an intracellular solution containing (in mM): 140 KCl, 2 MgCl<sub>2</sub>, 10 EGTA, 10 HEPES, 5 Mg-ATP, pH 7.4 (adjusted with KOH). Current was recorded using an Axopatch-200A amplifier, filtered at 5 kHz, and digitized using a DigiData 1440A (Molecular Devices). The pCLAMP software (version 10.2) was used for data acquisition and analysis (Molecular Devices).

To generate conductance/voltage curves, cells were held at -80 mV, then depolarized for 1.5 s from -80 mV to +20 mV in 10 mV increments, followed by an isopotential pulse at 0

mV (Figure 16). Current values recorded at the beginning of the 0mV pulse were measured, normalized, and expressed as a function of the preceding voltage. The data obtained were then fit to a Boltzmann distribution of the following form:

$$y = \text{max} / [1 + \exp (V_{1/2} - V)/k]$$

where  $V$  is the test potential,  $V_{1/2}$  indicate the half-activation potential, and  $k$  the slope factor (Figure 16). Current densities (expressed in picoamperes per picofarad, pA/pF) were calculated as peak  $K^+$  currents (pA) measured at 0 mV divided by the capacitance of the same cell (expressed in pF) (Figure 16).

To evaluate the effects of drugs on Kv7, cells were clamped at - 80 mV and currents were elicited by 3-s voltage ramps from -80 mV to +20 mV in the presence and absence of each compound.

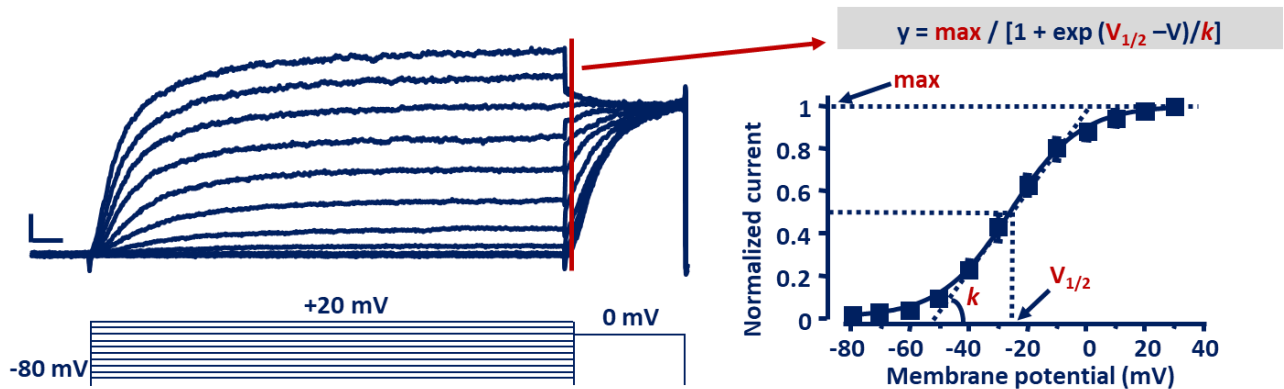


**Figure 16. Whole-cell configuration of patch-clamp technique.** On the left, representative trace obtained by application the voltage protocol in the bottom. On the right, conductance/voltage curve obtained fitting to a Boltzman distribution the data.

### 3.7 FluxOR™ II Green Potassium Ion Channel Assay

Screening of retigabine derivatives have been performed on stable CHO cell lines co-expressing Kv7 channel subunits of interest by using a fluorescence based (FluxOR Green Potassium Ion Channel Assay). Briefly, the assay is based on the uses of Thallium ( $Tl^+$ ) as a surrogate for  $K^+$  ions and a fluorescent  $Tl^+$ -sensitive dye called FluxOR™. The dye is loaded into cells as a membrane-permeable aminomethyl (AM) ester and its permeation is facilitated by the presence of the surfactant PowerLoad™. Once in the cytosol, AM ester dye is cleaved by endogenous esterase to obtain fluorogenic thallium-sensitive form and its cell extrusion is inhibited by the presence of probenecid, a blocker of the organic anion transporter. During the assay, a small amount of thallium is added to the cells with a stimulus to open channels. Thallium then passes into cells through open potassium channels according to a strong inward driving force. Upon binding cytosolic thallium, the de-esterified FluxOR™ dye exhibits a strong increase in fluorescence intensity at its peak emission of 525 nm (Figure 17A)

Chinese hamster ovary (CHO) cells that stably expressed KCNQ channels were resuspended to  $2 \times 10^5$  cells/ mL in complete growth medium, and 80  $\mu$ L/well were plated into a Biocoat Poly-D-Lysine Celldware 96-well plates (Corning,USA) and incubated overnight at 37 °C in a 5% CO<sub>2</sub> incubator. The next day, after manual removal of the medium, 80  $\mu$ L of 1X Loading Buffer (PowerLoad™ Concentrate 100X 100 $\mu$ L/10ml, FluxOR™ II Reagent 10  $\mu$ L/ 10ml, deionized water 8.8 mL/10ml, FluxOR™ II Assay Buffer, 10X 1 mL/10ml and probenecid 100 $\mu$ L/10ml) were added into the cell plate, and then incubated in the dark at room temperature for 60 minutes. Subsequently the Loading Buffer was removed and replaced with 70  $\mu$ L/well of Assay Buffer (Deionized water 8.9mL/10mL, FluxOR™ II Assay Buffer 10X 1 mL/10mL, Probenecid 100  $\mu$ L/10mL). Additionally, 10 $\mu$ L/well of the test compounds were added into the plate. Cell plates were loaded onto an FLUOstar OPTIMA microplate reader (BMG LABTECH). FITC green filters were used ( excitation wavelength

485 nm and emission wavelength 520 nm) After 5 seconds of recording, 20  $\mu\text{L}$ /well of stimulus buffer (Chloride-free Stimulus Buffer 2 mL/10mL, thallium Sulfate ( $\text{Ti}_2\text{SO}_4$ ) 1 mL/10mL, deionized water 7 mL/10mL) were added and each well was read every second for 50 seconds. The OPTIMA data Analytics software was used for data acquisition.

To evaluate drugs effects of retigabine derivatives, two different parameters were calculated; the ratio between the maximal fluorescent signal and the fluorescent signal at time 0 ( $F_{\text{max}}/F_0$ ) and the slope of the fluorescent curve calculated between 5" and 15" (Figure 17B)

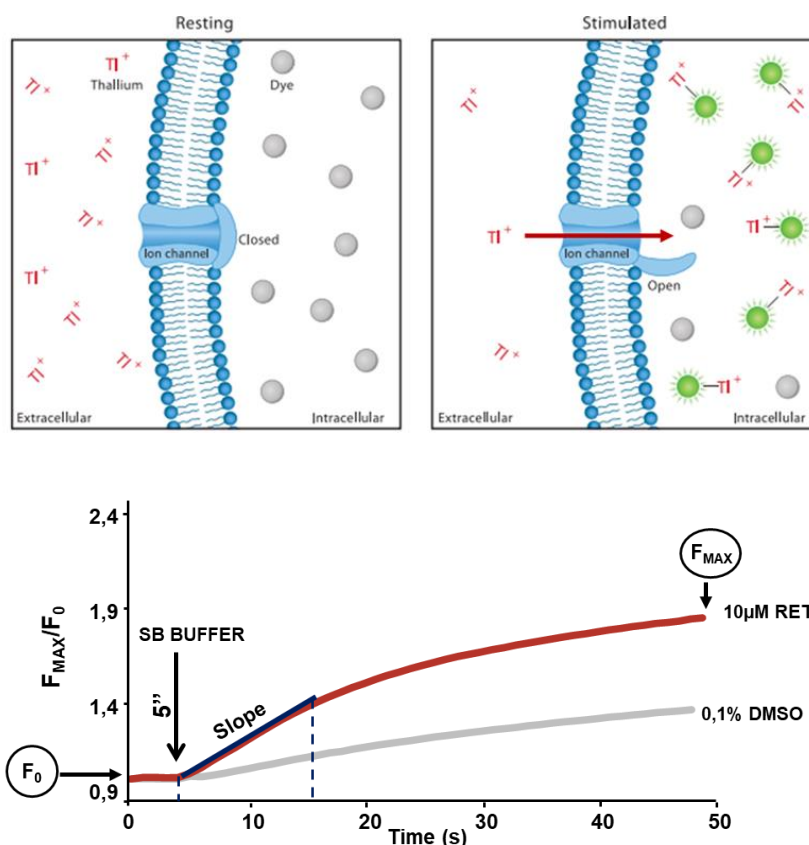


**Figure 17. The FluxOR™ assay.** A) Low basal fluorescence from cells loaded with FluxOR™ dye until potassium channels stimulation (left panel). Subsequently the addition of the stimulus, thallium flows down its concentration gradient into the cells, activating the dye (right panel). B) Representative fluorescent curve recoded on Kv7.2/Kv7.3 in presence of 10 $\mu\text{M}$  RET (activator) and 1% DMSO (vehicle).

The normalized slope values were plotted versus log(concentration) of the compound, fitted to a four-parameter logistic equation, and EC<sub>50</sub> values were calculated with SigmaPlot (version 12.3). Indicated EC<sub>50</sub> values are the mean of at least three independent experiments ± standard deviation (SD).

Assay quality is typically determined according to the Z' factor. The Z factor has a range of 0 to 1; an assay with a Z factor of greater than 0.5 is considered appropriately robust for compound screening (Zhang et al., 1999).

$$Z'=1-3\times\frac{(SD\ VEHICLE+SD\ CONTROL)}{|(MEAN\ OF\ VEHICLE-MEAN\ OF\ CONTROL)|}$$

### 3.8 Photochemical Stability Assay

Compounds were dissolved in DMSO and then diluted in buffered aqueous solutions at pH 7.4 to a final concentration of 10 µM. 1cm quartz cells, filled with the above-mentioned solutions were irradiated by an UV lamp (UV Consulting TQ 150 equipped with duran 50 sleeve and 150W power supply unit, Peschl, Germany) at a fixed distance of 20 cm from the UV source. Control samples were maintained at 37°C and wrapped by aluminium foils to avoid light exposure. At predetermined intervals aliquots were withdrawn and analysed by HPLC in order to assess the concentration decrease of the starting materials and the presence of the dimers usually formed by retigabine. UHPLC analyses were performed on a Nexera UHPLC system (Shimadzu, Kyoto, Japan) consisting of a CBM-20A controller, two LC-30AD pumps, a DGU-20 A5R degasser, an SPD-M20A photo diode array detector, a CTO-20AC column oven, a SIL-30AC autosampler.

The separation was carried out on a Kinetex<sup>TM</sup> C18 150 × 2.1 mm × 2.6 µm (100 Å) column (Phenomenex, Bologna, Italy). The optimal mobile phase consisted of 0.1% TFA/H<sub>2</sub>O v/v (A) and 0.1% TFA/ACN v/v (B). Analysis was performed in gradient elution as follows: 0–



13.0 min, 5–65% B; 13–14.0 min, 65–95% B; 14–15.0 min, isocratic to 95% B; 15–15.01 min, 95–5% B; then three minutes for column re-equilibration. Flow rate was 0.5 mL min<sup>-1</sup>. Column oven temperature was set to 45°C. Injection volume was 7 µL of sample. The following PDA parameters were applied: sampling rate, 12.5 Hz; detector time constant, 0.160 s; cell temperature, 40°C. Data acquisition was set in the range 190–800 nm and chromatograms were monitored at 224 nm to assess the decrease in concentration of the starting material, while a wavelength of 550 nm was used to eventually detect dimerization.

### **3.9 Homology model**

Three-dimensional models of Kv7.2 subunits were generated by homology modelling by using SWISS-MODEL. A chimeric channel in which the voltage-sensor paddle (corresponding to the S3b–S4 region) of Kv2.1 was transferred into the Kv1.2 subunit was used as a template (PDB ID code 2R9RH). The model was optimized through all-atom energy minimization process by using the GROMOS96 implementation of Swiss-PDBViewer and analyzed by using both the DeepView module of Swiss-PDBViewer (version 4.0.1; <http://spdbv.vital-it.ch/>) and PyMOL (<http://www.pymol.org/>) (Miceli et al 2013).

### **3.10 Protein preparation**

The homology models were amended using the Protein Preparation Wizard Schrodinger tool characterized by three different sections: 1) Import and Process, in which the protein structure is uploaded and basic preparation tasks are performed, such as assignment of bond orders, addition of hydrogen atoms, refinement of side chains and loops, etc; 2) Review and Modify, that allows to select chains and waters of interest, and fix or delete unconventional groups; 3) Refine, in which orientations of hydrogen-bonded groups are optimized and the structure is minimized.

In this study, the Kv7.2 potassium channel was prepared using the Schrodinger Protein Preparation Wizard default settings. H-bonds were optimized using the hydrogen bonds assignment tool, water molecules were removed and then, the whole protein structure could relax and minimize by applying OPLS3e force field with an in-built constraint of RMSD (Root mean square deviation) = 0.3 Å.

### **3.11 Molecular docking**

#### **3.11.1 Ligand preparation**

In addition to the protein structures, also ligands must be pre-processed for molecular modeling experiments. Here, the ligand retigabine was converted from 2D to 3D structure and prepared with Schrödinger's LigPrep tool. LigPrep, through Epik Schrödinger package (J.C. Shelley et al 2007), generates ionization and tautomeric states for the ligand; for the aim of this study, possible states were generated at a pH of  $7 \pm 2$ . A conformational search was performed using ConfGen (K.S. Watts et al 2010), generating ten different conformations which represented the input for the subsequent docking studies.

#### **3.11.2 Glide**

Docking calculations were performed using the commercial package Schrödinger's Glide (Friesner RA et al 2004). Retigabine has been docked into all four active sites and evaluated by the Standard Precision (SP) scoring function. For each chain, a grid around the active site was generated considering the binding pocket of known ligands. In detail, a 20 Å docking box was set to cover the assumed binding pocket and centred at Trp236, Leu299, Leu 275 and Leu243 residues. For each retigabine binding site, six different docking conditions were applied (Table 9). In particular, we considered: 1) the scaling of atomic van der Waals radii of both protein and ligand, 2) a constraint imposing the formation of a hydrogen bond between Trp236 and retigabine, 3) the number of retigabine poses stored in the output. As for condition 1, we tested different scale factors in ligand docking for both ligand and protein,

as reported in Table 1. Van der Waals scale factors smaller than 1.0 make the protein site “roomier” by “moving back” the surface of non-polar regions of the protein and/or ligand.

**Table 9. Docking conditions applied for each retigabine binding site.**

vdW scaling		Constraint	N° Poses
Protein	Ligand	H-bond W236	
1	0,8	No	1
0,9	0,8	No	1
0,8	0,8	No	1
0,8	0,7	No	10
0,8	0,7	No	10
0,8	0,7	Yes	10

Schrödinger’s proprietary GlideScore multi-ligand scoring function is used to score the poses.

$$G_{\text{Score}} = 0.05 \cdot \text{vdW} + 0.15 \cdot \text{Coul} + \text{Lipo} + \text{Hbond} + \text{Metal} + \text{Rewards} + \text{RotB} + \text{Site (Table 10)}$$

**Table 10. GlideScore components.**

<b>Component</b>	<b>Description</b>
vdW	Van der Waals energy. This term is calculated with reduced net ionic charges on groups with formal charges, such as metals, carboxylates, and guanidiniums.
Coul	Coulomb energy. This term is calculated with reduced net ionic charges on groups with formal charges, such as metals, carboxylates, and guanidiniums.
Lipo	Lipophilic term, which is a pairwise term in SP but is derived from the hydrophobic grid potential for XP. Rewards favorable hydrophobic interactions.
HBond	Hydrogen-bonding term. This term is separated into differently weighted components that depend on whether the donor and acceptor are neutral, one is neutral and the other is charged, or both are charged.
Metal	Metal-binding term. Only the interactions with anionic or highly polar acceptor atoms are included. If the net metal charge in the apo protein is positive, the preference for anionic or polar ligands is included; if the net charge is zero, the preference is suppressed.
Rewards	Rewards and penalties for various features, such as buried polar groups, hydrophobic enclosure, correlated hydrogen bonds, amide twists, and so on. This category covers all terms other than those explicitly mentioned.
RotB	Penalty for freezing rotatable bonds.
Site	Polar interactions in the active site. Polar but non-hydrogen-bonding atoms in a hydrophobic region are rewarded.

### **3.11.3 InducedFit**

Induced-fit docking was performed using the program InducedFit as implemented in the Schrodinger Suite, using the prepared Kv7.2 potassium channel structure and a 20 Å grid centred on residues Trp236, Leu299, Leu 275 and Leu243. In this calculation, we applied the extended sampling protocol. Briefly, induced-fit docking included four steps:

1) the initial docking with Glide to generate an ensemble of a maximum of 20 poses. In order to eliminate or at least significantly reduce steric clashes, the vander Waals radii of ligand and receptor atoms were scaled by 50%, and residues predicted to be highly flexible were temporarily replaced with alanine. 2) The resulting 20 poses were used as a basis for protein structure prediction via Prime program. Residues previously replaced with alanine were

restored to their original type, followed by side-chain prediction and minimization. Only residues having at least one atom within 5 Å of any of the 20 ligand poses were sampled.

3) The ligand was redocked into induced-fit structures within 30 kcal/mol of the best structure.

4) The binding energy for each output pose was estimated as Glide Score.

### **3.12 Molecular Dynamics Simulations**

Molecular dynamics (MD) simulations were performed using the commercial package Schrödinger's Desmond. The simulated environments were built using the Desmond system builder utility; the proteins were inserted into 1-palmitoyl-2-oleoyl phosphatidylcholine (POPC) bilayer, based on the coordinates of the Kv1.2 structure (PDB 2a79) from the Orientations of Proteins in Membranes (OPM) database (Lomize MA et al 2006). Simple point charge water (SPC) model was used for solvating the system in an orthorhombic box (13 Å × 13 Å × 13 Å). To balance the net charge, Na<sup>+</sup> and Cl<sup>-</sup> ions were added to a final concentration of 0.15 M. In the protocols, different conditions were tested depending on the application of the Grand-canonical Monte Carlo algorithm (GCMC) and the Surface Tension 4000 bar·Å. Protein/membrane systems were submitted to minimization and short MD simulations with the aim to relax the system before performing the production steps using the default equilibration settings. Finally, MD simulations were carried out at a temperature of 300 °K and pressure of 1.01325 bar in the NP<sub>γ</sub>T ensemble using a Nose-Hoover chain thermostat and a Martyna-Tobias-Klein barostat.

Apo protein MD simulations were run for 1.2, 10 and 100 ns and the trajectory recording interval was set at 4.8 ,10 , and 20 ps respectively. Trajectory analyses were performed using the Desmond simulation event analysis tool and VMD version 1.9.4a37. Docking poses were also studied via Molecular Dynamics using the best conditions from simulations of the apoprotein.

In the simulations analyses four parameters were considered the protein and ligand RMSD and the protein and ligand RMSF.

**The Root Mean Square Deviation (RMSD)** is used to measure the average change in displacement of a selection of atoms for a particular frame with respect to a reference frame. It is calculated for all frames in the trajectory. The RMSD for frame x is:

$$RMSD_x = \sqrt{\frac{1}{N} \sum_{i=1}^N (r'_i(t_x) - r_i(t_{ref}))^2}$$

where N is the number of atoms in the atom selection; t ref is the reference time, (typically the first frame is used as the reference and it is regarded as time t=0); and r' is the position of the selected atoms in frame x after superimposing on the reference frame, where frame x is recorded at time t x . The procedure is repeated for every frame in the simulation trajectory.

**Protein RMSD** All protein frames are first aligned on the reference frame backbone, and then the RMSD is calculated based on the atom selection. Monitoring the RMSD of the protein can give insights into its structural conformation throughout the simulation. RMSD analysis can indicate if the simulation has equilibrated

**Ligand RMSD** could be into two different parameters. The 'Lig fit Prot' shows the RMSD of a ligand when the protein-ligand complex is first aligned on the protein backbone of the reference and then the RMSD of the ligand heavy atoms is measured. If the values observed are significantly larger than the RMSD of the protein, then it is likely that the ligand has diffused away from its initial binding site. 'Lig fit Lig' shows the RMSD of a ligand that is aligned and measured just on its reference conformation. This RMSD value measures the internal fluctuations of the ligand atoms.

## Protein RMSF

The Root Mean Square Fluctuation (RMSF) is useful for characterizing local changes along the protein chain. The RMSF for residue  $i$  is:

$$RMSF_i = \sqrt{\frac{1}{T} \sum_{t=1}^T \langle (r'_i(t)) - r_i(t_{ref}) \rangle^2}$$

where  $T$  is the trajectory time over which the RMSF is calculated,  $t_{ref}$  is the reference time,  $r_i$  is the position of residue  $i$ ;  $r'$  is the position of atoms in residue  $i$  after superposition on the reference, and the angle brackets indicate that the average of the square distance is taken over the selection of atoms in the residue.

Resulting peaks indicate areas of the protein that fluctuate the most during the simulation. Typically you will observe that the tails (N- and C-terminal) fluctuate more than any other part of the protein. Secondary structure elements like alpha helices and beta strands are usually more rigid than the unstructured part of the protein, and thus fluctuate less than the loop regions

## Ligand RMSF

The Ligand Root Mean Square Fluctuation (L-RMSF) is useful for characterizing changes in the ligand atom positions. The RMSF for atom  $i$  is:

$$RMSF_i = \sqrt{\frac{1}{T} \sum_{t=1}^T (r'_i(t)) - r_i(t_{ref})^2}$$

where  $T$  is the trajectory time over which the RMSF is calculated,  $t_{ref}$  is the reference time (usually for the first frame, and is regarded as the zero of time);  $r$  is the position of atom  $i$  in the reference at time  $t_{ref}$ , and  $r'$  is the position of atom  $i$  at time  $t$  after superposition on the reference frame..

### **3.13 Statistics**

Data are expressed as the mean  $\pm$  standard error of the mean (SEM). Statistically significant differences between the data were evaluated with the Student's t test, with the threshold set at  $p < 0.05$ .



## 4 Results

### 4.1 Ligand Docking

As previously described, Kv7 channels are tetramers composed of six transmembrane segments called from S1 to S6: among these, the region encompassing S1-S4 segments forms the Voltage Sensing Domain (VSD) whereas the segments S5-S6 constitute the Pore Domain (PD). The Kv7 activator retigabine recognizes an intracellular hydrophobic pocket located in the pore domain (Main et al 2000); within this cavity, a residue of tryptophan (W236 in Kv7.2 and W265 in Kv7.3) in the cytoplasmic part of S5 was found to be crucial for the retigabine effect. Rationalized as generic hydrophobic contact by Lange et al. in 2015, Kim and collaborators have hypothesized that H-bond interactions are established between the carbamate group of retigabine and the tryptophan residue in the channel pore (Figure 11). As four retigabine binding sites are present within the homotetrameric Kv7.2 potassium channel, the docking of ligand was performed individually in each of the four sites (Figure 18). The rationale to carry out ligand docking in a single site, rather than in all four binding sites simultaneously, was supported by a recent study showing that a single retigabine-sensitive subunit is sufficient to generate nearly the full retigabine gating effect (Yau et al 2018).

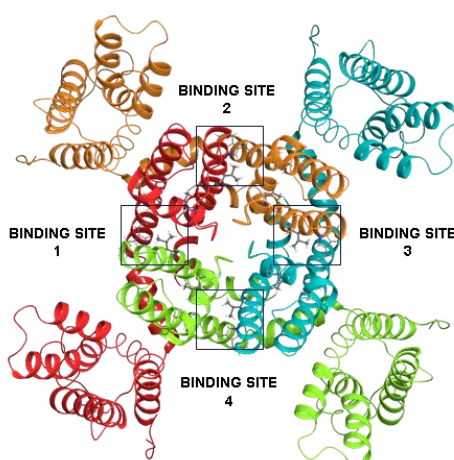


**Figure 18. Representation of the four retigabine binding sites in the homotetrameric Kv7.2 potassium channel.**

For our docking experiments, the ligand retigabine and the optimized Kv7.2 channel structure, generated by homology modeling starting from Kv1.2 / 2.1 paddle chimera (PDB2R9R) were used. As previously reported in *Materials and Methods*, six different Glide setups were used for each retigabine binding site considering: 1) the scaling of atomic van der Waals radii of both protein and ligand, 2) a constraint imposing the formation of a hydrogen bond between Trp236 and retigabine, 3) the number of retigabine poses stored in the output (Table 11). According to the scaling of atomic van der Waals radii, Glide does not allow for receptor flexibility in docking, but scaling of van der Waals radii of nonpolar atoms, which decreases penalties for close contacts, can be used to the receptor and the ligand. Overall, among 132 poses obtained, the retigabine binding mode was similar to that described by Kim et al., in which the retigabine carbamate group was in the vicinity of the W236. However, starting from more rigid conditions (scaling 1.0/0.8 and 0.9/0.8) the H-bond interaction between the carbamate group of retigabine and the tryptophan residue was not found in any of the four retigabine binding sites considering only one output pose. Instead, other types of interactions were established between tryptophan residue and ligand, like  $\pi-\pi$  interaction and aromatic H-bond. Proceeding to the 0.8/0.8 scaling condition, we observed the interaction described by Kim with tryptophan only in binding sites 2 and 4. With unchanged scaling values and increased output poses up to 10, the visual analysis showed that the interaction of interest was established also in the binding site 3. Moving to the application of the softer scaling ligand radii 0.7 (and scaling protein 0.8), the desired H-bond network was not obtained. Finally, retigabine was able to reproduce the reference binding mode in all binding sites when ligand-receptor interaction requirement (constraints) and protein/ligand scaling radii 0.8/0.7 were applied. Although these scaling were used to decrease penalties of close contacts, induced-fit effects leading to receptor conformational changes upon ligand binding were not considered in the docking calculation.

Consequently, the poses obtained were not optimal due to close distances between the ligand and some residues of the binding site (Figure 19).

**Table 11. Docking conditions applied for each retigabine binding site**

Binding site	vdWscaling		Constraint H-bond W236	N° of Output poses
	Protein	Ligand		
1	1	0,8	No	1
	0,9	0,8	No	1
	0,8	0,8	No	1
	0,8	0,8	No	10
	0,8	0,7	No	10
	<b>0,8</b>	<b>0,7</b>	<b>Yes</b>	<b>10</b>
2	1	0,8	No	1
	0,9	0,8	No	1
	0,8	0,8	No	1
	0,8	0,8	No	10
	0,8	0,7	No	10
	<b>0,8</b>	<b>0,7</b>	<b>Yes</b>	<b>10</b>
3	1	0,8	No	1
	0,9	0,8	No	1
	0,8	0,8	No	1
	0,8	0,8	No	10
	0,8	0,7	No	10
	<b>0,8</b>	<b>0,7</b>	<b>Yes</b>	<b>10</b>
4	1	0,8	No	1
	0,9	0,8	No	1
	0,8	0,8	No	1
	0,8	0,8	No	10
	0,8	0,7	No	10
	<b>0,8</b>	<b>0,7</b>	<b>Yes</b>	<b>10</b>

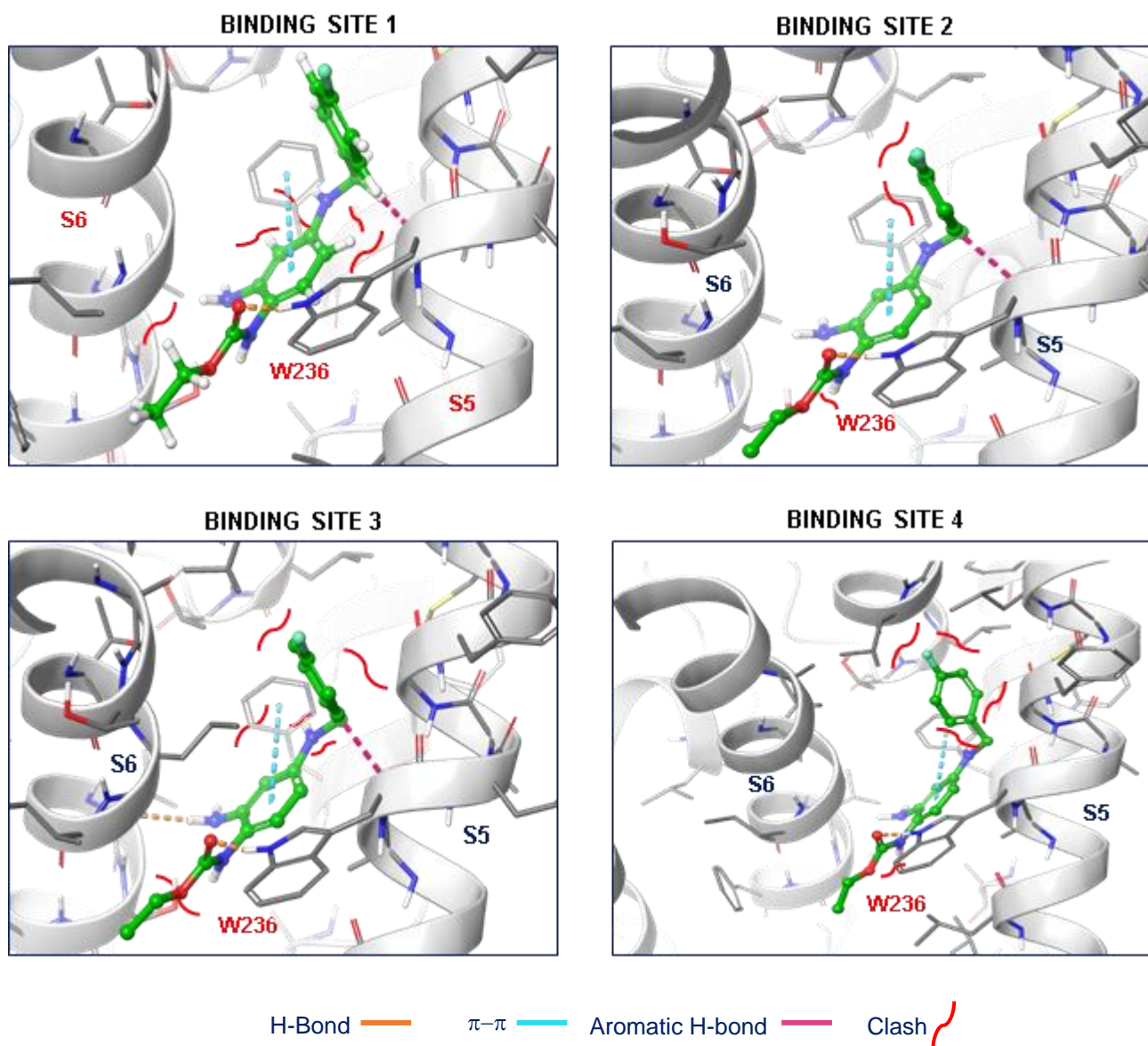


**Figure 19.** Best docking poses obtained with 0.8/0.7 scaling factors and interaction constraints, for each retigabine binding site.

Thus, to overcome this limitation and considering the receptor flexibility, the InducedFit Docking protocol was applied (*see Materials and Methods*).

Considering the flexibilities of both ligand and side chains of a target protein, the retigabine poses obtained of all four binding sites, were characterized by the absence of unfavorable interactions, the presence of the H-bond interaction between the carbamate group of the ligand and the side chain of tryptophan residue 236 (Figure 20), and better docking scores compared to the previous calculation (Table 12).

**Table 12. Comparison of GlideScore between the best poses obtained with the rigid receptor docking and InducedFit protocol.**

Binding site	InducedFit	Rigid receptor docking
	Gscore (kcal/mol)	Gscore (kcal/mol)
1	-10,29	-6,9
2	-10,17	-7,1
3	-9,65	-6,8
4	-9,49	-6,7

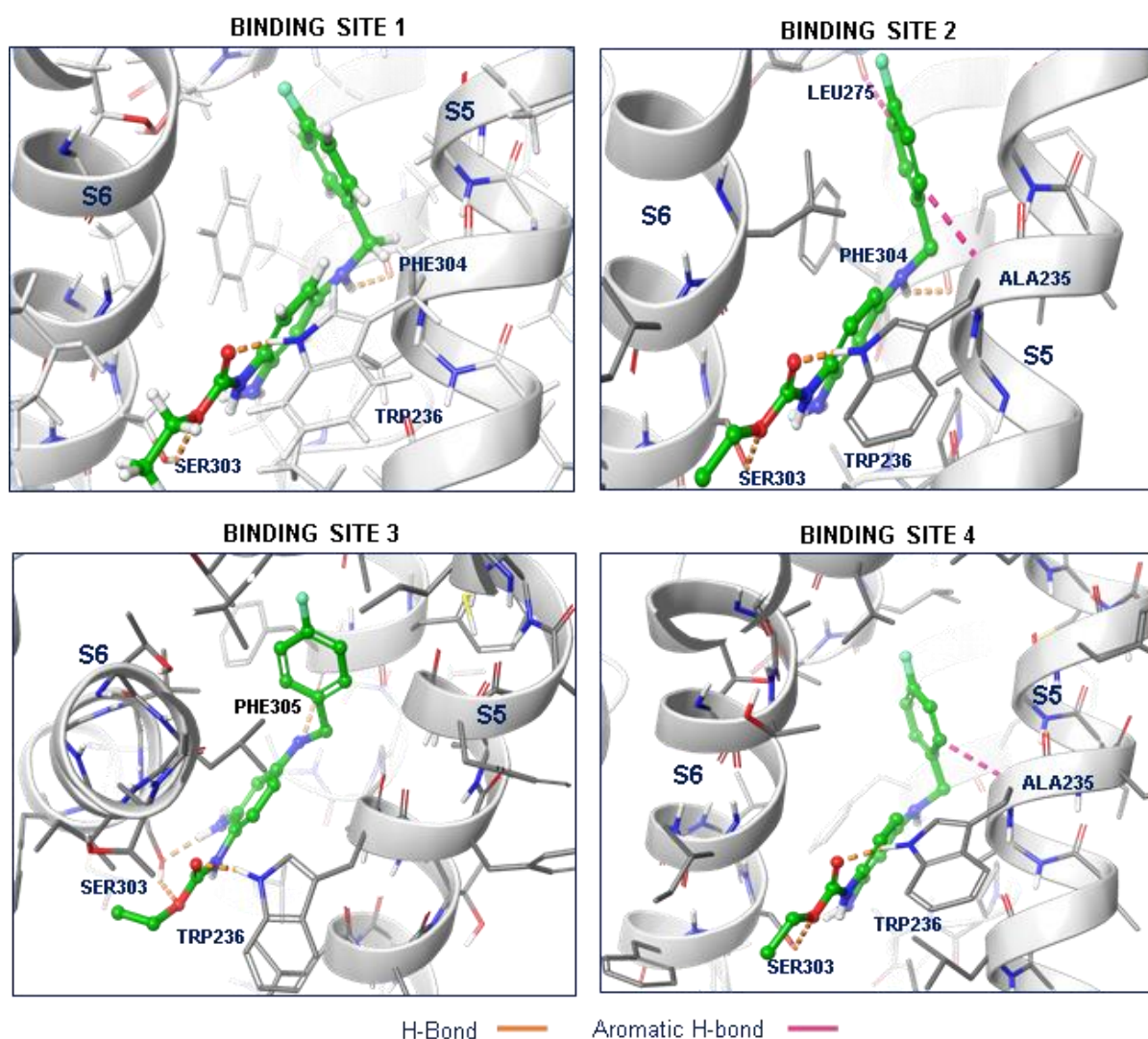


**Figure 20. Best docking poses, for each retigabine binding site, obtained by InducedFit docking.**

In addition to the H-bond between the W236 and the ligand, in Figure 20 it is also possible to appreciate the H-bond interaction between the aniline group or the carbamate group of retigabine and Ser303 in all active sites. Moreover, a hydrogen bond was established with the Phe304 in the binding site 1 and 2 and with Phe305 in the site 3, while an aromatic H-bond interaction was found with Ala235 in the binding sites 2 and 4.

To verify the reliability of these results, we submitted the most relevant docking poses to MD simulations.

## 4.2 Molecular Dynamics Simulations of the Apo form

To assess the stability of the system and identify the ideal conditions to be applied to the Holo form (with ligand) of the Kv7.2 potassium channel, the first MD simulations were performed on the Apo (without ligand) tetrameric form of the channel. Different MD conditions were applied (Table 13; *see also Materials and methods*) and two variants have been considered such as the timescale and application of the Grand canonical Monte Carlo (GCMC).

**Table 13. Conditions applied to the MD simulations of the Apo form of Kv7.2 potassium channel.**

MEMBRANE	SOLVENT	PERIODIC BOUNDARY CONDITIONS	IONS	TIME	ENSEMBLE	GCMC
POPC	SCP	Orthorombic	NaCl 0,15M	1,2ns	NP <sub>γ</sub> T	NO
POPC	SCP	Orthorombic	NaCl 0,15M	10ns	NP <sub>γ</sub> T	YES
POPC	SCP	Orthorombic	NaCl 0,15M	10ns	NP <sub>γ</sub> T	NO
POPC	SCP	Orthorombic	NaCl 0,15M	10ns	NP <sub>γ</sub> T	YES
POPC	SCP	Orthorombic	NaCl 0,15M	10ns	NP <sub>γ</sub> T	NO
POPC	SCP	Orthorombic	NaCl 0,15M	100ns (n=3)	NP <sub>γ</sub> T	YES
POPC	SCP	Orthorombic	NaCl 0,15M	100ns (n=3)	NP <sub>γ</sub> T	NO

### 4.2.1 Selection of simulation timescale

The conformational stability across MD simulations was evaluated by calculating the root mean square deviation (RMSD). The RMSD has been used to measure the average change in displacement of a selection of atoms for a particular frame with respect to a reference

frame. In our study, 250, 1000 and 5000 frames were considered respectively for simulation times of 1,2, 10 and 100 ns and the RMSD was measured considering the backbone atoms of the structure. In the MD simulations performed for 1,2 and 10 ns, the RMSD value of the backbone atoms with respect to the starting position (frame 0) reached 2,5 Å and 4,0 Å, respectively, with unobserved convergence (Figure 20). Conversely, the 100 ns simulation showed the maximum RMSD value around 4,0 Å with no relevant fluctuations after 30ns (Figure 21). According to these results, we selected 100 ns timescale for next simulations, as good compromise of exhaustive sampling and calculation cost.

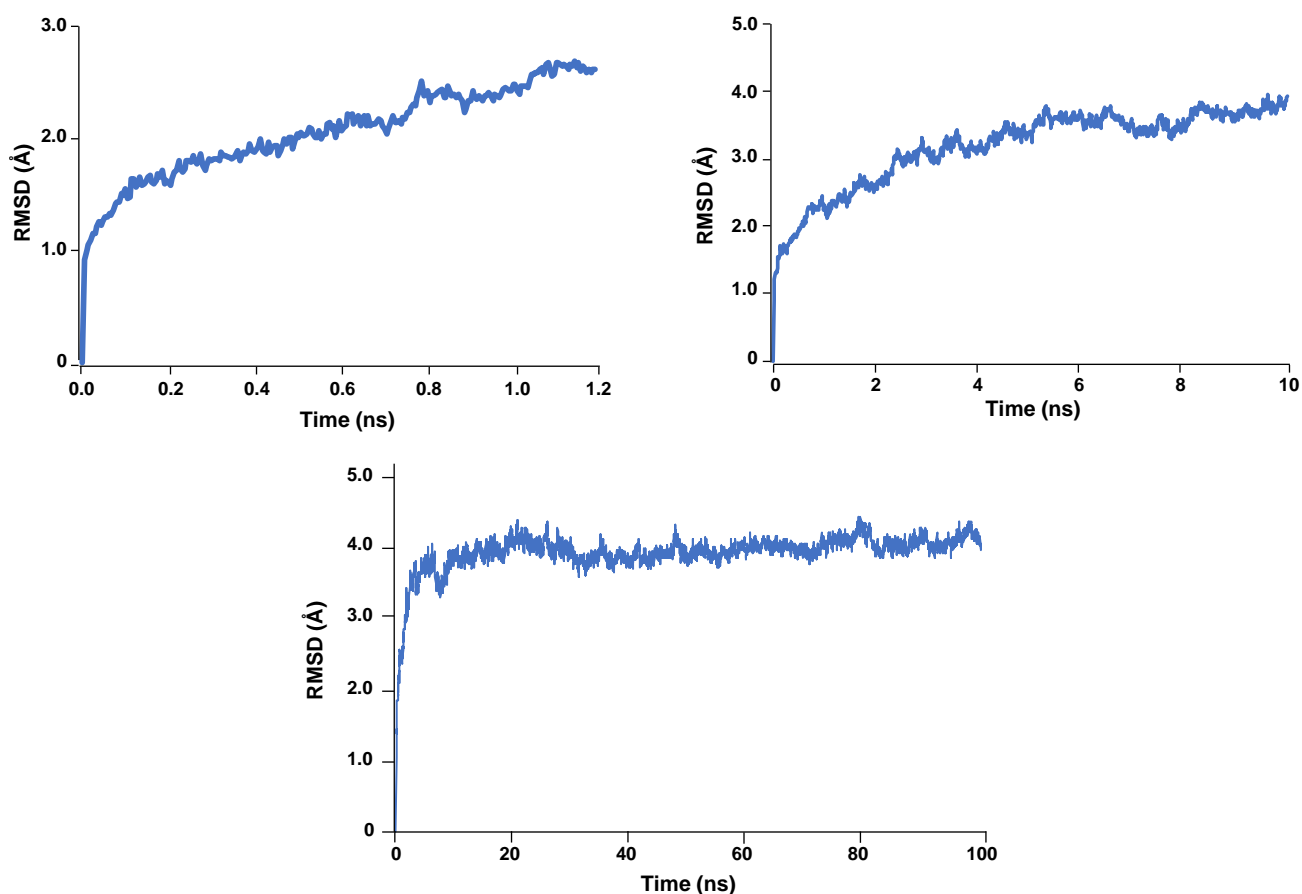


**Figure 21.** Graphical representation of RMSD results throughout 1,2ns 10ns and 100ns MD simulations.



Consider the 100 ns MD simulation, evaluation of local changes along the protein chain have been performed by calculating the Root Mean Square Fluctuation (RMSF). The results obtained suggest that the largest fluctuations in the RMSF values were observed, as expected, at the loop regions between the transmembrane segments and in the N-terminal of segments S1 and C-terminal of segments S6 (Figure 22); particularly, in all four subunits, the maximum RMSF values were observed around the residues Ser121-Glu123, Gly149-Arg155, and Ser187-Asn190 corresponding to the extracellular loop regions.

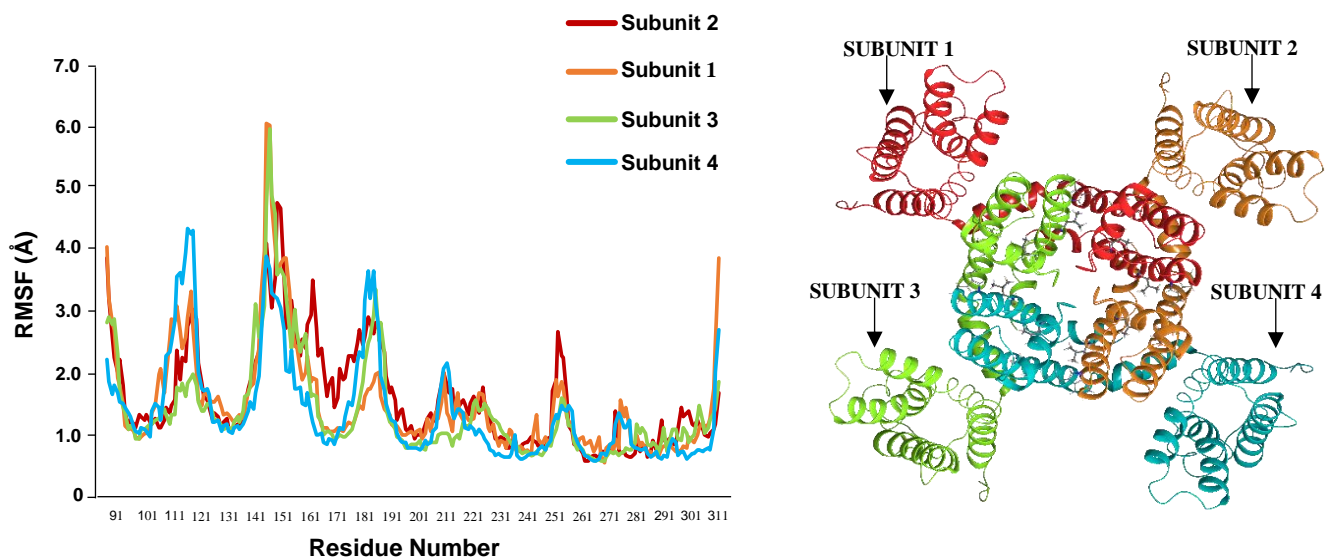


**Figure 22. RMS Fluctuations of protein backbone residues throughout 100ns MD simulations.** The graph shows the overall fluctuation of amino acids for each subunit constituting the Kv7.2 homotetramer (left). Representation of the four subunits composing homotetrameric Kv7.2 potassium channel (right).

#### 4.2.2 Application of GCMC

In statistical mechanics, a grand canonical ensemble is a statistical ensemble that is used to represent the possible states of a mechanical system of particles that are in thermodynamic equilibrium (thermal and chemical) with a reservoir; thus, the system is open and can exchange energy and particles with a reservoir. In that way, various possible states of the system can exist and differ in both their total energy and the total number of particles. As resulted from visual inspection analysis of our MD simulation, the application of GCMC determined a better water distribution, filling the empty spaces. Moreover, solvent molecules never interposed between the protein and the lipids.

According to the results collected, we defined the optimal MD settings for next simulations (Table 14).

Table 14. Optimal MD conditions

MEMBRANE	SOLVENT	PERIODIC BOUNDARY CONDITIONS	IONS	TIME	ENSEMBLE	GCMC
POPC	SCP	Ortorhombic	NaCl 0,15M	100ns	NP $\gamma$ T	YES

#### 4.3 Molecular Dynamics Simulations of the Holo form

To evaluate the stability of the Kv7.2 potassium channel/retigabine complex and of the observed interaction network, 100ns MD simulations of the best poses for each retigabine binding site obtained by InducedFit docking were performed. In total, 12 simulations were carried out (n=3 for each system).

Considering MD trajectories, both proteins, the ligand/protein complex and ligand RMSDs were assessed (for more details see *Materials and Methods*). As observed in Figure 23, both protein and protein-ligand complex reached stability during the simulation. Considering

Protein RMSD, in all systems, the average values of RMSD were around 4,0 Å (Table 15), whereas the average value for the protein-ligand complex, (Lig fit Prot pratameters) was lower than the RMSD of the protein suggesting that the ligand didn't diffuse away from its initial binding site.

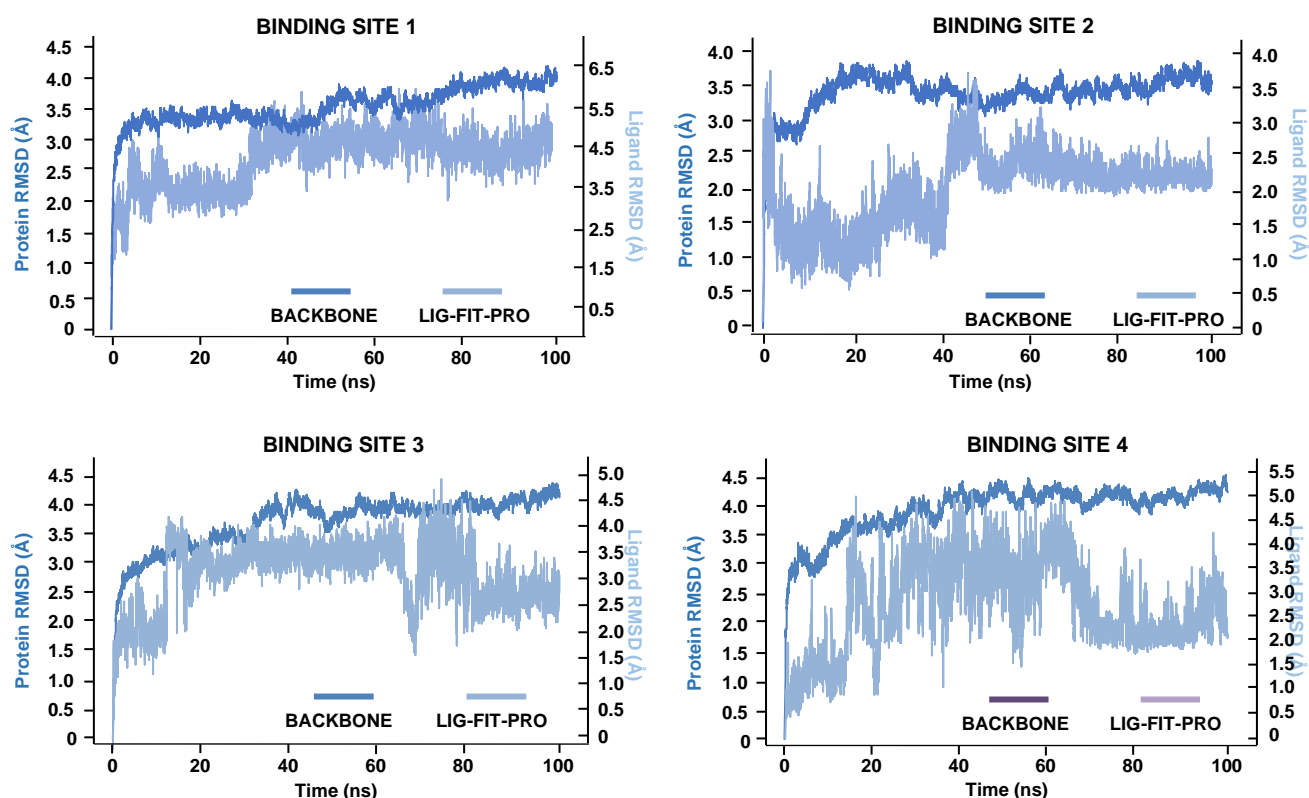


**Figure 23.** The Root Mean Square Deviations (RMSD) of protein backbone atoms and protein complex with retigabine in the binding site 1, 2, 3 and 4 during 100 ns MD simulation. Each plot shows the RMSD of protein on left Y-axis whereas the ligand RMSD in the complex with the protein (LigfitPro) is represented on right Y-axis.

**Table 15. Average RMSD values of protein backbone atoms and protein complex with retigabine in the binding site 1, 2, 3 and 4 during 100 ns MD simulation**

Retigabine binding site	Average values of RMSD	
	Protein Backbone	Ligand/Protein Complex (LigfitPro)
1	4,0 Å	3,6 Å
2	4,3 Å	2,8 Å
3	3,7 Å	3,3 Å
4	3,9 Å	2,8 Å

Subsequently, evaluation of the internal fluctuations of the ligand atoms have been measured by means of the Lig fit Lig parameters (see Materials and methods). As shown in Figure 24, in all binding sites, fluctuations in the RMSD value are observed, suggesting certain motion of the ligand in the binding pocket.

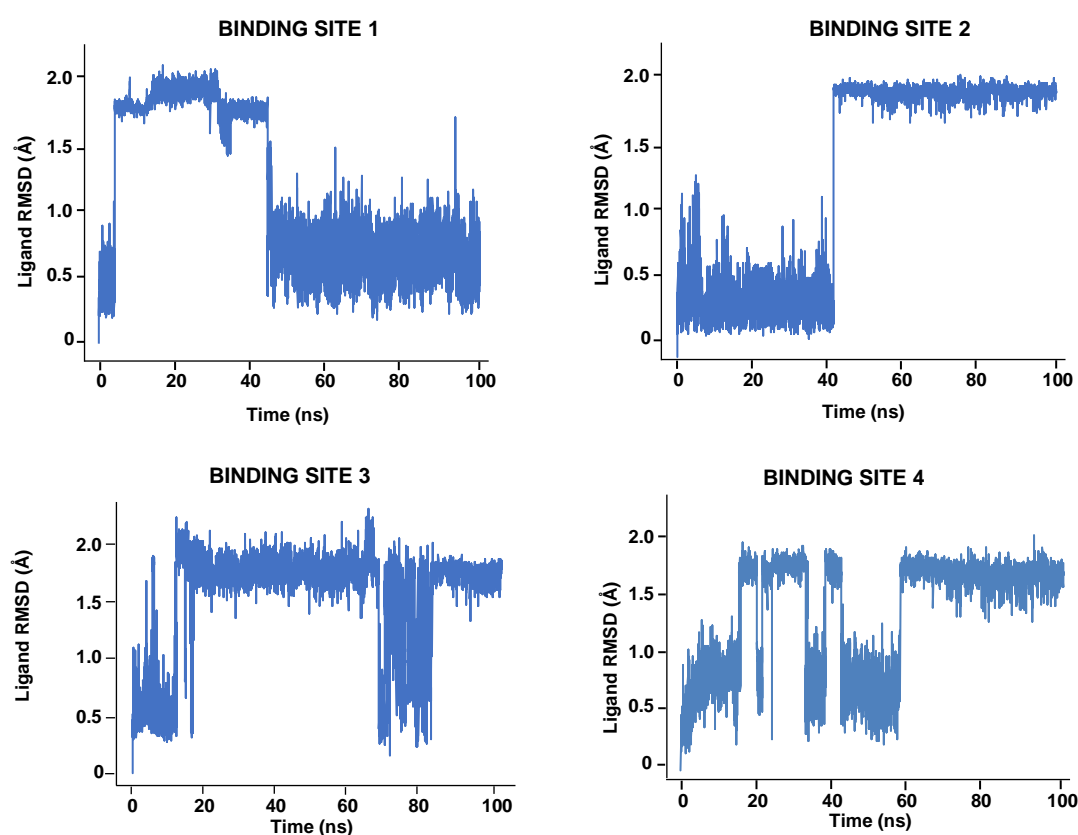


**Figure 24. Lig-Fit-Lig RMSD graphs of retigabine.**

Subsequent evaluation of ligand RMSF, useful to characterize the most fluctuating atoms composing the ligand along the simulations, was considered to understand which moiety of the molecules could be subject to a higher mobility. As shown in the figure, higher RMSD values were related to atom numbers 2, 3, 5 and 6 belonging to the fluorophenyl group (Figure 25).

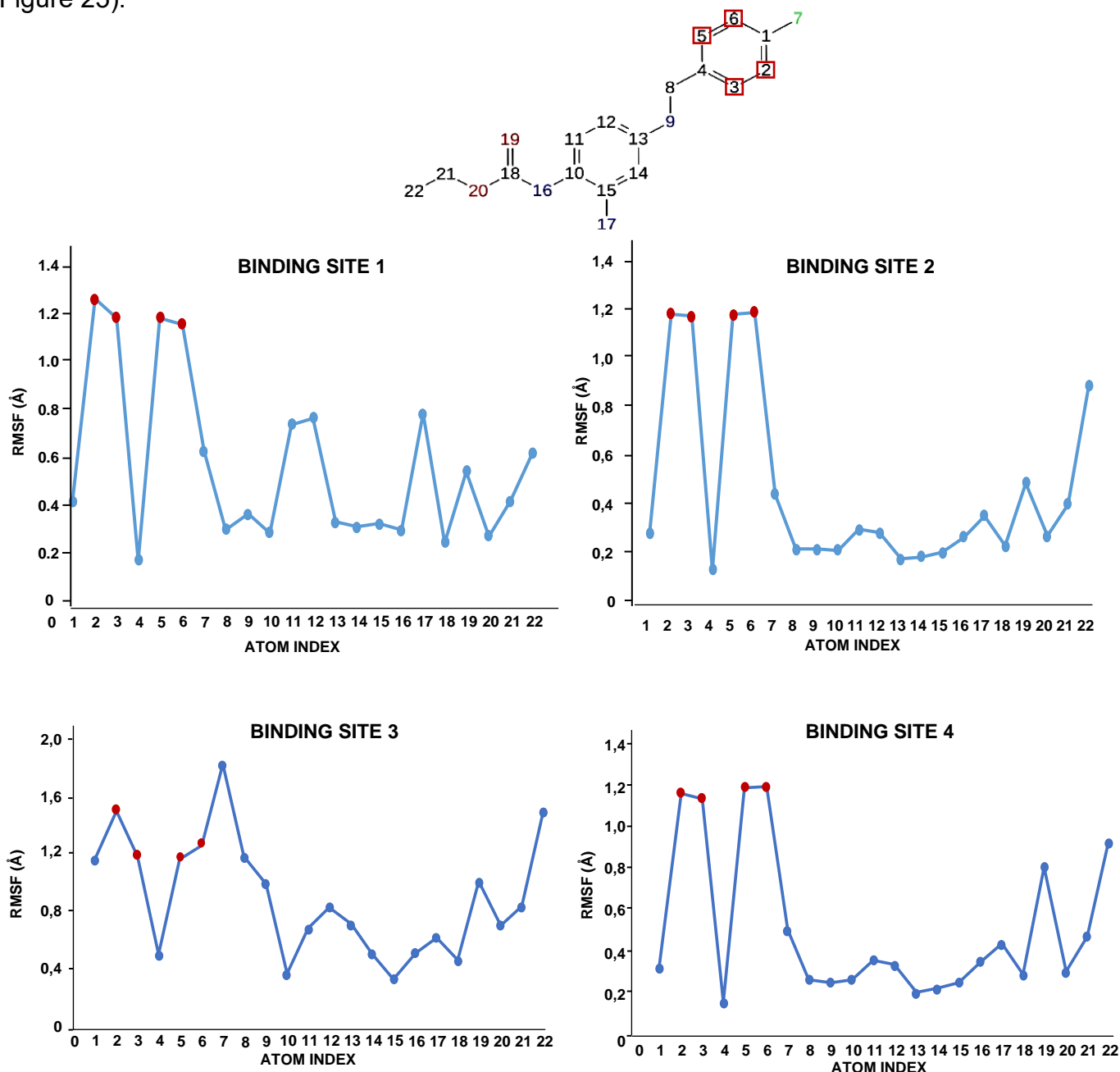


**Figure 25. Ligand RMSF broken down by atom, corresponding to the 2D structure in the top panel.** In the bottom panel, the 'Ligand' line shows fluctuations where the ligand in each frame is aligned on the ligand in the reference frame, and its fluctuations are measured for the ligand heavyatoms. These RMSF values reflect the internal atom fluctuations of the retigabine located in all four binding sites.

To evaluate if rotational movements of the fluorophenyl moiety were responsible for the RMSD values fluctuation, dihedral angles formed between atoms 9, 8, 4 and 3 were calculated during the simulations. A dihedral angle describes the geometric relation of two parts of a molecule joined by a chemical bond. Every set of three not-colinear atoms of a molecule defines a plane. When two such planes intersect (i.e., a set of four consecutively bonded atoms), the angle between them is a dihedral angle. Dihedral angles are used to specify the molecular conformation. As reported in figure 25, the trend of the dihedral angles calculated for the fluorophenyl group is highly similar to the RMSD of the ligand (Figure 26). The results obtained demonstrated that the fluctuation in RMSD values of Retigabine was due to rotation of fluorophenyl moiety, so suggesting two different conformations (Figure 27).

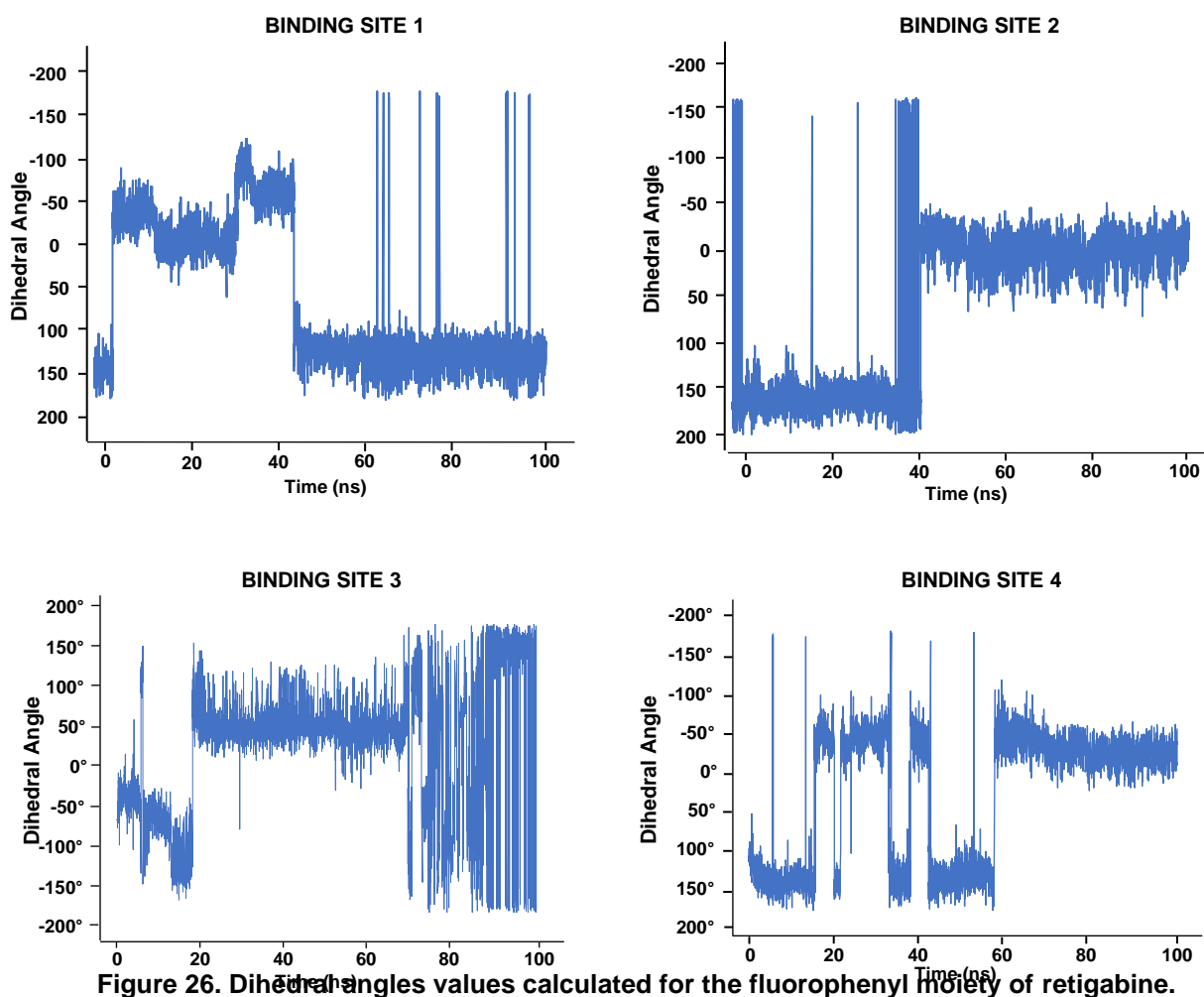
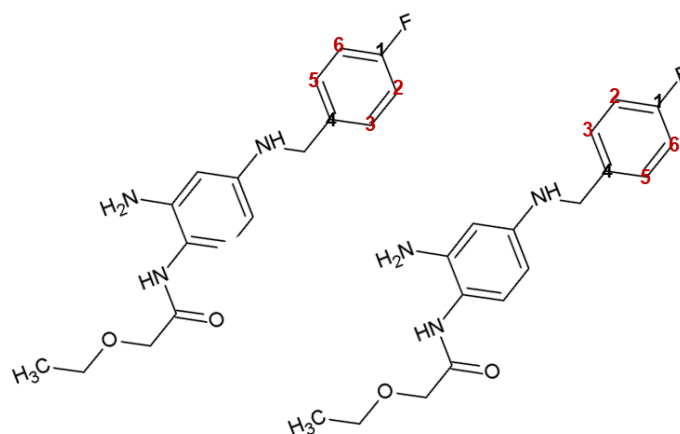


Figure 26. Dihedral angles values calculated for the fluorophenyl moiety of retigabine.



**Figure 27.** 2D representation of two different conformation of fluorophenyl moiety.

MD simulations were run to verify if the interaction pattern established in the docking results is maintained (involving for example Ser303, Phe304, Phe305 and Ala235) and if other interactions can occur. As stated before, tryptophan 236 at the end of the S5 helix in the Kv7.2 channel, was found to be crucial for retigabine effect. Beside this residue, also other amino acids are involved in the binding of retigabine, like Leu243 in S5, Leu275 in the pore, Leu299 in the S6; however, none of them seems to be as crucial as Trp236. Figure 28 shows that Trp236 established hydrogen bonds and hydrophobic interactions for 100% of the simulation time, in all active sites. Moreover, in all the chains, Retigabine made hydrophobic interactions with Leu243 for less than 10% of the trajectory, while hydrogen or hydrophobic contacts were observed with Leu275 for less than 20%. Except for site 1, Leu299 maintained more than 100% interactions, in all binding sites. This high persistency is possible as some residues may have multiple contacts with the ligand. In addition to residues that are known to be involved in the binding of the activator, also other residues whose role in the binding is unknown, were found to strongly interact with the ligand. Significant interactions were observed with Phe304 and Phe305 through hydrogen bonds, hydrophobic interactions and

some water bridges. Persistent contacts were established with Pro308 through hydrophobic interactions and with Ser303 via hydrogen bonds (Figure 28).

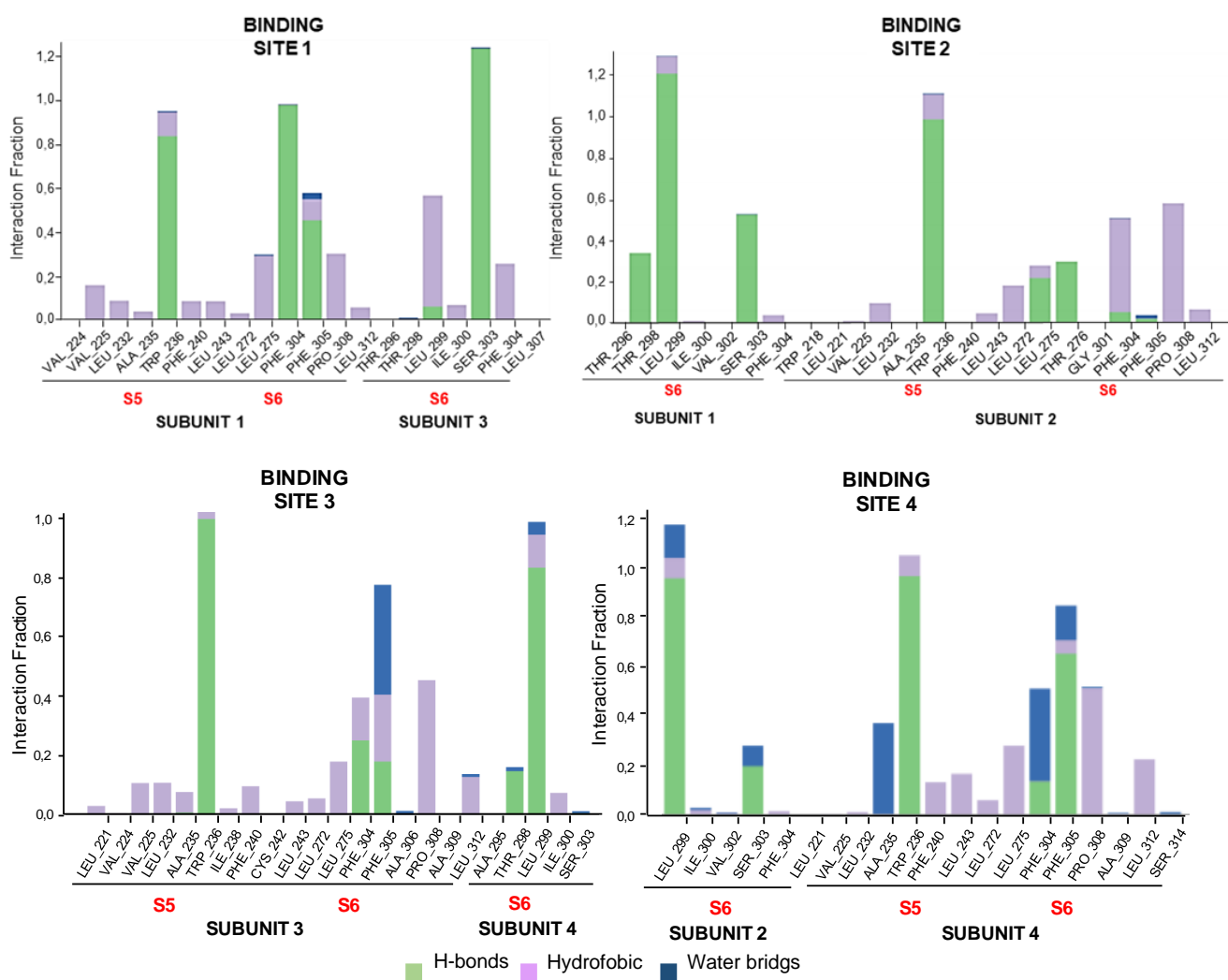


**Figure 28. Protein interactions with the ligand retigabine, in all four binding sites, monitored throughout the simulations.** Protein-ligand interactions are categorized into three types: Hydrogen Bonds, Hydrophobic, and Water Bridges. The stacked bar charts are normalized over the course of the trajectory: a value of 0.7 suggests that 70% of the simulation time the specific interaction is maintained. Values over 1.0 are possible as some protein residue may make multiple contacts of same subtype with the ligand.



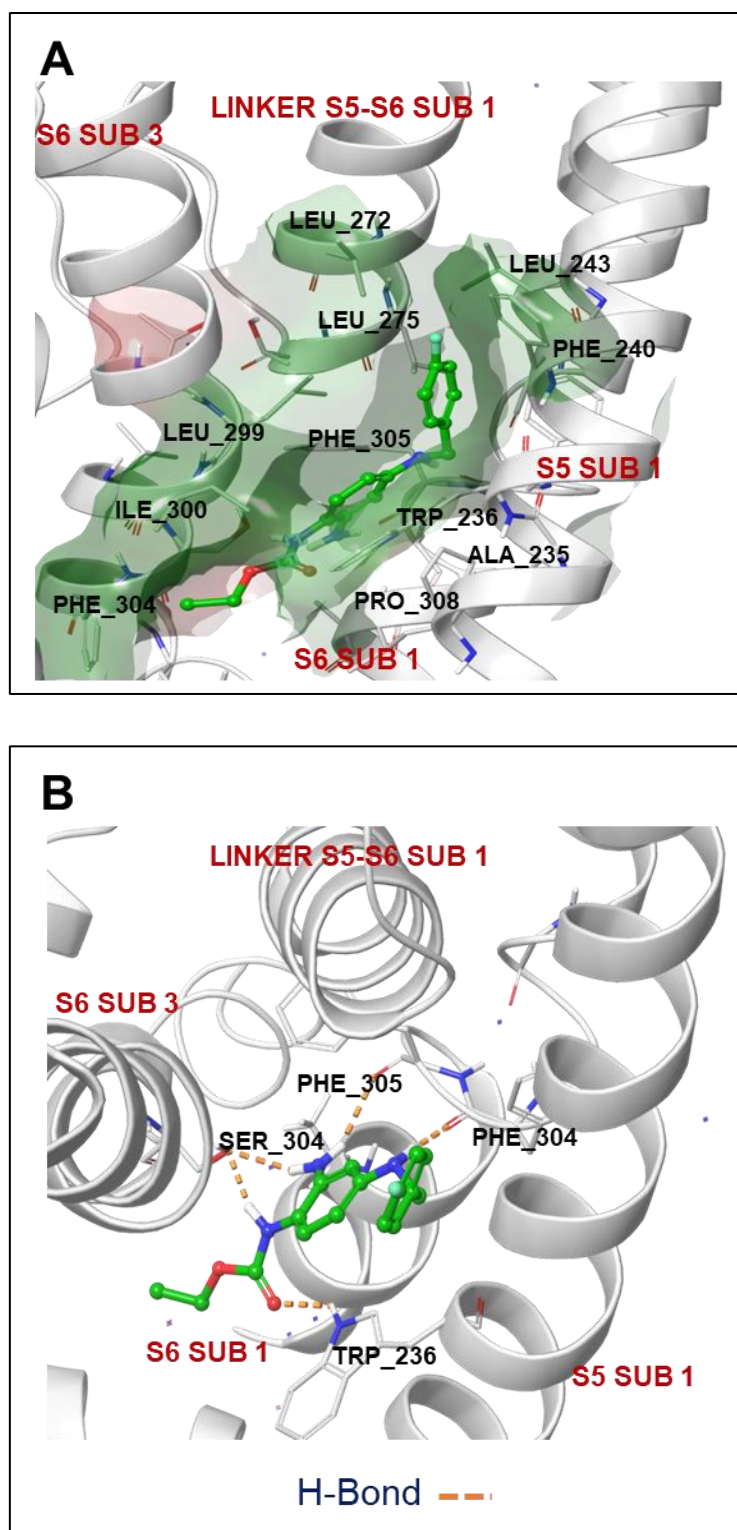
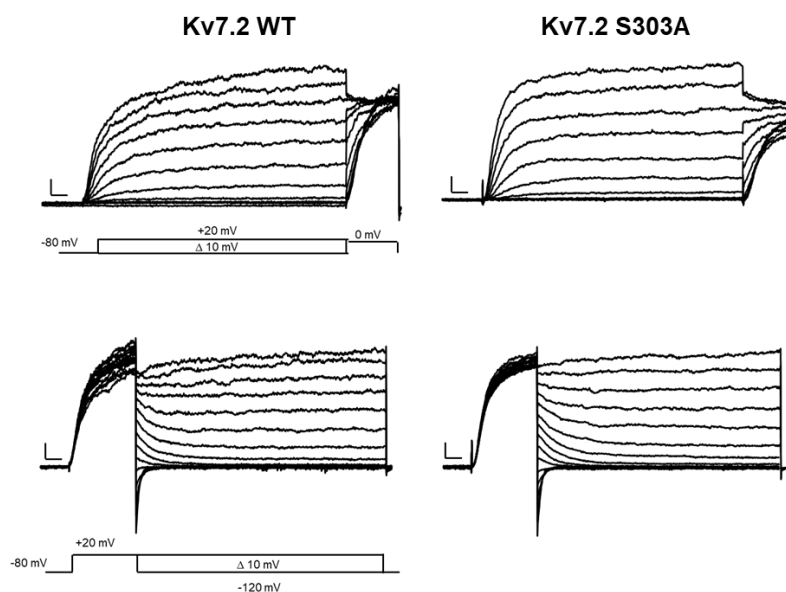


Figure 29. A) Representation of the hydrophobic pocket and residues implicated in hydrophobic interactions with the ligand. B) Interactions that occur more than 30.0% of the simulation time in the selected trajectory

#### 4.4 Functional characterization of Kv7.2 S303A mutant

According to previous MD results, to confirm whether the serine residue in position 303 is involved in the binding of the retigabine, site direct mutagenesis was performed. In particular, the residue of serine was substituted with a residue of alanine, which is not able to act either as an acceptor or as a donor of H-bonds. In a first series of experiments, patch-clamp recordings were performed on CHO cells transiently transfected with wild-type or mutant Kv7.2 cDNA. Outward  $K^+$  currents were recorded, in response to incremental depolarizing voltage steps ( $\Delta 10$  mV) from -80 to +20 mV. CHO cells expressing wild-type channels produce a robust  $K^+$  currents ( $30.1 \pm 8.1$  pA/pF;  $n=9$ ;  $p<0.05$ ) by contrast, cells expressing Kv7.2 subunits carrying S303A mutation show a reduced current amplitude ( $13.1 \pm 4.5$  pA/pF;  $n=6$ ;  $p<0.05$ ). The calculated  $V_{1/2}$  was  $-23.9 \pm 1.8$  mV in Kv7.2-S303 and  $-29 \pm 1.7$  mV in Kv7.2 whereas the slope  $13.1 \pm 1.5$  and  $10.3 \pm 1.0$  for Kv7.2 and Kv7.2-S303, respectively. This, suggested that, no major alteration in voltage sensitivity of the Kv7.2 channel activation were introduced by the mutant. Both Kv7.2 WT and Kv7.2-S303 show similar activation and deactivation kinetics and absence of inactivation (Figure 30).



**Figure 30. Functional characterization of Kv7.2 and Kv7.2 S303A mutant.** Representative current traces recorded in CHO cells expressing the indicated subunits, in response to the voltage protocol shown in bottom part. Current scale, 200 pA ; time scale, 0.2 s.

To evaluate the retigabine sensitivity of the Kv7.2 S303A mutant channel we performed time-course experiments at increasing drug concentrations (0.1-100  $\mu\text{M}$ ) using a ramp protocol in which Kv7.2 currents were activated by 3 s voltage ramps from  $-100$  to  $+20$  mV. As we can see in Figure 31, retigabine induced a dose-dependent leftward shift in the voltage-dependence of Kv7.2 WT channels and a slight increase of current at depolarized potential; whereas, in Kv7.2S303A we observed a dose-dependent leftward shift in the voltage-dependence and a marked increase in the current size at depolarized potentials (Figure 31).

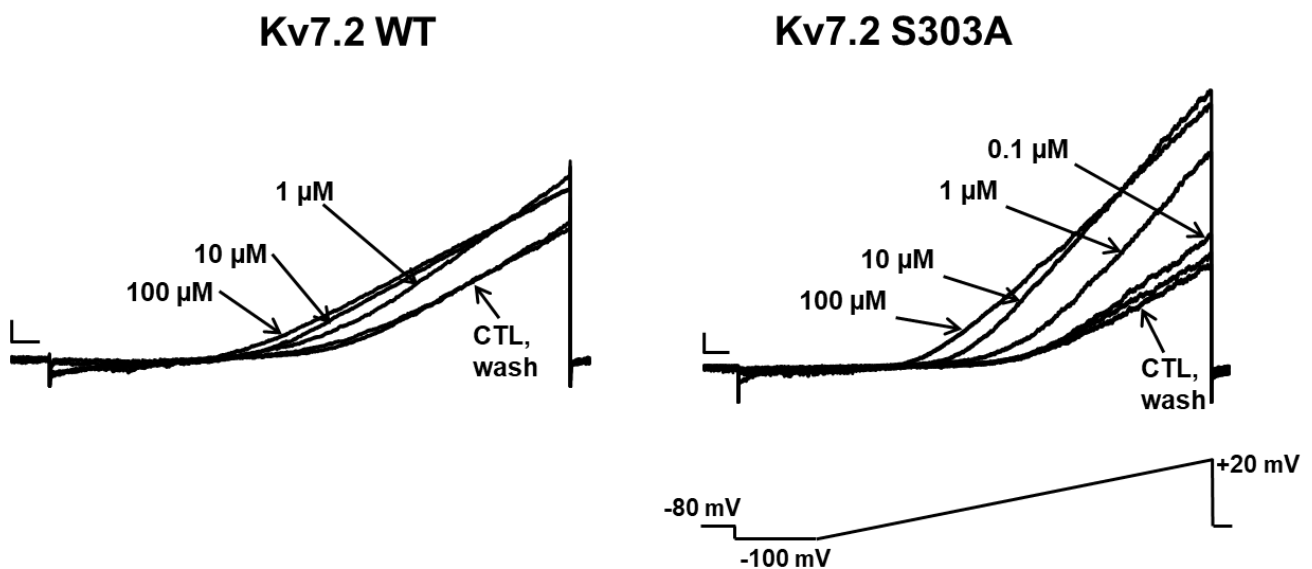


**Figure 31. Effect of retigabine on ramp-evoked Kv7.2 and Kv7.2 S303A currents.** Representative whole-cell current traces from Kv7.2WT and Kv7.2S303A channels activated by the indicated ramp protocol recorded in control conditions and upon exposure to 0.1–10  $\mu\text{M}$  RET (for the mutant) 1–100  $\mu\text{M}$  RET (for WT). Current scale, 100 pA (for WT), 200 pA (for mutant); time scale, 0.2 s.

The  $EC_{50}$  of retigabine on Kv7.2 WT and Kv7.2 S303A current activation was  $0.72 \pm 0.38 \mu M$  for WT, while for the mutant the calculated  $EC_{50}$  was  $2.77 \pm 0.78 \mu M$  (Figure 32). The reduced potency observed in the mutant channels when compared to Kv7.2 WT, suggests that the serine at position 303 may contribute to the formation retigabine binding site.

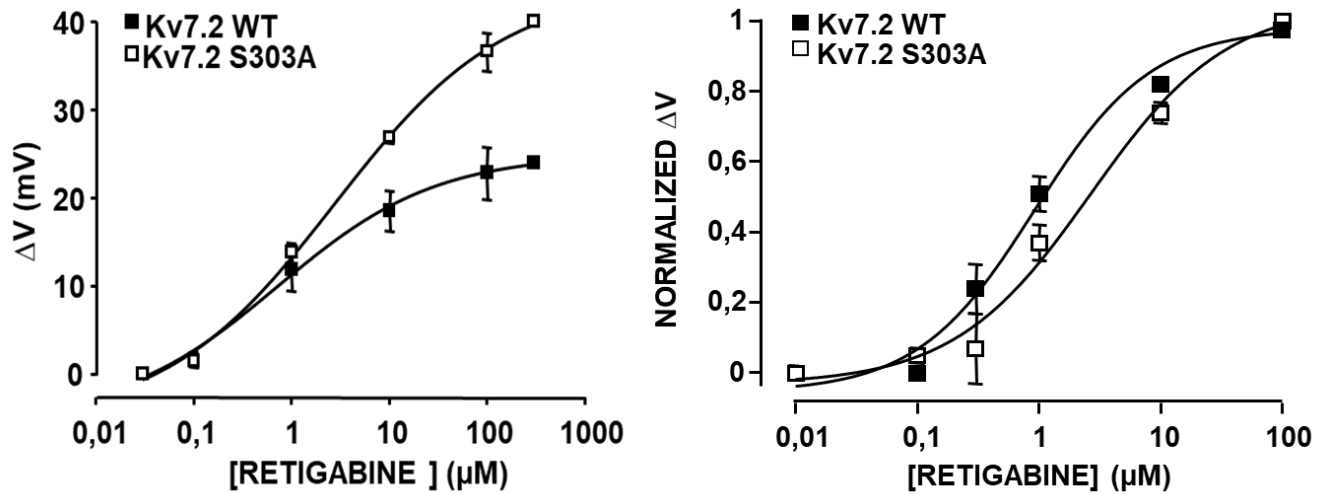
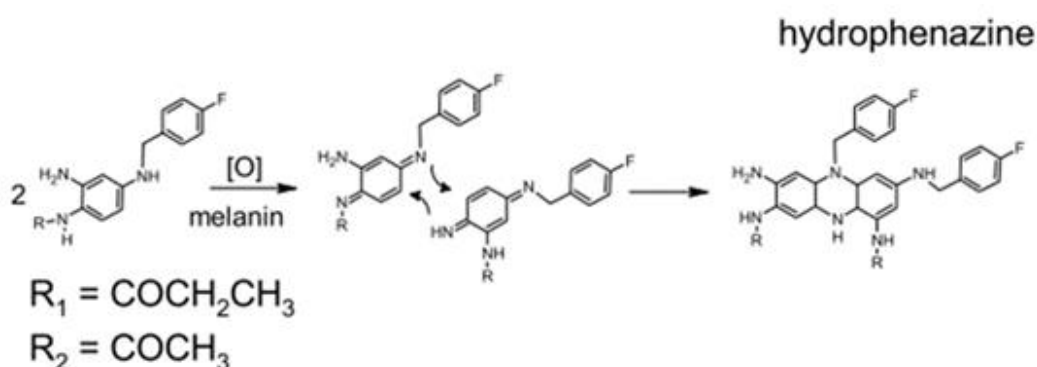


Figure 32. Dose-response curve for RET-induced  $\Delta V$  shift.

## 4.5 Synthetic strategy

To overcome some limitation of retigabine, in collaboration with the Department of Pharmacy of the University of Salerno we developed a library of retigabine derivatives. Docking results obtained suggested that retigabine binds a pocket characterized by a central hydrophilic core flanked by two hydrophobic regions. Retigabine contains three major functional groups: fluorophenyl group (zone A), the middle phenylaniline ring (zone B), the carbamate and the methoxy group (zone C) (Figure 33). The most important chemical interaction evidenced is represented by a hydrogen bond between the carbamate group of retigabine and a tryptophan residue in S5 (W265 in Kv7.3, W236 in Kv7.2). For that reason, in our derivatives, no changes were made on the carbamate group. On the other hand, the compounds showed one or more of the following features: I) modification on the fluorophenyl moiety to increase the potency. According to the structure of the potent retigabine analogue, RL-81, (Kumar et al., 2016), a larger electron withdrawing group such as the  $-CF_3$  has been inserted. II) To prevent dimers formation, subsequent to the formation of the two new C–N bonds of the hydrophenazine ring following initial oxidation of retigabine to the diimide quinone (Scheme 2)



Scheme 2. Proposed mechanism for the formation of dimers

substitutions on the aniline group or on NH-linker were made (Zone B). In particular, three types of modifications were made, such as insertion of -CH<sub>3</sub> group at the -NH linker and/or introduction electron withdrawing group (-F) in the aniline moiety, or substitution of the amino group with a heterocycles (e.g.piperidine, pyrrolidine). III) introduction of longer chains (e.g. hexane, heptane, tert-butyl and, cyclohexane) at the methoxy group to explore the deep part of the hydrophobic retigabine binding site (Zone C) (Figure 33). Screening of newly-synthesized drugs have been performed in stable cell lines expressing Kv7.2/3, Kv7.4 and, Kv7.3A315T.

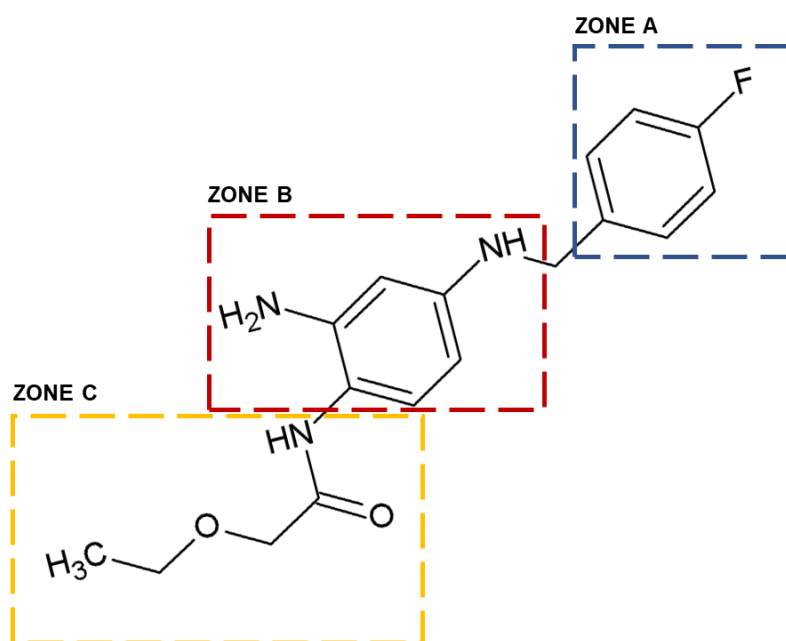


**Figure 33. Drug optimization. Representation of the three “zones” of the retigabine manipulated.**

#### 4.6 Electrophysiological characterization of Kv7.2/Kv7.3, Kv7.2, Kv7.3, Kv7.3A315T, Kv7.4 stable cell lines

Characterization and screening of stable cell lines obtained, as described above in *Materials and Methods*, was carried out using the patch-clamp electrophysiological technique.

To compare current expression, patch-clamp recordings were performed in CHO stable cell lines and in a control group represented by CHO cells transiently transfected with the cDNAs of interest. To generate conductance-voltage curves, the cells were held at  $-80$  mV, then depolarized for 1.5 s from  $-80$  mV to  $+20$  in 10-mV increments, followed by an isopotential pulse at 0 mV. Cells transiently transfected with the cDNAs encoding for Kv7.2 and Kv7.3 generated a voltage-dependent  $K^+$  selective current with a current density of  $119.7 \pm 13.2$  pA/pF and a half-activation potential ( $V_{1/2}$ ) of  $-35.1 \pm 1.6$ . Among the 7 clones stably expressing Kv7.2/Kv7.3, clone number 5 exhibited biophysical properties similar to the control group; in fact, the calculated  $V_{1/2}$  was  $-32.2 \pm 1.7$  while the current densities at 0 mV was  $71.1 \pm 17.4$  pA/pF. (Figure 34)

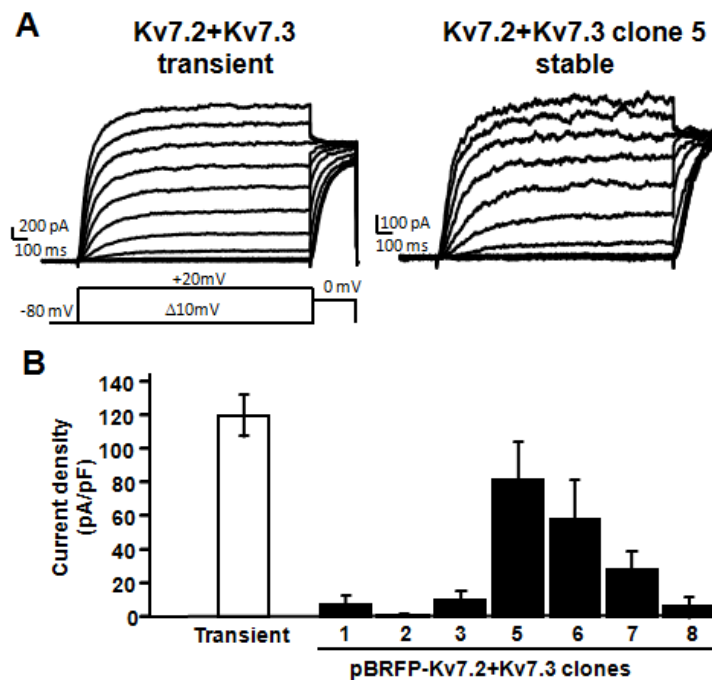


**Figure 34. Functional characterization of Kv7.2/Kv7.3 stable cell lines.** Representative current traces recorded in CHO cells expressing, stably or transiently, the indicated subunits, in response to the voltage protocol shown in bottom part. Current scale, 200 pA (for stable) 100 pA (for transient); time scale, 0.1 s.

To ensure that both Kv7.3 and Kv7.2 subunits were expressed and formed into heteromeric channels, Kv7.2/3 stable transfected cells, pharmacological experiments with tetraethylammonium (TEA) were performed. Homomeric Kv7.2 and Kv7.3 channels, and heteromeric Kv7.2/7.3 channels, show significant differences in their pharmacological sensitivity to the TEA blocker; while Kv7.2 is highly sensitive to TEA, showing an  $IC_{50}=0.3$  mM, Kv7.3 is TEA-insensitive exhibiting an  $IC_{50}=30$  mM. On the other hand, heteromeric Kv7.2/7.3 channels show an intermediate sensitivity ( $IC_{50}=3$  mM) (Hadley et al., 2000). The high TEA sensitivity of Kv7.2 might result from the presence of a tyrosine residue in the pore loop of the channel (Kavanaugh et al., 1991), by contrast this residue is replaced by a threonine in Kv7.3 which may confers low sensitivity to TEA (MacKinnon et Yellen, 1990). The effect of TEA block has been investigated using a ramp protocol in which Kv7.2/Kv7.3 currents were activated by 3 s voltage ramps from  $-80$  to  $+20$  mV. As shown in Table 16, perfusion of 3 mM TEA in CHO transiently transfected with Kv7.2 and Kv7.3 induce a current inhibition at 0 mV of about  $56.01\pm0.06\%$  while in the selected clone 5 the inhibition current is about  $36\pm7\%$ , suggesting that both subunits are likely expressed, possibly with a slightly higher participation of Kv7.3 subunits (Figure 35).

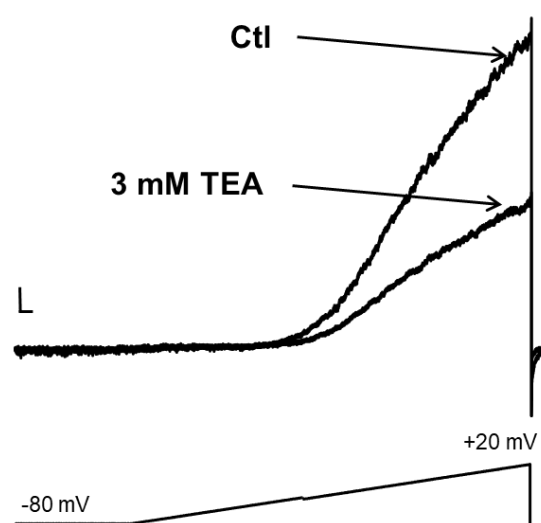


**Figure 35. Effects of TEA on ramp-evoked Kv7.2/Kv7.3 current.** Representative current traces from CHO cells stable expressing Kv7.2/Kv7.3 subunits in response to the indicated voltage ramp protocol before TEA exposure (CTL, control), during TEA exposure (TEA, 3 mM). Current scale, 100 pA; time scale, 0.1 s.



## Kv7.2

As we can see from the Table 16, cells transiently transfected with Kv7.2 generate a K<sup>+</sup> selective currents ( $22.9 \pm 4.5$  pA/pF) and exhibit a half-activation potential of  $-25.2 \pm 1.5$  mV. Among 4 clones, the selected clone number 1, show comparable  $V_{1/2}$   $-29.2 \pm 3.4$  mV and current density ( $13.7 \pm 3.8$  pA/pF) to transiently transfected with Kv7.2 (Figure 36).

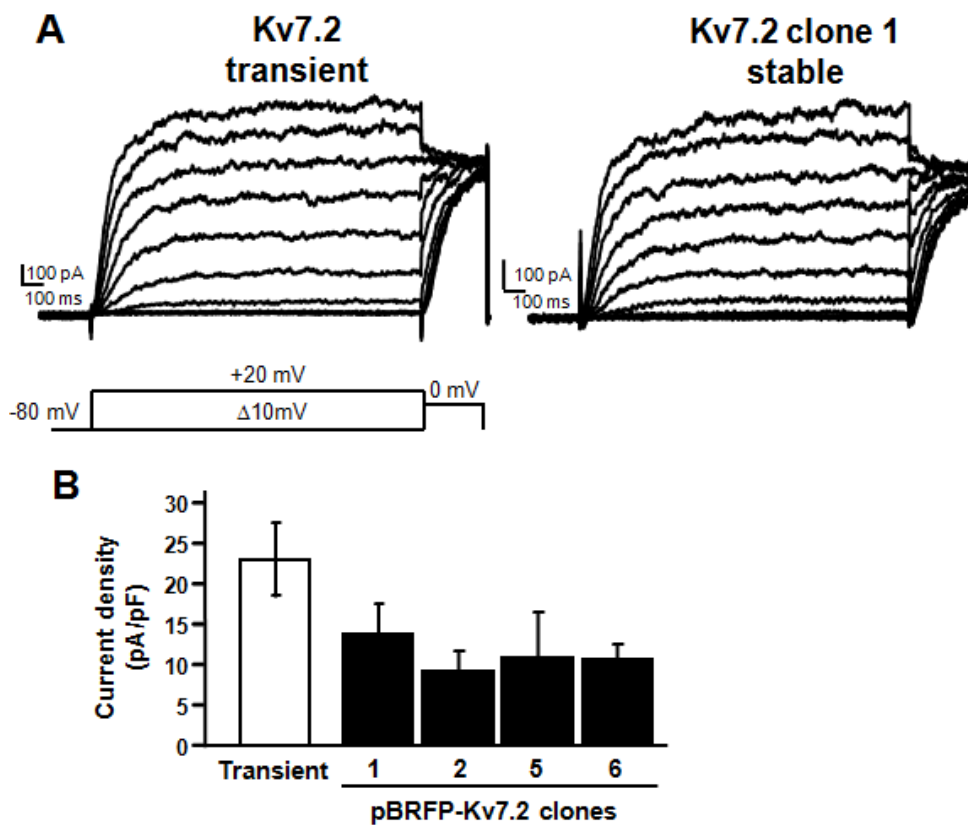


**Figure 36. Functional characterization of Kv7.2 stable cell lines.** Representative current traces recorded in CHO cells expressing, stably or transiently, the indicated subunits, in response to the voltage protocol shown in bottom part. Current scale, 100 pA; time scale, 0.1 s.

### Kv7.3 AND Kv7.3\*

Compared with other members of the family, Kv7.3 homomeric channels yield very small macroscopic currents. CHO transiently transfected, show current density at 0 mV of  $17.2 \pm 6.1$  pA/pF and a  $V_{1/2}$  of  $-36.4 \pm 2.3$  mV. Same results are also obtained for stable cell lines; the selected clone 1 exhibit a current density of  $-10.1 \pm 3.0$  pA/pF and a  $V_{1/2}$  of  $-44.8 \pm 1.6$  (Table 16; Figure 37).

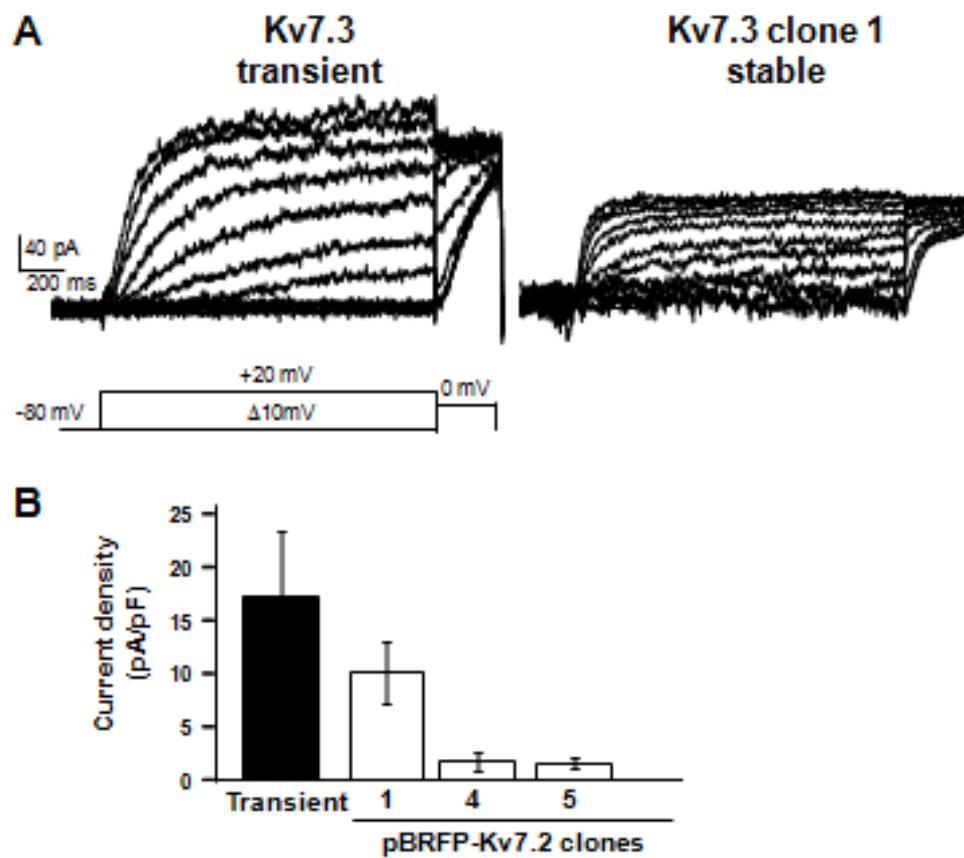


**Figure 37. Functional characterization of Kv7.3 stable cell lines.** Representative current traces recorded in CHO cells expressing, stably or transiently, the indicated subunits, in response to the voltage protocol shown in bottom part. Current scale, 50 pA; time scale, 0.1 s.

For this reason, we decided to generate stable cell lines carrying the mutant Kv7.3 A315T (Kv7.3\*), which has been demonstrated, to strongly increase the current density by nearly ~15-fold relative to Kv7.3 WT. In particular, the increased current amplitude is not relying on an increase in the expression of channels in the membrane but, to the stabilization of the selectivity filter (SF) in a conductive conformation by the creation of a network of H-bonds around I312 residue and van der Waals interactions with F344 residue triggered by the A/T substitution (Choveau et al., 2012). As shown in Table 16, the obtained Kv7.3\* stable cell lines showed similar current density and  $V_{1/2}$  values when compared to those measured in the control group (Figure 38).

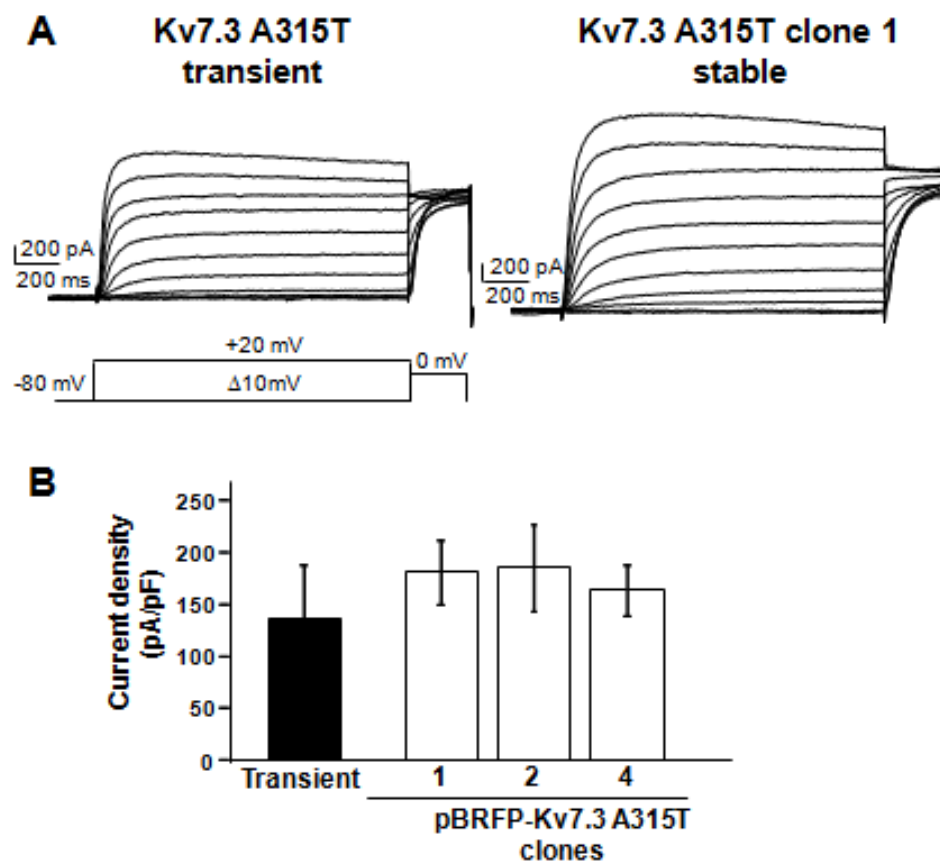


**Figure 38. Functional characterization of Kv7.3 A315T stable cell lines.** Representative current traces recorded in CHO cells expressing, stably or transiently, the indicated subunits, in response to the voltage protocol shown in bottom part. Current scale, 400 pA (for transient) 500 pA (for stable); time scale, 0.1 s.

## Kv7.4

Finally, among the six clones stably expressing Kv7.4 subunit, the selected clone 4, show similar current densities and  $V_{1/2}$  value when compared to those measured in the control group (Figure 39)

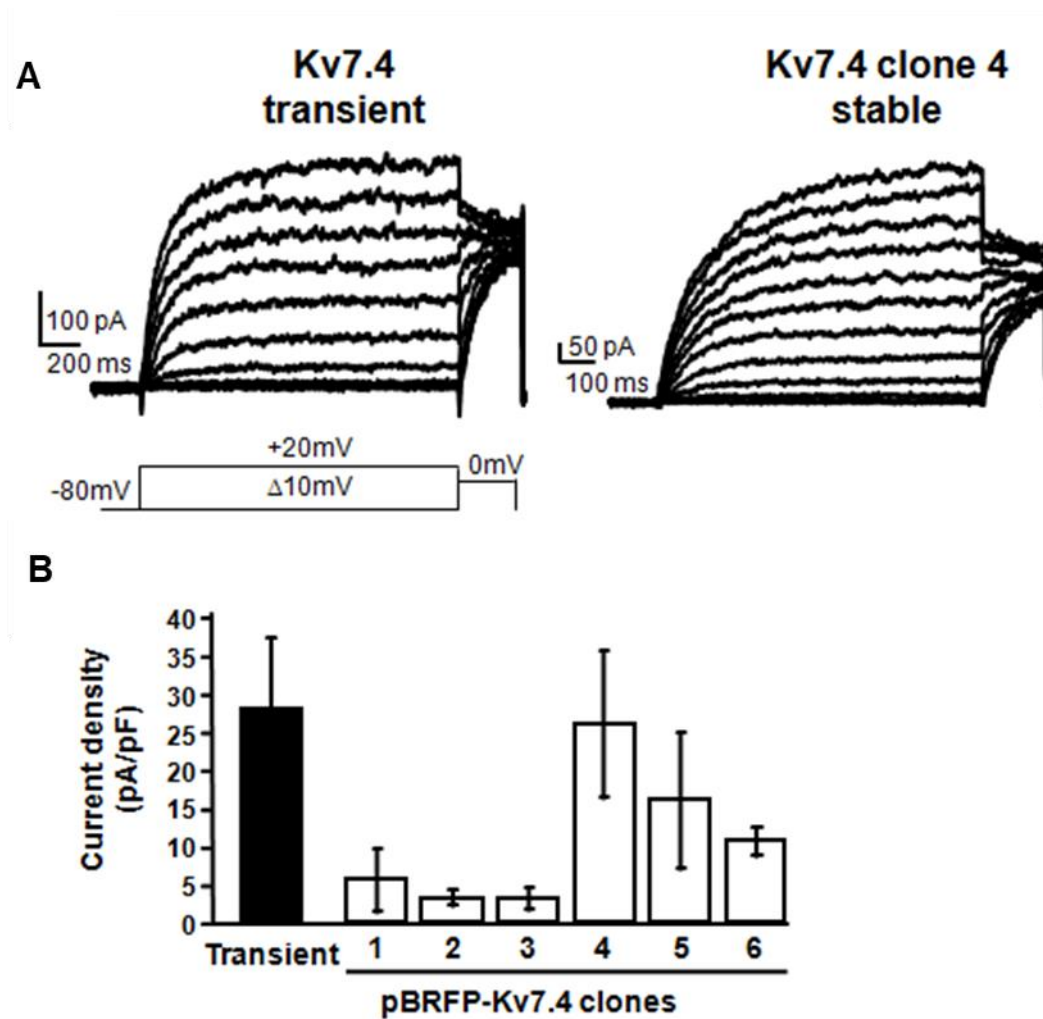


**Figure 39. Functional characterization of Kv7.4 stable cell lines.** Representative current traces recorded in CHO cells expressing, stably or transiently, the indicated subunits, in response to the voltage protocol shown in bottom part. Current scale, 50 pA; time scale, 0.1

**Table 16. Functional and pharmacological characteristic of stable and transient Kv7 cell lines.**

	n	V <sub>1/2</sub> (mV)	k (mV/efold)	Current density (pA/pF at 0 mV)	Blockade by 3mM TEA (%)
<b>pcDNA3-Kv7.2/Kv7.3</b>	16	-35.1±1.6	13.0±0.7	119.7±13.2	56.1±0.06
<b>pBRFP-Kv7.2/Kv7.3 cl.5</b>	12	-32.2±1.7	9.4±1.7	66.7±16.9	36±7
<b>pBRFP-Kv7.2</b>	13	-25.2±1.5	13.3±1.5	22.9±4.5	
<b>pBRFP-Kv7.2 cl.1</b>	7	-29.2±3.4	10.4±0.6	13.7±3.8	
<b>pBRFP-Kv7.3</b>	5-7	-36.4±2.3	8.2±0.6	17.2±6.1	
<b>pBRFP-Kv7.3 cl. 1</b>	9	-44.8±1.6	8.0±0.7	10.1±3.0	
<b>pBRFP-Kv7.3 A315T</b>	5-7	-39.3±3.0	8.9±0.8	132.3±50.5	
<b>pBRFP-Kv7.3 A315T cl. 1</b>	3-4	-41.1±4.0	9.6±1.6	179.2±31.6	
<b>pcDNA3-Kv7.4</b>	6	-30.8 ±2.7	13.1 ±0.6	28.0 ± 9.3	
<b>pBRFP-Kv7.4</b>	9	-24.2 ± 4.1	17.0 ± 2.9	25.9 ± 9.6	

TEA: tetraethylammonium. Student's t test. Each data is the mean-SEM of cells recorded in at least three separate experimental sessions.

For simplicity, in the next sections, the stable cell lines expressing Kv7.2/3, Kv7.4 and, Kv7.3A315T will be named CHO- Kv7.2/3, CHO- Kv7.4, CHO-Kv7.3\*, respectively.

## 4.7 Screening of the compound library

### 4.7.1 Effects of known Kv7 activators and inhibitor on fluorescence in CHO-Kv7.2/Kv7.3

In a first set of experiments, the effects of the Kv7 activator retigabine and of the inhibitor Xe991 were compared between CHO cells, that do not express Kv7 channels, and stable Kv7.2/Kv7.3 cell lines. As shown in Figure 40A, in control CHO cells both retigabine (10  $\mu$ M) and Xe991 (10  $\mu$ M) didn't modify the fluorescent signal. By contrast, in CHO-Kv7.2/Kv7.3 cells retigabine increased both the maximal fluorescence and the initial slope of the fluorescent signal; this effect is abolish in presence of Xe991 (Figure 40B).

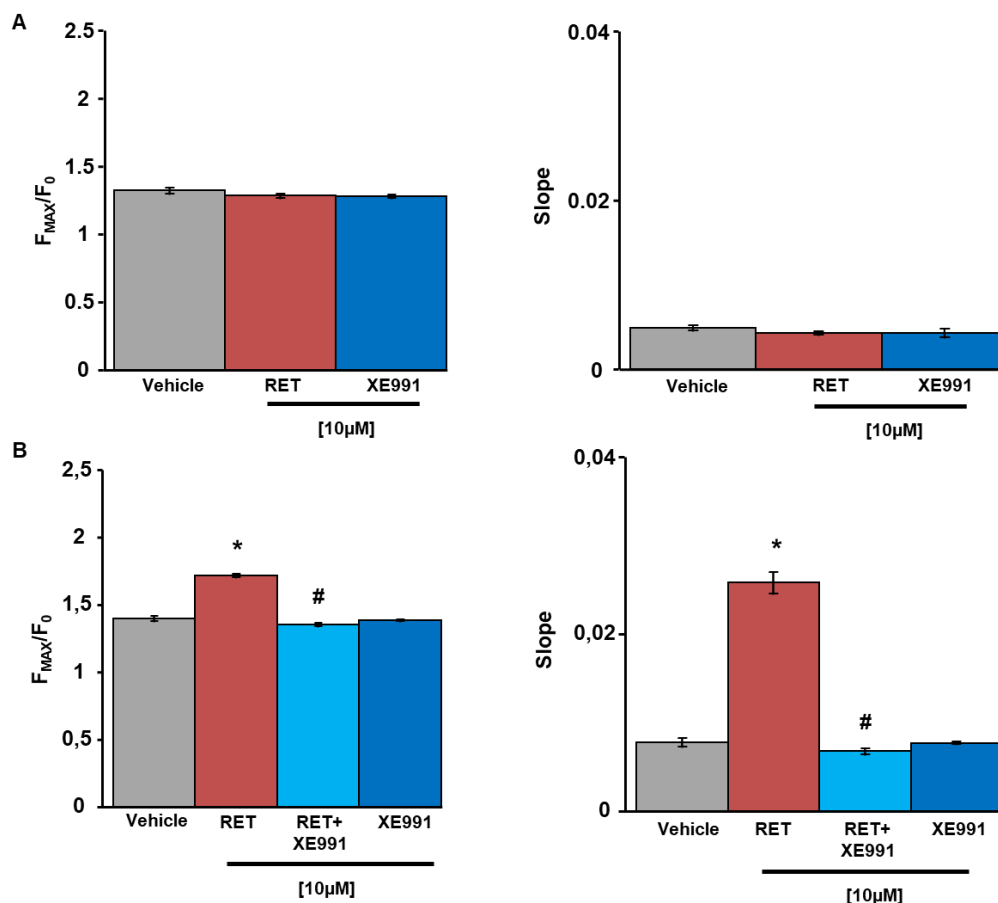


**Figure 40. Effects of retigabine and Xe991 on the fluorescent signal.** A) Effect of activator and inhibitor in CHO cells and B) in CHO-Kv7.2/Kv7.3 cells. \* $p < 0.05$  vs Vehicle; # $p < 0.05$  vs RET;  $n = 3$ . Vehicle; DMSO 1%

Moreover, in CHO-Kv7.2/Kv7.3 cells, retigabine (1 to 100  $\mu\text{M}$ ) dose-dependently increased both the maximal fluorescence and the initial slope of the fluorescent signal (Figure 41A). The calculated  $\text{EC}_{50}$  for retigabine was  $11 \pm 0.04 \mu\text{M}$ , a value slightly higher than that calculated by electrophysiological techniques ( $\text{EC}_{50} = 4.8 \pm 1.8 \mu\text{M}$ ) (Figure 41B).

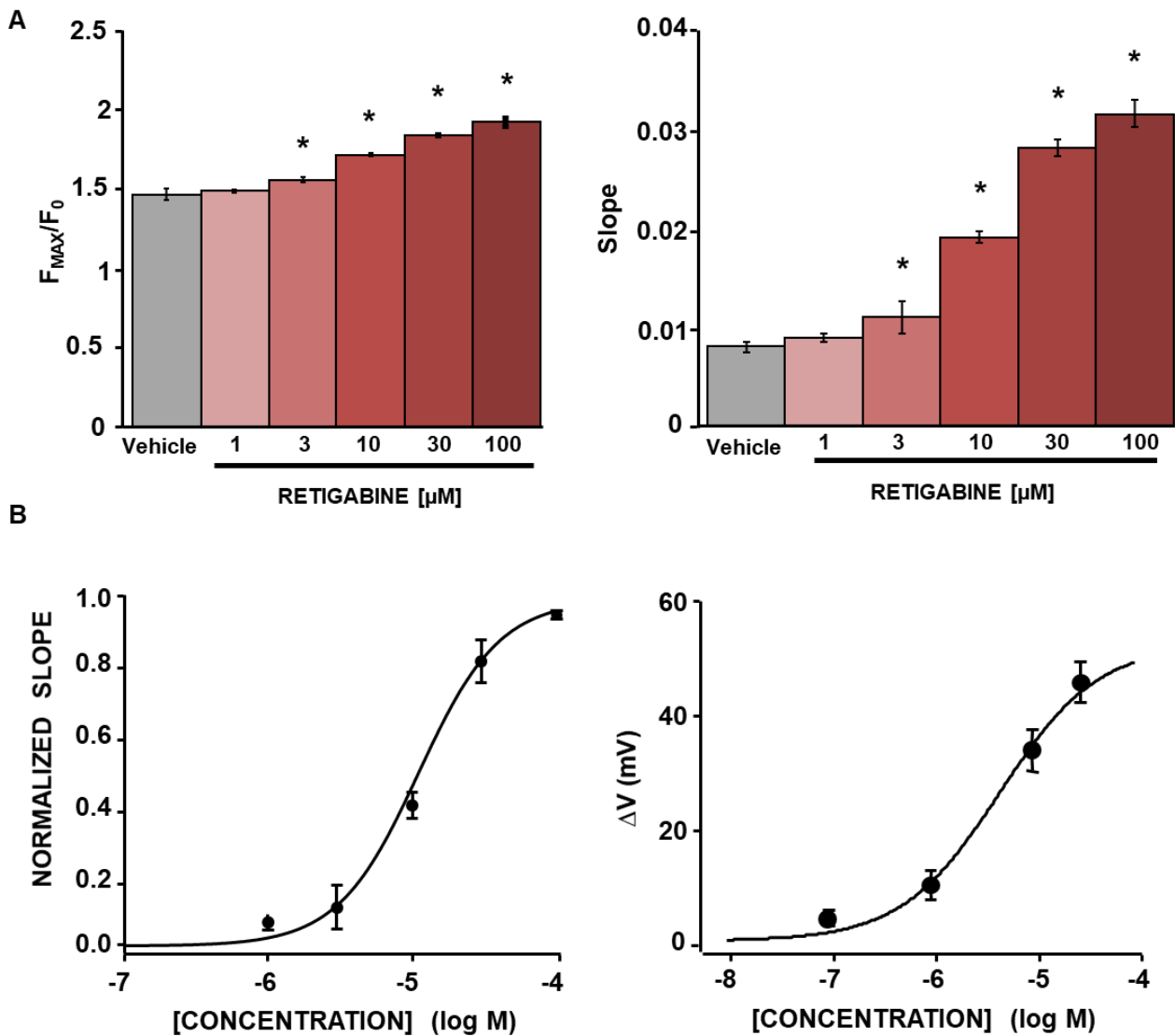


**Figure 41. A) Concentration-dependent effects of retigabine on stable Kv7.2/Kv7.3 cell lines. B) Comparison between the retigabine  $\text{EC}_{50}$  calculated on fluorescent (left) and electrophysiological (right) assays. \* $p < 0.05$  vs Vehicle;  $n = 3$ . Vehicle; DMSO 1%**

To evaluate the ability of the assay to detect compounds which have been described to act as more potent Kv7.2/3 activator when compared to retigabine, concentration-response curves of RL648\_81 were performed (Kumar et al., 2016). To this aim we synthesized, RL648\_81 is retigabine analogues previously described by Kumar and colleagues, as more potent and chemically stable than the reference compound. Here in the Fluxor assay, using concentration from 0.01 to 100  $\mu$ M, RL648\_81 dose-dependently increased both slope and maximal fluorescence (Figure 42A). The compound test resulted more potent; in fact, the calculated  $EC_{50}$  was  $1.2 \pm 0.2$   $\mu$ M, a value lower than that calculated for the control retigabine  $7.2 \pm 1.9$   $\mu$ M (Figure 42B).

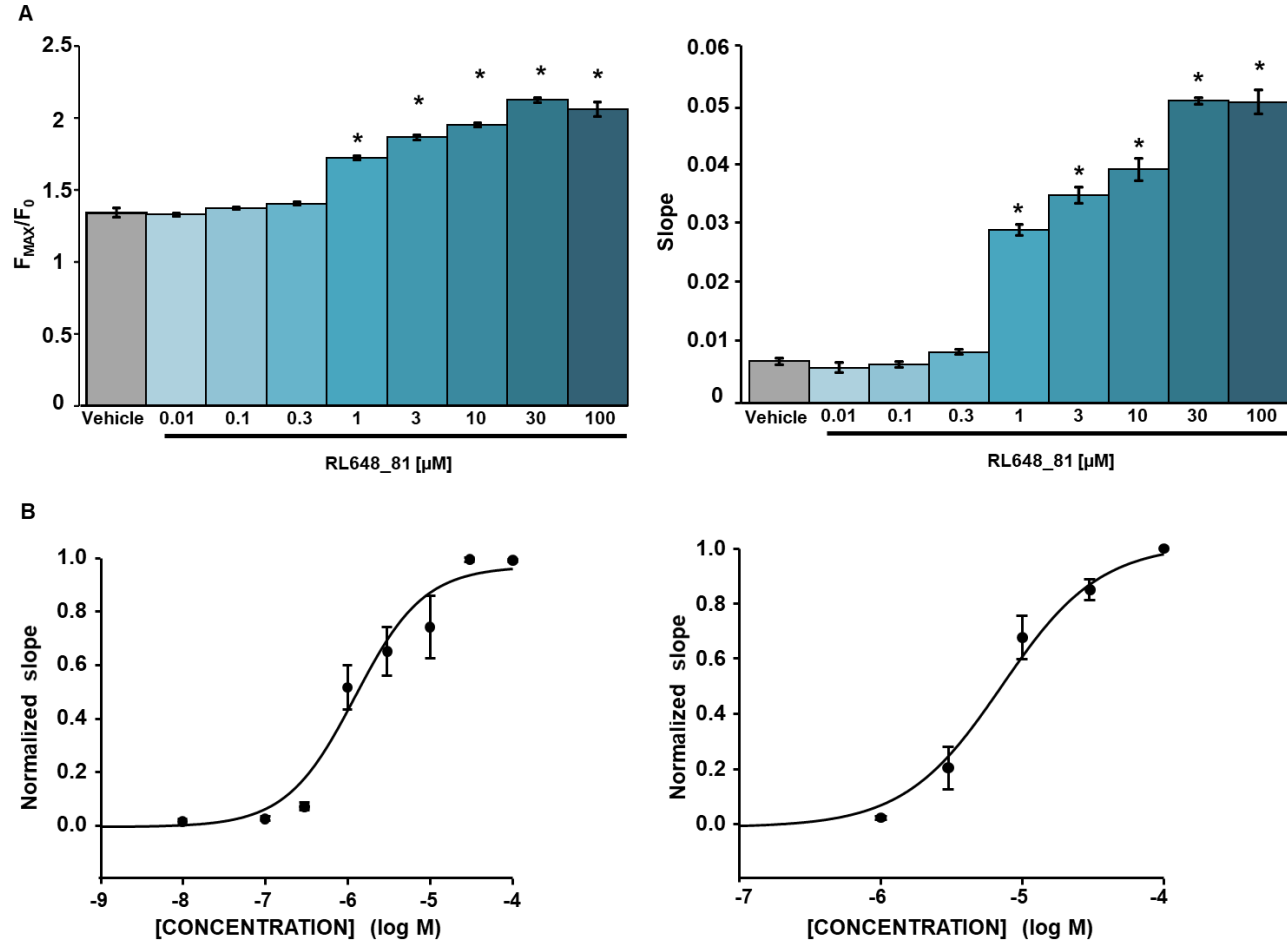
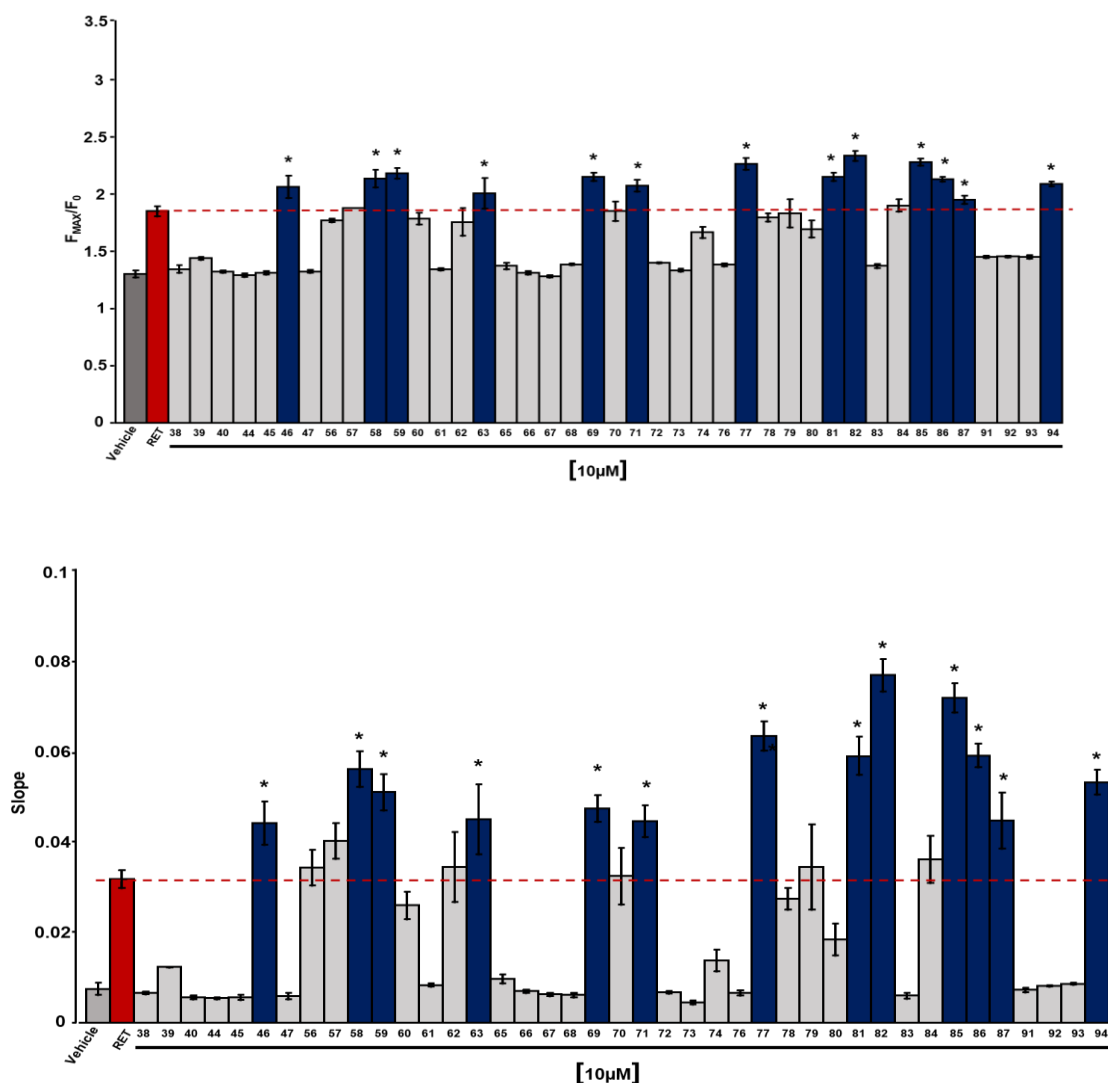


**Figure 42. A) Concentration-dependent effects of RL648\_81 on stable Kv7.2/Kv7.3 cell lines. B) Comparison between the RL648\_81 (left) and retigabine (right)  $EC_{50}$ s calculated on fluorescent assay.**  
 \* $p < 0.05$  vs DMSO 0.1%;  $n = 3$



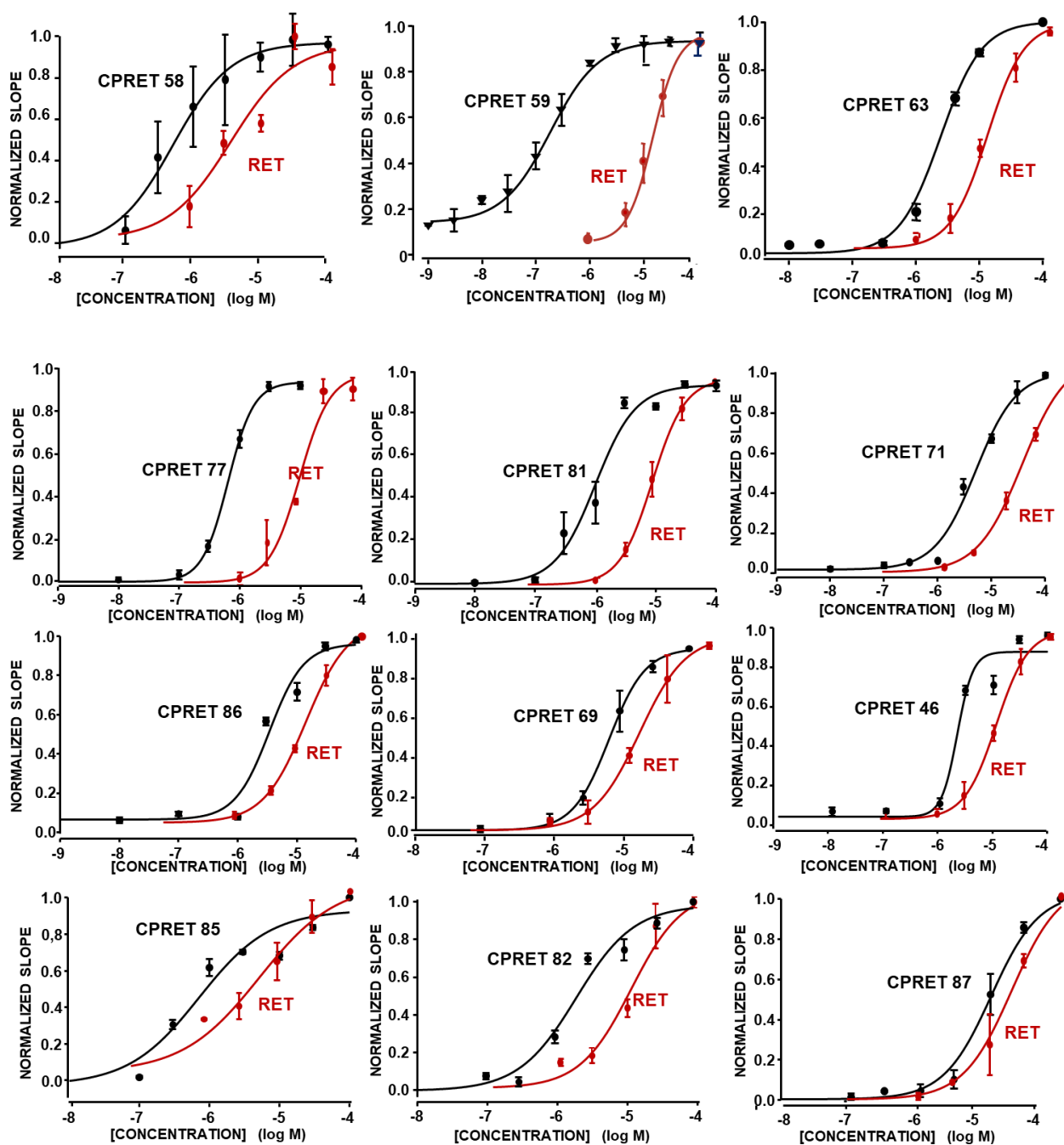
#### 4.7.2 Library screening on CHO-Kv7.2/Kv7.3

The fluorescence assay has been than used to evaluate the activity of 41 retigabine derivatives, structurally characterized by one or more modifications as described above. A 10  $\mu$ M concentration was used to evaluate the activity of each drug; as a reference, we used the same concentration for retigabine. Of the 41 tested compounds, thirteen derivatives (CPRET-46-58-59-63-69-71-77-81-82-85-86-87-94) results more effective than retigabine in terms of both maximal fluorescence and initial slope of the fluorescent signal (Figure 43). To evaluate the robustness of the assay the Z'factor value (see *Materials and Methods*) was calculated, resulting  $\geq 0.5$ , consistent whit the assay quality requirement.



**Figure 43. Effect of retigabine derivatives at 10  $\mu$ M on stable Kv7.2/Kv7.3 cell lines.** \*  $p < 0.05$  vs RET; n=3 Vehicle; DMSO 1%

For these 13 compounds concentration-responses curves experiments for the control retigabine and for the derivatives were performed (Figure 44). As we can see from the Table 17, all derivatives tested appeared about 5-10 times more potent than retigabine.



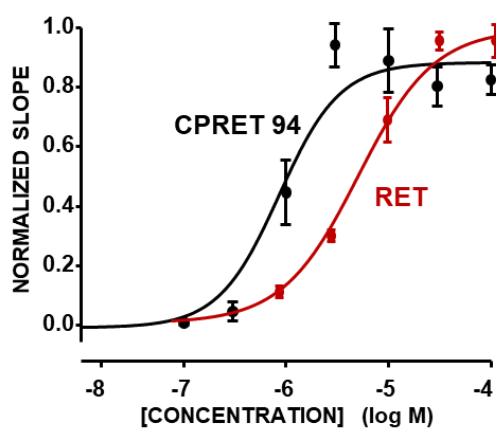
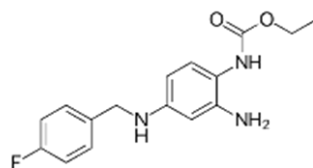


Figure 44. Dose–response curve for RET- and CPRET derivatives-induced slope of the Fluxor signal.

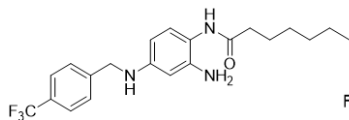
Table 17. EC<sub>50</sub> of retigabine derivatives on Kv7.2/Kv7.3 channels

DERIVATIVES	EC <sub>50</sub> ; [μM]	
	CP RET	RET control
46	2,1± 0,5	11 ± 0,4
58	0.7±0.2	3,5 ±2,5
59	0.17±0.8	4,6±1,2
63	2,2±0.5	11 ± 0.4
69	7,05±0,5	13,3± 1,2
71	5,1 ±1	17,9 ± 3,9
77	0,6 ± 0,03	11 ± 3,8
81	0,9±0,2	9,8±0,5
82	2,0 ± 0,7	11,3 ± 5
85	0,7 ± 0,4	5,7±3,4
86	3,4 ±1,01	14,5±0,8
87	10,0 ± 1,9	16,7 ± 4,5
94	0,8 ± 0,3	5,3± 1,3

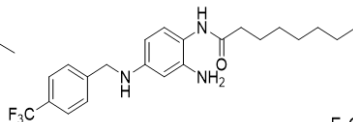
# RETIGABINE



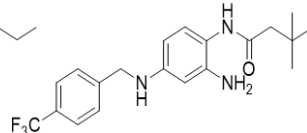
**CP RET 46**



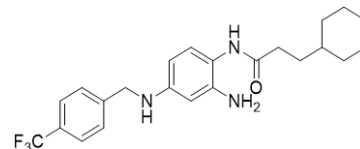
**CP RET 58**



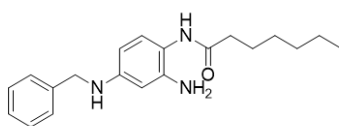
**CP RET 59**



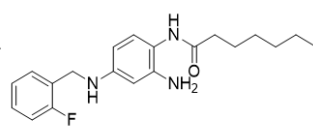
**CP RET 63**



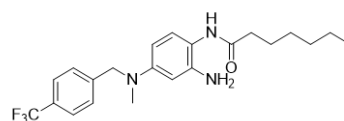
**CP RET 69**



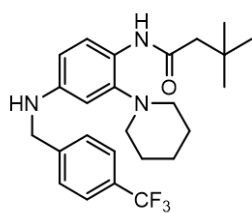
**CP RET 71**



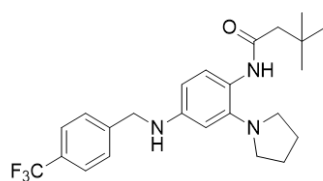
**CP RET 77**



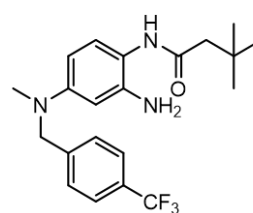
**CP RET 81**



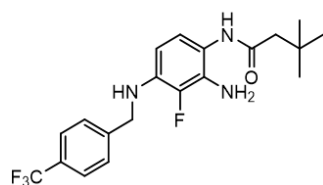
**CP RET 82**



**CP RET 85**



**CP RET 86**



**CP RET 87**

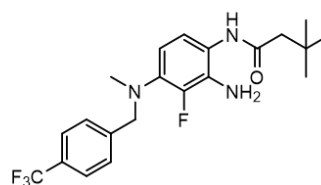


**Figure 45. Structures of more potent retigabine derivatives (PCT/EP200/052156).**

#### 4.7.3 Electrophysiological characterization of CP RET 46, 59, 63, and 86 on Kv7.2/Kv7.3 channels.

The effects of some of the retigabine derivatives were also evaluated on Kv7.2+Kv7.3 currents by means of whole-cell patch-clamp electrophysiological experiments in mammalian CHO cells transiently transfected with Kv7.2+Kv7.3 cDNA. The effect of these compounds was investigated using increasing drug concentrations (0.1, 1, 10, 30 and 100  $\mu$ M), using a voltage-clamp protocol in which Kv7.2+Kv7.3 currents were activated by depolarizing steps from -120/-80 to +20 mV, followed by an isopotential pulse at 0 mV.

Application of 1  $\mu$ M retigabine caused a leftward shift of about 15 mV in the half-activation voltage ( $V_{1/2}$ ) of Kv7.2+Kv7.3 currents (Figure 46 A-B) with no change in the maximal current, whereas the same concentration CPRET-46, -59, -63, and -86 caused a marked leftward shift in the  $V_{1/2}$  and a significant increase of maximal current. The calculated  $V_{1/2}$  was  $-26.4 \pm 0.6$ ,  $-40.4 \pm 0.2$ ,  $-89.0 \pm 2.6$ ,  $-80.2 \pm 0.6$  and  $-82.3 \pm 0.4$  for control retigabine, CP RET 46, 59, 63, and 86, respectively (Figure 46 A-B). To quantify the potency of the tested compounds, we measured the shift in  $V_{1/2}$  ( $\Delta V_{1/2}$ ) at increasing concentrations and used a Hill equation fit to calculate their  $EC_{50}$ . The results obtained demonstrate that all four derivatives were 12-14 times more potent than RET. Indeed, the calculated  $EC_{50}$  was  $4.8 \pm 1.8$ ,  $0.39 \pm 0.02$ ,  $0.19 \pm 0.03$ ,  $0.28 \pm 0.04$  and  $0.12 \pm 0.04$  for retigabine, CP RET 46, 59, 63, and 86, respectively.

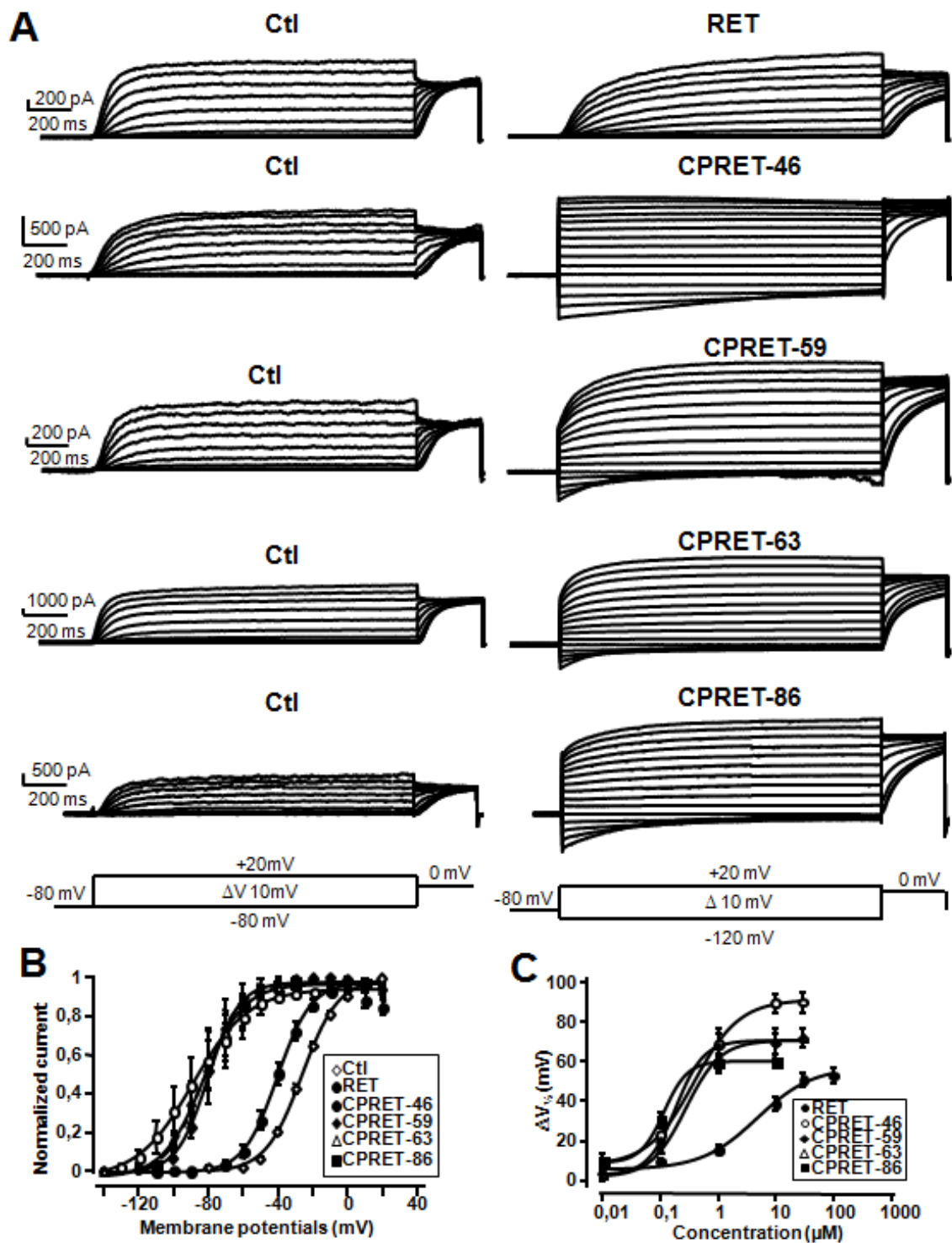


**Figure 46. Effect of RET and CPRET 46, 59, 63 and 86 on Kv7.2/Kv7.3 currents.** (A) Representative macroscopic current traces recorded from a CHO cell co-expressing Kv7.2 and Kv7.3 channel subunits in response to the indicated voltage protocol before and after application of 1  $\mu$ M RET, CPRET 46, 59, 63 and 86. (B) Kv7.2/Kv7.3 current/voltage curves before and after application of 1  $\mu$ M RET, CPRET 46, 59, 63 and 86. (C) Dose-response curve for 1  $\mu$ M RET, CPRET 46, 59, 63 and 86-induced  $\Delta V_{1/2}$  shift.

#### 4.7.4 Photostability Assays

One of the major pitfalls of retigabine is its chemical photo instability, resulting in dimers formation responsible for muco-cutaneous blue-grey discolorations in patient under chronic therapy. Recently, phenazinium, phenazine, and benzimidazole dimers of retigabine with high melanin affinity have been detected using MALDI mass spectrometry in the corneal tissue (Groseclose and Castellino et al., 2019). Considering that premise, always in collaboration with the Department of Pharmacy of the University of Salerno, compound that resulted more potent than retigabine in the fluorescence assay, were subjected to photostability assays.

Initially, an UV quartz cuvette containing an aqueous solution of RET or CPRET (10  $\mu$ M) was irradiated by an UV lamp for 3 h. After exposure, aliquot of the solution was withdrawn and analysed by HPLC to assess the concentration decrease of the starting materials and the presence of the dimers formed by retigabine.

Exposure to UV light led to significant photodegradation of retigabine; about  $63.3 \pm 0.1\%$  was degraded after 3 h. Similar % of photodegradation was show by CPRET 63, 77 whereas remarkable or almost complete degradation were obtained for CPRET 59,71,81,82,85,87 and 94. Finally, derivatives 46, 69 and 86 were the most photostable retigabine analogues (Table 18).

We then decided to further investigate the photodegradative behaviour of CPRET compounds and the control retigabine by analysing the corresponding by-products. Considering that the typical absorbance of retigabine photoinduced dimers is 550 nm, we decided to set the same wavelength for the UV detection. Compared to retigabine, the only derivatives which was not able to generate dimers were the CPRET 77,81,82,85,86,87 suggesting that the structural modification at the aniline group or at NH-linker, that characterized these compounds, was able to reduce the dimerization reaction (Figure 47).

**Table 18. Photoinduced degradation of retigabine and its derivatives under UV light.** Results are expressed as percentage of degradation  $\pm$  sd.

DERIVATIVE	TIME (3H) % OF DEGRADATION	DIMERS
46	30.6 $\pm$ 2.2	YES
59	79.8 $\pm$ 4.2	YES
63	64.8 $\pm$ 0.9	YES
69	19.5 $\pm$ 4.7	YES
71	74.9 $\pm$ 0.1	YES
94	98.4 $\pm$ 0.2	YES
77	63.3 $\pm$ 2.8	NO
81	98.0 $\pm$ 0.1	NO
85	99.5 $\pm$ 0.1	NO
86	34.8 $\pm$ 1.8	NO
82	97.7 $\pm$ 1	NO
87	86.5 $\pm$ 0.8	NO

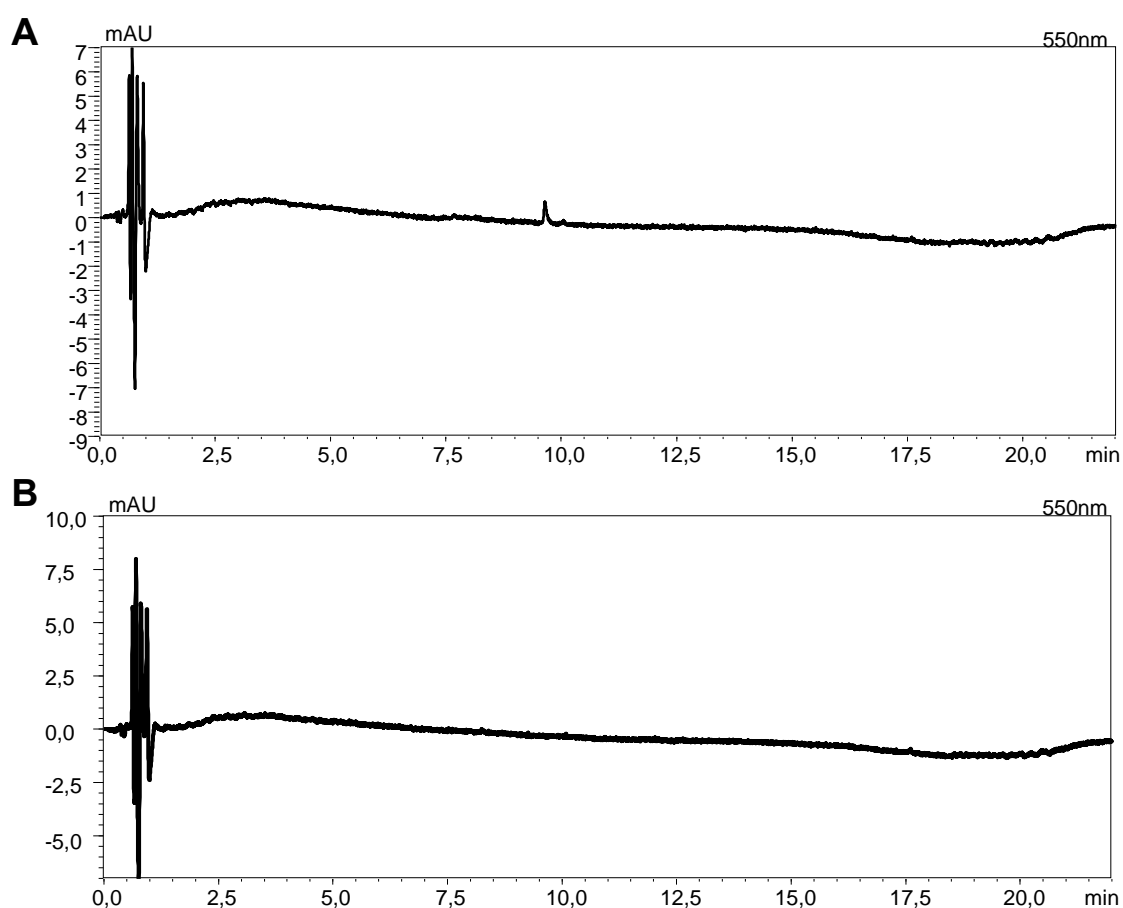


**Figure 47. HPLC trace of retigabine (A) and CP RET 86 (B).** Typical dimer peak is present in HPCL trace of retigabine (A) with a retention time between 7.00- and 10.00-min.



#### 4.7.5 Library screening on CHO-Kv7.4

The effect of retigabine derivatives was also investigated on Kv7.4 channels. Of the 41 tested compounds, at concentration 10  $\mu$ M, sixteen derivatives (CPRET-46-56-57-58-59-63-69-70-71-77-80-81-82-85-86-87) resulted more effective than retigabine in terms of both maximal fluorescence increase and initial enhancement of the slope of the fluorescent signal (Figure 48). The calculated Z' factor value resulted  $\leq 0.5$ , suggesting that the assay condition need to be further optimized.

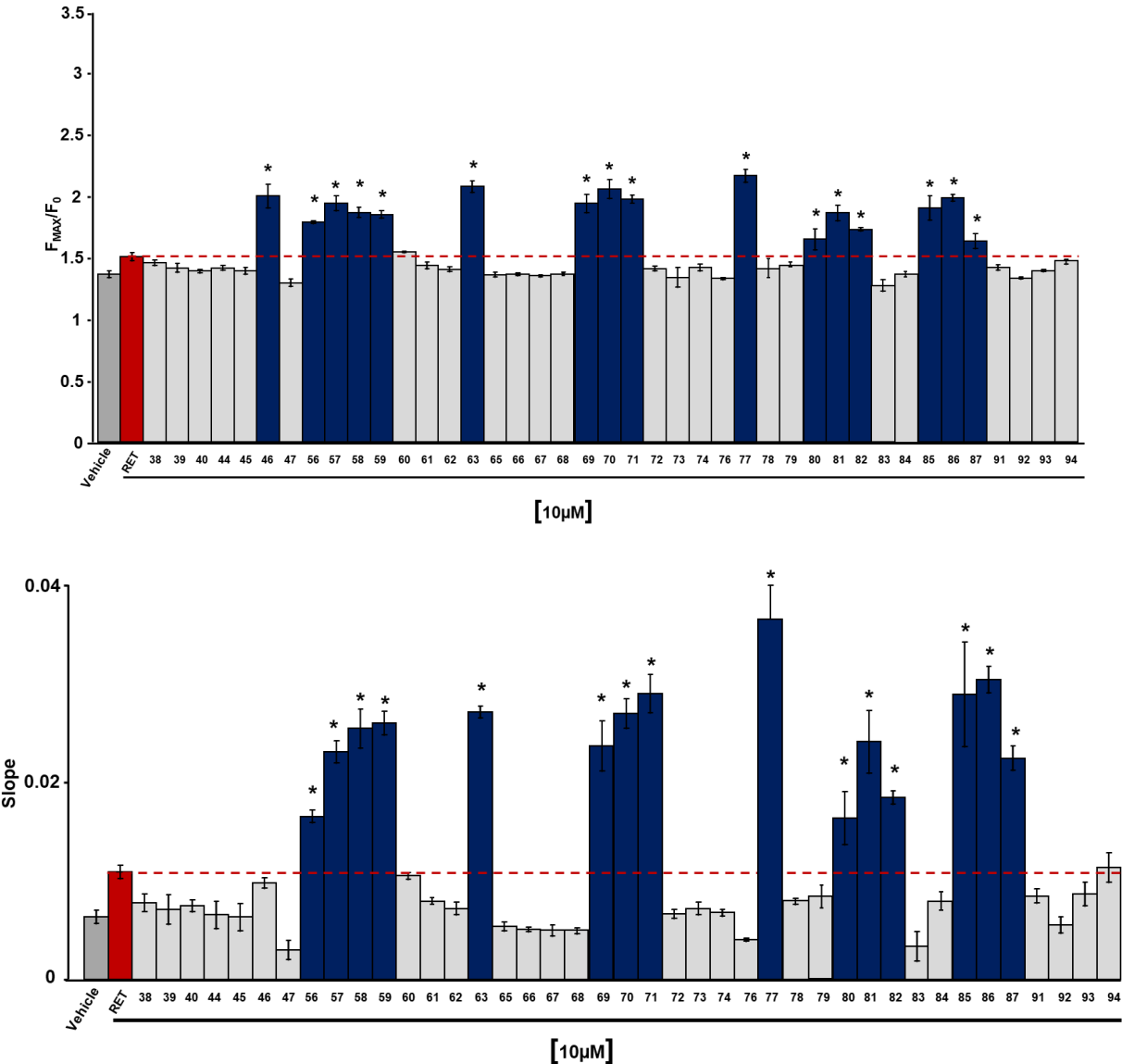


**Figure 48. Effect of retigabine derivatives at 10  $\mu$ M on stable Kv7.4 cell lines.** \*  $p < 0.05$  vs RET;  $n=3$ ; Vehicle; DMSO 1%

According to previous described photostability experiments, we quantify the potency of the compounds unable to form dimers. The calculated EC<sub>50</sub> for the CP RET 77, 81, 82, 85, 86,87 indicated that these compounds were about 5/10-times more potent than retigabine on Kv7.4 channels (Figure 49; Table 19)

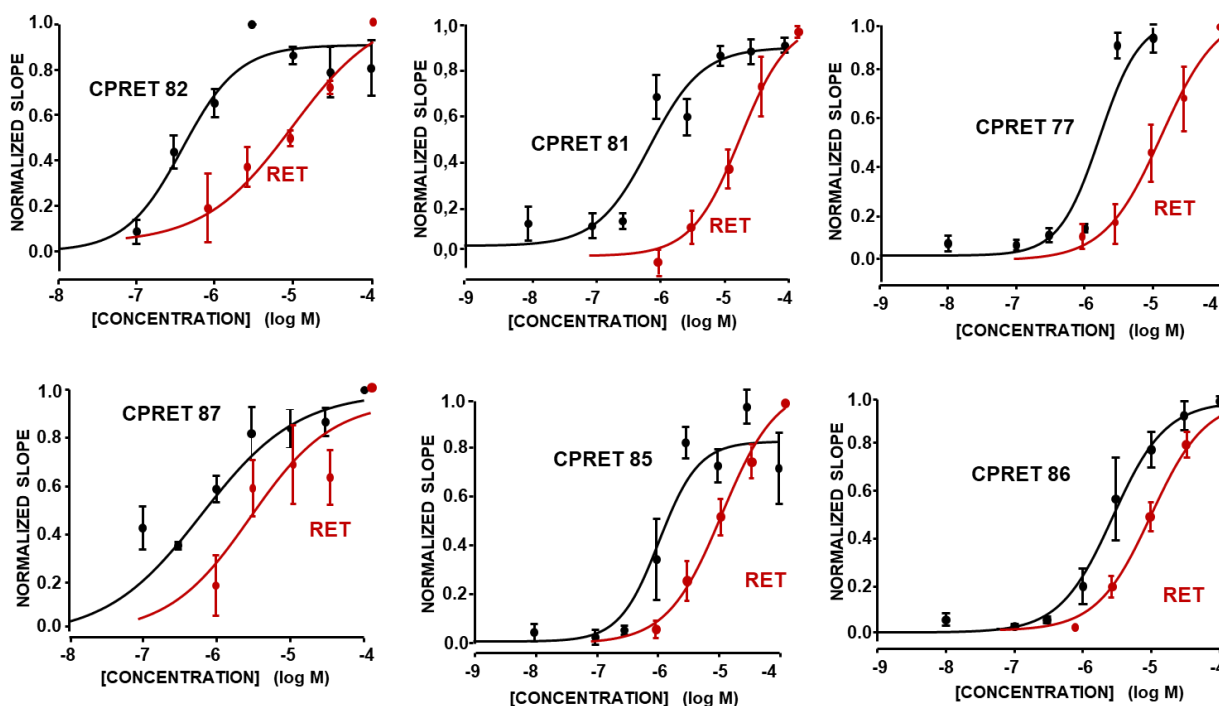


Figure 49. Dose-response curve for RET- and CP RET derivatives-induced slope of the Fluxor signal.

Table 19. EC<sub>50</sub> of retigabine derivatives on Kv7.4 channels

DERIVATIVE	EC <sub>50</sub> ; [μM]	
	CPRET	RET control
77	1.6 ± 1.3	14 ± 2.5
81	0.8 ± 0.3	14.7 ± 1.3
82	0.3 ± 0.2	10.5 ± 1
85	1.1 ± 0.4	10.4 ± 3.8
86	2.7 ± 0.4	9.9 ± 1.7
87	0.6 ± 0.4	2.8 ± 3.4

By comparing the EC<sub>50</sub> values of CP RET 77, 81, 82, 85, 86,87 and the mean of the EC<sub>50</sub> values of retigabine calculated on CHO-Kv7.2/Kv7.3 and CHO-Kv7.4 (Figure 50), we can observe that there were no statistically significant differences between the EC<sub>50</sub> values calculated, for both compounds except CP 87, on CHO-Kv7.2/Kv7.3 and CHO-Kv7.4. These results suggest that the selective prolife for CP 77 was Kv7.2/3=Kv7.4; for CP 81 was Kv7.4=Kv7.2/3; for CP 82 was Kv7.4=Kv7.2/3; for CP 85 was Kv7.4=Kv7.2/3; for CP 86 was Kv7.4=Kv7.2/3; for CP 87 was Kv7.4> Kv7.2/3.

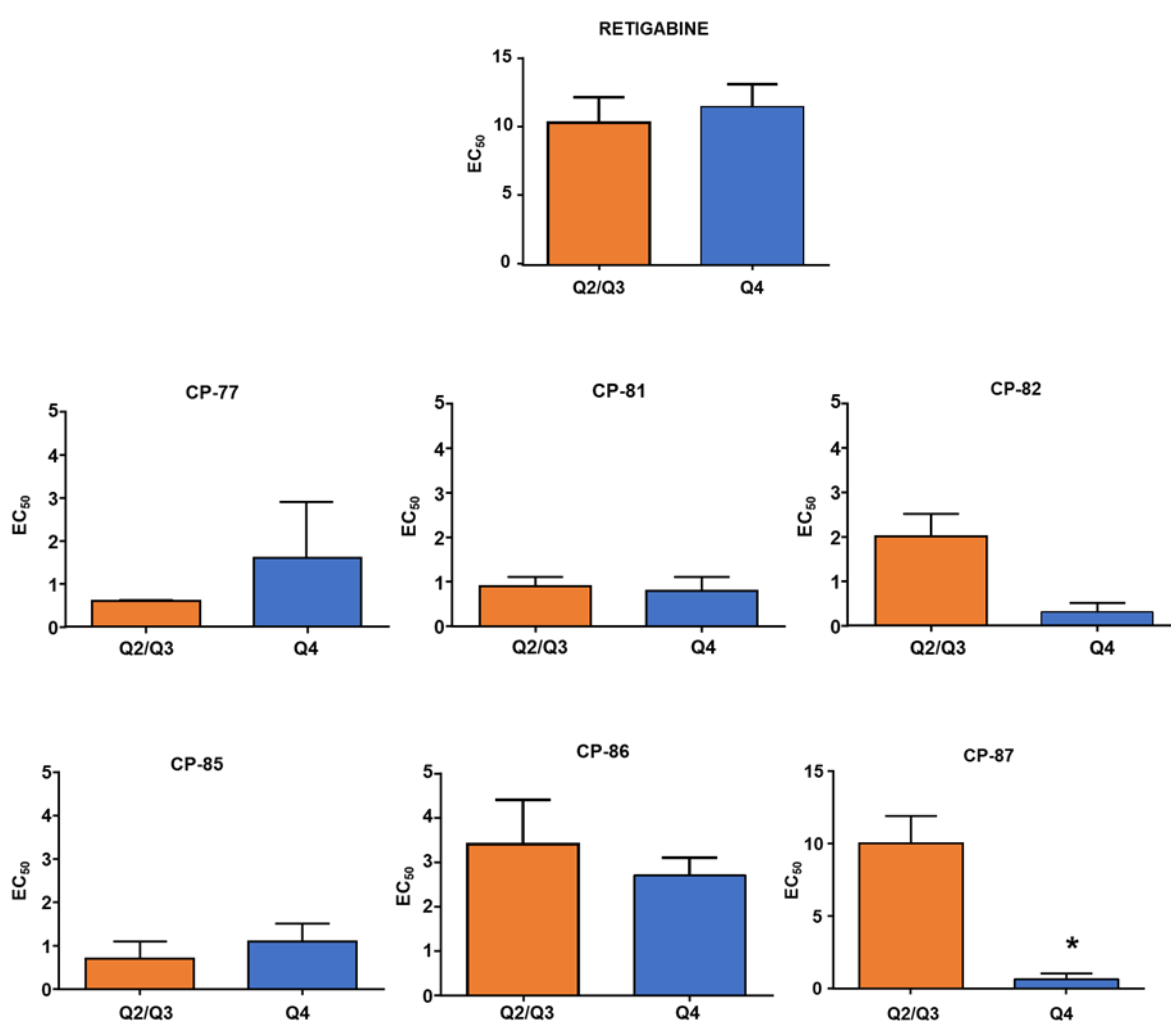
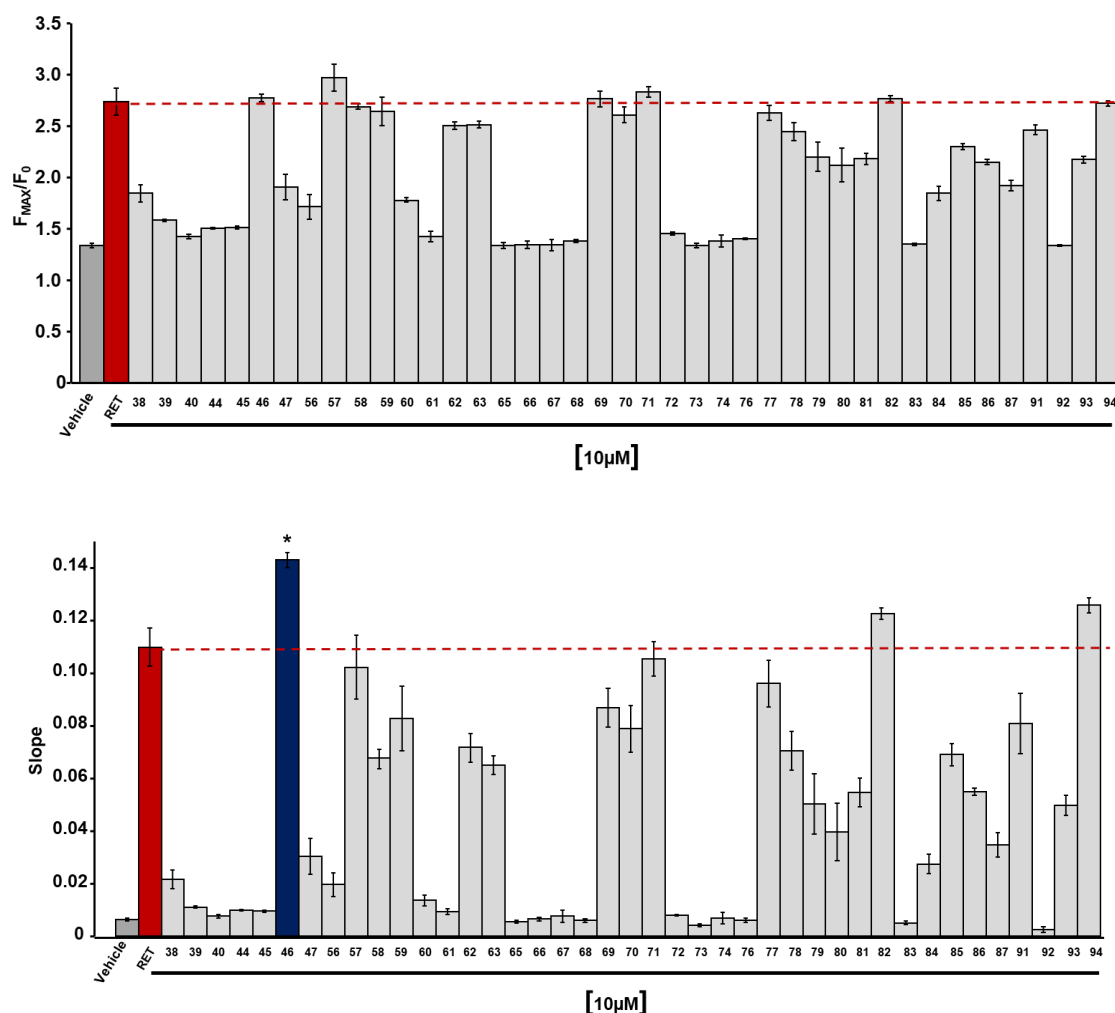


Figure 50 Comparison between the EC<sub>50</sub> values CP RETs and RET control calculated on Kv7.2/3 and Kv7.4 (CP<sub>s</sub> n=3; RET n=6; \*p< 0,05).

#### 4.7.6 Library screening on CHO-Kv7.3\*

Finally, retigabine derivatives were also studied on Kv7.3\* channels.

Considering the  $F_0/F_{\max}$  parameter, none of the derivatives resulted more effective, at concentration 10  $\mu$ M, than retigabine whereas regarding the slope of the fluorescence curve, only the CP46 appeared more effective than control. Nevertheless, for most of these, in particular for the CPRET-46-57-58-59-62-63-69-70-71-77-78-79-80-81-82-85-86-91-94 the effect on the maximal fluorescence was similar to retigabine while only the CPRET-57-69-71-77-94 exhibited an effect in terms of slope similar to the reference compound (Figure 50). The calculated Z' factor was  $\geq 0.5$ .



**Figure 51. Effect of retigabine derivatives at 10  $\mu$ M on stable Kv7.3\* cell lines.** \*  $p < 0.05$  vs RET;  $n = 3$   
Vehicle; DMSO 1%

## 5 Discussion and conclusion

Epilepsy is a complex neurological disorder that affects ~50 million people worldwide. Epilepsy can be acquired as a result of an insult to the brain such as trauma, infection, stroke or a tumour, or can result from a genetic mutation in one or more of the ion channel or neurotransmitter genes or proteins that control brain excitability. Despite the development of novel anticonvulsant drugs (AEDs), the proportion of epilepsy patients with drug resistant epilepsies has remained stable at 30%, making necessary the identification of new molecular targets that may lead to the discovery of novel drugs to treat drug resistant epilepsy. In particular, Kv7 potassium channels represent an attractive pharmacological target for several neurologic disorder, including epilepsy. Retigabine, the first antiepileptic drug acting on Kv7 channels and approved as an add-on treatment for drug-resistant partial onset seizures with or without secondary generalization in adults. Retigabine enhances the M-current activation through the voltage-gated K<sup>+</sup> channel Kv7; this action is unique compared with the existing AEDs and highlight the advantages of exploring alternative targets for the control of seizures. Unfortunately, post-marketing studies revealed that chronic treatment produced retinal and mucocutaneous blue-grey discoloration.

The long-term outcome of this side effect is currently unknown; in particular, is not yet clear if these alterations are permanent and if pigment changes in the retina are possible cause of vision damage. Additionally, retigabine cause urinary retention, probably because it activates KCNQ4, a potassium channel belonging to the same family of KCNQ2, expressed in the smooth muscle of the bladder, where it regulates contractility.

## **5.1 Evaluation of retigabine binding mode and refinement of ligand binding site**

On Kv7 channels, retigabine binds a small hydrophobic pocket located between the segments S5 and S6; here a tryptophan (W) residue, present at the end of the S5 segment (W236 or W265 according to Kv7.2 or Kv7.3 sequence, respectively) was found to be crucial for the retigabine effect. Substitution of this residue with a leucine resulted in a complete loss ability of retigabine to activate Kv7.2 currents (Schenzer et al., 2005; Wuttke et al., 2005). Originally rationalized as generic hydrophobic contact between the fluorophenyl ring of retigabine and the aromatic side chain of the tryptophan residue (Lange et al 2009), more recent studies have demonstrated the ability of the carbamate group of retigabine to establish an H-bond interaction with the tryptophan residue in the channel pore (Kim et al 2015). Currently, this hypothesis has been confirmed by the two Cryo-EM structures of the human Kv7.2 and Kv7.4 channels in complex with retigabine Li X et al., 2020; Li T et al., 2020).

Our docking studies have demonstrated that retigabine was able to form a hydrogen bond with the W236 present in the binding site; particularly, the interaction occurred between the carbamate group of the ligand and the side chain of tryptophan residue. Therefore, the binding mode obtained, correspond to those firstly described by Kim et al. and recently confirmed by the two hKCNQ2<sub>EM</sub> and hKCNQ4<sub>EM</sub> structures in complex with retigabine.

However, even though different scaling condition were used to decrease penalties of close contacts, unoptimal contacts were observed between the ligand and the residues of the binding sites; this results from the fact that we started from the basic assumption of a rigid receptor. For this reason, to consider the flexibility of the receptor and the conformational changes that occur upon ligand binding, and therefore to improve the poses of the ligand, the InducedFit Docking protocol has been applied. Hence, better retigabine poses and absence of unfavourable interactions were obtained.

To verify the reliability of the poses obtained, it has been necessary to submit them to molecular dynamic simulations. The first MD simulations performed considered the Apo form (without ligand) in order to assess the stability of the system and identify the ideal conditions to be applied to the Holo form (with the ligand retigabine docked in his binding site). Analysis of 11 MD simulations performed on the Apo form has demonstrated that; I) simulation times of 100ns are reasonable for the system to reach stability. II) Visual inspection analysis has demonstrated that the solvent molecules never interpose between the protein and the lipids, furthermore, the application of the Grand canonical Monte Carlo (GCMC) determines a better water distribution, filling the empty spaces. The optimal condition includes POPC bilayer, SPC water model, Periodic Boundary Conditions orthorhombic box, System neutralization  $\text{Na}^+$  and  $\text{Cl}^-$  ions 0.15 M, statistical ensemble Np $\gamma$ t, simulation time 100ns, GCMG.

Subsequently, MD simulations of the top docking pose for each retigabine binding site obtained by InducedFit, were performed. Trajectories analysis showed good stability of protein, protein-ligand complex, and ligand, in all systems simulated. Particularly interesting was the behaviour of the ligand; fluctuation in RMSD values of retigabine was due to rotation of fluorophenyl moiety, which may adopt two different conformations. Interestingly, retigabine was able to establish persistent interactions with residues that are known to be crucial for the retigabine activity like; Trp236, Leu275, Leu299 and with residue never described before such as Ser303, Phe304, Phe305. It is not surprising that in the four subunits, the obtained protein-ligand interactions types, and the duration of the specific interaction during the simulation were not identical. This is because, MD simulations were performed starting from four different docking poses. Besides, it is important to highlight that MD simulations are inherently chaotic. Even the same input files, run on the same machines, may not produce an identical trajectory. The important thing is that different simulations should converge to the same ensemble average properties.

According to these results, we decided to focus our attention on the S303 residue. In our model, the aniline group of retigabine was able to form a H-bond with the serine side chain at position 303, located at the end of the S6 segment.

To assess the role of the serine residue, mutagenesis experiments were performed; the residue was substituted with an alanine, which is not able to act either as an acceptor or as a donor of H-bonds. Whole-cell patch-clamp electrophysiological recordings performed on CHO cells transiently transfected with the Kv7.2-S303A and Kv7.2 WT demonstrated that the mutant was functional and exhibited a  $V_{1/2}$  and a slope values similar to the WT. By contrast the mutant showed a reduced current density compared to those calculated for the WT.

Application of increasing retigabine concentrations determined a different effect in Kv7.2-S303A and Kv7.2 WT. In both cases retigabine induced a dose-dependent leftward shift in the voltage-dependence; at 10  $\mu$ M concentration, in the WT, the calculated  $\Delta V$  was  $-18,6 \pm 2,3$ , while in the mutant  $-26,8 \pm 0,5$ . Moreover, retigabine, elicited only a slight increase of current at depolarized potential in Kv7.2 WT channels, whereas a marked increase in the current size at depolarized potentials was observed in Kv7.2-S303A.

The calculated  $EC_{50}$  of retigabine on Kv7.2 WT and Kv7.2 S303A current activation was  $0.72 \pm 0.38 \mu$ M for WT, and  $2.77 \pm 0.78 \mu$ M for the mutant; the significant potency reduction, observed in the mutant channels when compared to Kv7.2 WT, suggests that the serine at position 303 may contribute to the retigabine binding. While my thesis work was being performed, this hypothesis was confirmed by the Cryo-EM structures of the human Kv7.2 and Kv7.4 (Ser 303 and 309, respectively) channels in complex with retigabine (Li X et al., 2020; Li T et al., 2020). In both model an H-bond interaction occur between the aniline group of retigabine and the side chain of serine. In Kv7.4 the mutant Ser309H (Histidine) completely abrogated retigabine's ability to activate the channel (Li T et al., 2020) while in Kv7.2, Ser303A mutation, decreased the potentiation activity of retigabine on Kv7.2 by



attenuating the left-shift of the G-V curves; concentration of 5  $\mu$ M retigabine was able to induce in the WT a  $\Delta V_{1/2}$  of about -30 mV, while in the mutant the  $\Delta V_{1/2}$  was about -20 mV (Li X et al., 2020), suggesting an opposite effect compared to our results. Additional experiment could be made to better understand the differences highlighted.

## **5.2 Screening of newly synthesized retigabine derivatives**

Screening of a library of 41 retigabine derivatives was performed in stable CHO-Kv7.2/Kv7.3, CHO-Kv7.4 and CHO-Kv7.3\* channel subunits (generated by means of the PiggyBac Transposon System) using the FluxOR Green Potassium Ion Channel Assay; a fluorescent-based assay, that uses thallium as surrogates for potassium and a fluorescent thallium-sensitive dye.

In a first series of experiment, to evaluate the feasibility and sensibility of the assay the activator retigabine and its potent analogue RL648\_81 (Kumar et al., 2016) were tested on CHO-Kv7.2/Kv7.3 cells. In both cases, the drugs dose-dependently increased the maximal fluorescence and the initial slope of the fluorescent signal. The calculated  $EC_{50}$  for retigabine was slightly higher than that calculated by electrophysiological techniques. On the other hand, RL648\_81 showed an  $EC_{50}$  of  $1.2 \pm 0.2 \mu$ M, whereas that for retigabine was  $7.2 \pm 1.9 \mu$ M, revealing that, in the fluorescent assay the analogue was 6-times more potent than the reference control. By contrast, using electrophysiological techniques the RL648\_81 was reported to be 15-time more potent than retigabine (Kumar et al., 2016). These two examples highlight that the fluorescence assay was slightly less sensitive than the electrophysiological technique, but still able to detect compounds more potent than retigabine.

Among the newly synthesized retigabine analogues tested at a single concentration of 10 $\mu$ M, in CHO-Kv7.2/Kv7.3 cells, thirteen (46-58-59-63-69-71-77-81-82-85-86-87-94) were found to increase the maximal fluorescence and the initial slope of the fluorescent signal

significantly more than retigabine. EC<sub>50</sub> calculations for these compounds demonstrated that the derivatives were from 5 to 10 times more potent than retigabine (Table 17).

Electrophysiological characterization of some of these compounds was also performed showing that, compared to retigabine, the CPRET-46, -59, -63, and -86 (1  $\mu$ M) caused a marked leftward shift in the  $V_{1/2}$  and a significant increase of maximal current and the calculated  $V_{1/2}$  was  $-26.4 \pm 0.6$ ,  $-40.4 \pm 0.2$ ,  $-89.0 \pm 2.6$ ,  $-80.2 \pm 0.6$  and  $-82.3 \pm 0.4$  for control retigabine, CP RET 46, 59, 63, and 86, respectively.

Similar to those obtained in the fluorescent assay, all four derivatives were 12-14 times more potent than retigabine; the calculated EC<sub>50</sub> was  $4.8 \pm 1.8$ ,  $0.39 \pm 0.02$ ,  $0.19 \pm 0.03$ ,  $0.28 \pm 0.04$  and  $0.12 \pm 0.04$  for retigabine, CP RET 46, 59, 63, and 86, respectively.

### 5.2.1 Structure–Activity Relationship of retigabine derivatives

Retigabine structure was divided and modified in three major zones: fluorophenyl group (zone A), the middle phenyl ring (zone B), and the methoxy group (zone C). The structural modification made in these three zones were carried out to increase both potency and chemical stability.

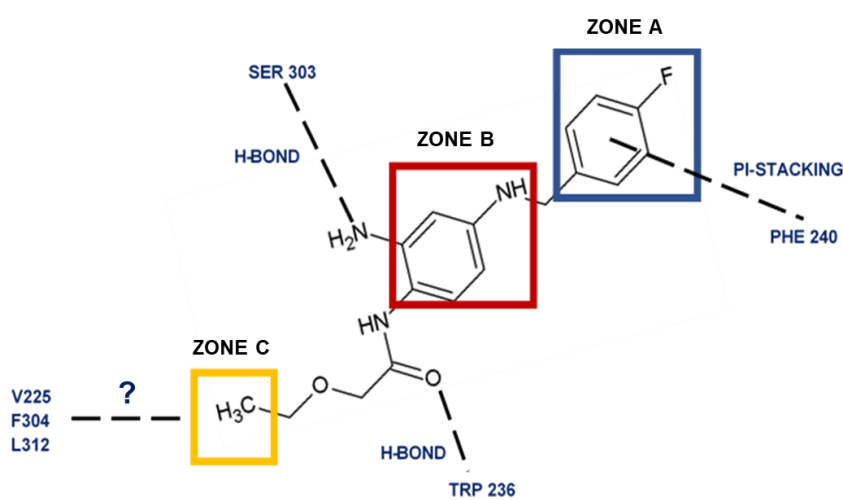
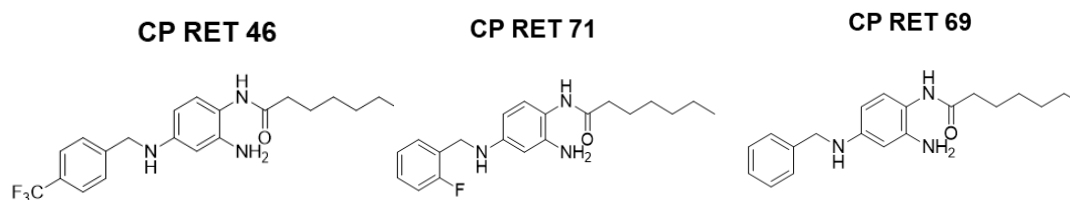


**Figure 52. Structure–Activity Relationship of retigabine derivatives.**

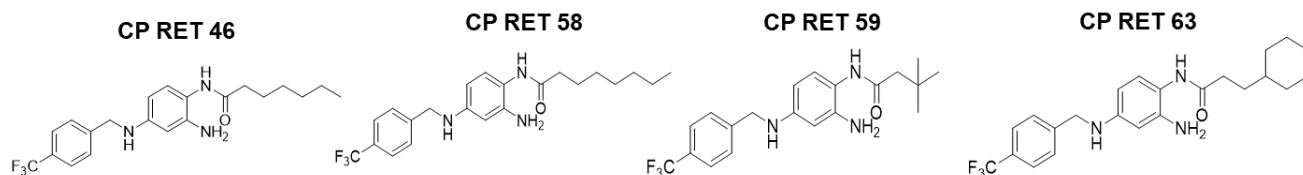
The increased potency of these derivatives was justified by the modification on the fluorophenyl moiety (zone A). In fact, as also demonstrated by Kumar and collaborators (Kumar et al., 2016), the substitution of the –F group, with a larger electron withdrawing group such as the –CF<sub>3</sub>, increased hydrophobic interactions and improved the activity of retigabine derivatives. All derivatives that resulted more potent than retigabine were characterized, except CP 69 and CP 71, by the presence of the –CF<sub>3</sub> group *in para* on the phenyl moiety (Figure 45).

CP46, CP 71, and CP 69 were structurally identical except for the substituent on the phenyl moiety. In fact, CP 46 showed a –CF<sub>3</sub> group *in para* position, CP 71 showed a –F group *in*

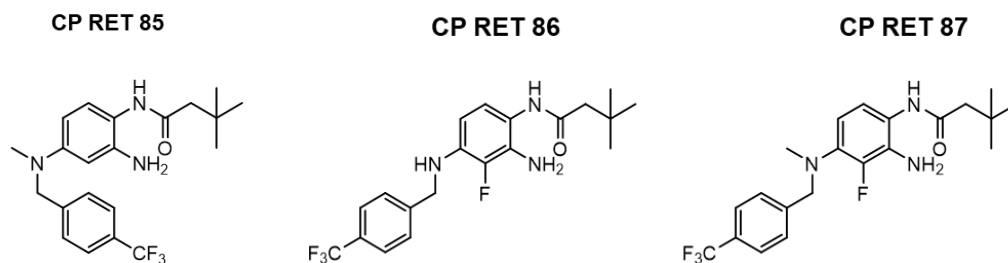
*ortho* position while no electron withdrawing groups were present on CP 69. By comparing the ratio of potency CP 46, 71, and 69 appeared to be respectively 5, 3,5 and 2 times more potent than retigabine, suggesting that higher increase of potency were obtained after the insertion of the -CF<sub>3</sub> group.



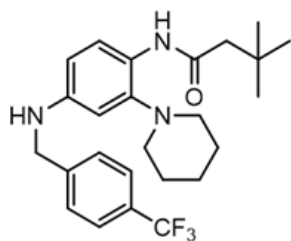
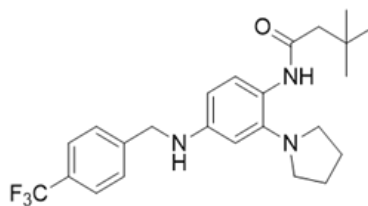
These results suggest that, probably, the increased potency was not only ascribed to the CF<sub>3</sub> substitution but also to the introduction of longer chain at the methoxy group (zone C). In fact, CP 69, despite the absence of the -CF<sub>3</sub> or the -F groups, resulted more potent than the control retigabine. To understand if additional interactions can occur between this part of the molecule and residues located in the deepest part of the hydrophobic binding site, MD simulations were performed by our collaborators of the Department of Pharmacy of the University of Naples. The results obtained suggested that during the simulation, these longer chains interacted mostly with the side chains of V225, F304 and L312 residues, generating hydrophobic interactions that could be responsible for the improved potency of these derivatives when compared to retigabine. Based on potency results obtained both in electrophysiological and fluorescence experiments, comparing CP 46,58,59,63, we can hypothesize that both hexane, heptane, tert-butyl and, cyclohexane lateral chain were well tolerated but the best compromise in terms of potency was obtained incorporating the tert-butyl group.



Finally, evaluation of chemical stability of compounds resulting more effective than retigabine on CHO-Kv7.2/Kv7.3, has proven that the structural modification on the aniline moiety and/or on NH-linker (zone B), were able to inhibit the dimerization reaction. In particular, the insertion of -CH<sub>3</sub> group at the -NH linker (CP 85, 87) or the introduction electron withdrawing group (-F) in the aniline moiety (CP 86, 87), prevented the formation of dimers. These results agree with those previously reported by Kumar in 2016 and Kalappa in 2015. Indeed, in both RL-81 and SF0034, the insertion of -F group on the aniline moiety, improved the chemical stability by reducing dimers by products.



Also the substitution of the amino group with a piperidine (CP81) or a pyrrolidine (CP82), prevented dimers formation.

**CP RET 81****CP RET 82**

It is important to underline that all modification in the zone B does not prevent the amino group's ability to form an H-bond interaction with the S303.

### 5.3 Search for selectivity

As previously described, one of the drawbacks of retigabine is its capability of activating also Kv7.4 currents, resulting in urinary retention. To evaluate the subtype selectivity, the library compounds was also tested in CHO-Kv7.4 cells.

Several compounds including CPRET-46-56-57-58-59-63-69-70-71-77-80-81-82-85-86-87 resulted more effective than retigabine in term of both slope and maximal fluorescence. Unfortunately, the compounds CPRET-46-58-59-63-69-71-77-80-81-82-85-86-87 were more active than retigabine also on Kv7.2/Kv7.3.

The comparison of EC<sub>50</sub> values, of those compound that did not formed dimers such as CPRET-77-81-82-85-86-87 and retigabine, calculated on Kv7.4 and Kv7.2/Kv7.3 suggested that no significant difference in terms of selectivity were obtained. Only an increase selectivity of CP 87 for Kv7.4 was obtained, but additional experiment both electrophysiological and molecular modelling, are require to validate and better understand this result (Figure 50).

In CHO-Kv7.3\* the only derivatives that resulted more effective than retigabine was CP46. Conversely, compounds that were not able to form the typical retigabine by product were not found more effective but sowed a similar effect than retigabine, consider the F<sub>0</sub>/F<sub>max</sub> parameters. Probably, considering this channel subunit, the selected concentration of 10µM is too high and a lower concentration such as 1µM, could be used to better characterized the effect of this derivatives. Moreover, additional electrophysiological experiments are however necessary to define the selectivity of these compounds.

## 5.4 Conclusion and future direction

In conclusion, the refinement of the retigabine binding site allowed us to identify additional interaction sites and to develop rationally a library of retigabine derivatives. The compounds synthesized were screened by use a fluorescence-based assay which has proved to be suitable for evaluate the activity of Kv7 channels activators. This has been successfully used to identify novel promising compounds, that thanks to the structural modification, appeared more potent and more stable compared to retigabine. In the future, additional experiments by means of mutagenesis and electrophysiological techniques are required to better understand the functional consequence, due to the exploration of deepest part of the hydrophobic pocket, by the long chain incorporated at methoxy group of our derivatives.

Further investigations are also needed to evaluate the pharmacokinetic properties of synthesized compounds and the *in vivo* anticonvulsant activity. Among the different animal models of epilepsy, both acute and chronic could be used. The subcutaneous pentylenetetrazol (scPTZ) tests, characterized by the chemical induction of acute convulsions, remain one of the 'gold standards' for the detection of anticonvulsant activity. Consider that, in PTZ model seizures are evoke in healthy and neurologically intact rodents, chronic models e.g. Kainic acid Kindling, or genetic models (Milh et al.,2020) would provide the ideal condition to evaluate the possible neuroprotective action of the compounds.



## Referece

- Abbott, GW **(2015)** The KCNE2 K<sup>+</sup> channel regulatory subunit Ubiquitous influence, complex pathobiology. *Gene* 569(2),162-172.
- Abbott GW **(2020)** KCNQs: Ligand- and Voltage-Gated Potassium Channels. *Front Physiol.* 23;11:583.
- Abidi A, Devaux JJ, Molinari F, Alcaraz G, Michon FX, SuturaSardo J, Becq H, Lacoste C, Altuzarra C, Afenjar A, Mignot C, Doummar D, Isidor B, Guyen SN, Colin E, De La Vaissière S, Haye D, Trauffer A, Badens C, Prieur F, Lesca G, Villard L, Milh M, Aniksztejn L **(2015)** A recurrent KCNQ2 pore mutation causing early onset epileptic encephalopathy has a moderate effect on M current but alters subcellular localization of Kv7 channels. *Neurobiol Dis* 80:80–92.
- Aiken SP, Lampe BJ, Murphy PA, Brown, BS **(1995)** Reduction of spike frequency adaptation and blockade of M-current in rat CA1 pyramidal neurones by linopirdine (DuP 996), a neurotransmitter release enhancer. *Br J Pharmacol.* 115,1163-1168.
- Alaimo A, Gómez-Posada JC, Aivar P, Etxeberria A, Rodriguez Alfaro JA, Areso P, Villarroel A **(2009)** Calmodulin activation limits the rate of KCNQ2 K<sup>+</sup> channel exit from the endoplasmic reticulum. *J Biol Chem* 284:20668–20675
- Amato G, Roeloffs R, Rigdon GC, Antonio B, Mersch T, McNaughton-Smith G, Wickenden AD, Fritch P, Suto MJ **(2011)** N-Pyridyl and Pyrimidine Benzamides as KCNQ2/Q3 Potassium Channel Openers for the Treatment of Epilepsy. *ACS Med. Chem. Lett.* 2,481-484.
- Ambrosino P, Freri E, Castellotti B, Soldovieri MV, Mosca I, Manocchio L, Gellera C, Canafoglia L, Franceschetti S, Salis B, Iraci N, Miceli F, Ragona F, Granata T, DiFrancesco JC, Tagliatela M **(2018)** Kv7.3 compound heterozygous variants in early onset encephalopathy reveal additive contribution of Cterminal residues to PIP2-dependent K<sup>+</sup> channel gating. *Mol Neurobiol* 55:7009–7024.
- Ambrosino P, Soldovieri MV, Bast T, Turnpenny PD, Uhrig S, Biskup S, Döcker M, Fleck T, Mosca I, Manocchio L, Iraci N, Tagliatela M, Lemke JR. (2018) De novo gain-of-function variants in KCNT2 as a novel cause of developmental and epileptic encephalopathy. *Ann. Neurol.* 83:1198–1204
- Baraban SC, Dinday MT, Hortopan GA **(2013)** Drug screening in Scn1a zebrafish mutant identifies clemizole as a potential Dravet syndrome treatment. *Nat. Commun.* 4:2410
- Barrese V, Miceli F, Soldovieri MV, Ambrosino P, Iannotti FA, Cilio MR, Tagliatela M **(2010)** Neuronal potassium channel openers in the management of epilepsy: role and potential of retigabine. *Clin Pharmacol* 2:225-36.
- Battefeld A, Tran BT, Gavriliis J, Cooper EC, Kole MH **(2014)** Heteromeric Kv7.2/7.3 channels differentially regulate action potential initiation and conduction in neocortical myelinated axons. *J Neurosci* 34:3719–3732
- Barton ME, Klein BD, Wolf HH, White HS **(2001)** Pharmacological characterization of the 6 Hz psychomotor seizure model of partial epilepsy. *Epilepsy Res* 47:217–227
- Ben-Ari Y, Khalilov I, Kahle KT, Cherubini E **(2012)** The GABA excitatory/inhibitory shift in brain maturation and neurological disorders. *Neuroscientist* 18:467–486

- Bentzen BH, Schmitt N, Calloe K, Dalby Brown W, Grunnet M, Olesen SP **(2006)** The acrylamide (S)-1 differentially affects Kv7 (KCNQ) potassium channels. *Neuropharmacology* 51,1068-1077.
- Berg AT, Berkovic SF, Brodie MJ, Buchhalter J, Cross JH, van Emde Boas W, Engel J, French J, Glauser TA, Mathern GW, Moshé SL, Nordli D, Plouin P, Scheffer IE **(2010)**. Revised terminology and concepts for organization of seizures and epilepsies: report of the ILAE Commission on Classification and Terminology, 2005-2009. *Epilepsia* 51:676-85.
- Blom SM, Rottlander M, Kehler J, Bundgaard C, Schmitt N, Jensen HS **(2014)** From pan-reactive KV7 channel opener to subtype selective opener/inhibitor by addition of a methyl group. *PloS one* 9, (6), e100209.
- Bock C, Surur AS, Beirow K, Kindermann MK, Schulig L, Bodtke A, Bednarski PJ, Link A. Sulfide **(2019)** Analogues of Flupirtine and Retigabine with Nanomolar KV 7.2/KV 7.3 Channel Opening Activity. *ChemMedChem*. May 6;14:952-964.
- Boehlen A, Schwake M, Dost R, Kunert A, Fidzinski P, Heinemann U, Gebhardt C **(2013)** The new KCNQ2 activator 4-Chlor-N-(6-chlor-pyridin-3-yl)-benzamid displays anticonvulsant potential. *Br. J. Pharmacol.* 168:1182-1200
- Bosch DG, Boonstra FN, de Leeuw N, Pfundt R, Nillesen WM, de Ligt J, Gilissen C, Jhangiani S, Lupski JR, Cremers FP, de Vries BB **(2016)** Novel genetic causes for cerebral visual impairment. *Eur J Hum Genet* 24:660–665.
- Boscia F, Annunziato L and Taglialatela M **(2006)** Retigabine and flupirtine exert neuroprotective actions in organotypic hippocampal cultures. *Neuropharmacology* 51:283- 294.
- Brioni JD, Curzon P, Buckley MJ, Arneric SP, Decker MW **(1993)** Linopirdine (DuP996) facilitates the retention of avoidance training and improves performance of septal-lesioned rats in the water maze. *Pharmacol Biochem Behav* 44: 37-43.
- Brown DA, Adams PR **(1980)** Muscarinic suppression of a novel voltage-sensitive K<sup>+</sup> current in a vertebrate neurone. *Nature* 283: 673–676
- Brueggemann LI, Haick JM, Cribbs LL, Byron KL **(2014)** Differential activation of vascular smooth muscle Kv7.4, Kv7.5, and Kv7.4/7.5 channels by ML213 and ICA-069673. *Mol. Pharmacol* 86:330-341.
- Canafoglia, L., Castellotti, B., Ragona, F., Freri, E., Granata, T., Chiapparini, L et al. **(2019)** Progressive myoclonus epilepsy caused by a gain-of-function KCNA2 mutation. *Seizure*, 65, 106–108
- Castaldo P, del Giudice EM, Coppola G, Pascotto A, Annunziato L, Taglialatela M **(2002)** Benign familial neonatal convulsions caused by altered gating of KCNQ2/KCNQ3 potassium channels. *J Neurosci* 22:RC199
- Cavasotto CN, Phatak SS **(2009)** Homology modeling in drug discovery: current trends and applications *Drug Discov Today* 14:676-83.
- Charlier C, Singh NA, Ryan SG, Lewis TB, Reus BE, Leach RJ, Leppert M **(1998)** A pore mutation in a novel KQT-like potassium channel gene in an idiopathic epilepsy family. *Nat Genet* 18:53– 55
- Cherubini E, Gaiarsa JL, Ben-Ari Y **(1991)** GABA: an excitatory transmitter in early postnatal life. *Trends Neurosci* 14:515–519.
- Cheung YY, Yu H, Xu K, Zou B, Wu M, McManus OB, Li M, Lindsley CW, Hopkins CR **(2012)** Discovery of a series of 2-phenyl-N-(2-(pyrrolidin-1-yl)phenyl)acetamides as novel molecular switches that modulate modes of K(v)7.2 (KCNQ2) channel pharmacology: identification of (S)-2-

phenyl-N-(2-(pyrrolidin-1-yl)phenyl)butanamide (ML252) as a potent, brain penetrant K(v)7.2 channel inhibitor. *J. Med. Chem.* 55:6975-6979.

- Choi BH, Choi JS, Yoon SH, Rhie DJ, Min DS, Jo YH, Kim MS, Hahn SJ **(2001)** Effects of norfluoxetine, the major metabolite of fluoxetine, on the cloned neuronal potassium channel Kv3.1. *Neuropharmacology*. Sep 41:443-53.
- Citraro R, Leo A, Constanti A, Russo E, De Sarro G. **(2016)** mTOR pathway inhibition as a new therapeutic strategy in epilepsy and epileptogenesis. *Pharmacol Res* 107:333–343
- Cole BA, Johnson RM, Dejakaisaya H, Pilati N, Fishwick CWG, Muench SP, Lippiat JD **(2020)** Structure-based identification and characterization of inhibitors of the epilepsy-associated k na 1.1 (KCNT1) potassium channel *iScience*. 23:101100
- Cooper EC, Harrington E, Jan YN, Jan LY **(2001)** M channel KCNQ2 subunits are localized to key sites for control of neuronal network oscillations and synchronization in mouse brain. *J Neurosci* 21:9529–9540
- Cooper EC, Jan LY **(2003)** M-channels: neurological diseases, neuromodulation, and drug development *Arch Neurol*. 60:496-500
- Daci A, Bozalija A, Jashari F, Krasniqi S **(2018)** Individualizing Treatment Approaches for Epileptic Patients with Glucose Transporter Type1 (GLUT-1) Deficiency. *Int J Mol Sci* 19:E122.
- Dailey JW, Cheong JH, Ko KH, Adams-Curtis LE, Jobe PC. **(1995)** Anticonvulsant properties of D-20443 in genetically epilepsy-prone rats: Prediction of clinical response. *Neurosci Lett* 195:77–80
- Dalby-Brown W, Jessen C, Hougaard C, Jensen ML, Jacobsen TA, Nielsen KS, Erichsen HK, Grunnet M, Ahring PK, Christophersen P, Strobaek D, Jorgensen S **(2013)** Characterization of a novel high-potency positive modulator of K(v)7 channels. *Eur J Pharmacol* 709: 52-63.
- Davoren JE, Claffey MM, Snow SL, Reese MR, Arora G, Butler CR, Boscoe BP, Chenard L, DeNinno SL, Drozda SE, Duplantier AJ, Moine L, Rogers BN, Rong S, Schuyten K, Wright AS, Zhang L, Serpa KA, Weber ML, Stolyar P, Whisman TL, Baker K, Tse K, Clark AJ, Rong H, Mather RJ, Lowe JA **(2015)** 3rd, Discovery of a novel Kv7 channel opener as a treatment for epilepsy. *Bioorg. Med. Chem. Lett* 25:4941-4944.
- Dedek K, Kunath B, Kananura C, Reuner U, Jentsch TJ, Steinlein OK **(2001)** Myokymia and neonatal epilepsy caused by a mutation in the voltage sensor of the KCNQ2 K<sup>+</sup> channel. *PNAS* 98: 12272–12277.
- Dencker D, Dias R, Pedersen ML, Husum H **(2008)** Effect of the new antiepileptic drug retigabine in a rodent model of mania. *Epilepsy Behav* 12:49-53.
- de Sarro G, di Paola ED, Conte G, Pasculli MP, de Sarro A **(2001)** Influence of retigabine on the anticonvulsant activity of some antiepileptic drugs against audiogenic seizures in DBA/2 mice. *Naunyn Schmiedeberg's Arch Pharmacol* 363:330–336
- De Vivo M, Masetti M, Bottegoni G, Cavalli A **(2016)** Role of Molecular Dynamics and Related Methods in Drug Discovery *J Med Chem*. 59:4035-61
- Devaux JJ, Kleopa KA, Cooper EC, Scherer SS **(2004)** KCNQ2 is a nodal K<sup>+</sup> channel. *J Neurosci* 24:1236–1244.
- Dilella R, Striano P, Gennaro E, Bassi L, Olivotto S, Tadini L, Mosca F, Barbieri S, Zara F, Fumagalli M. **(2017)** Efficacy of sodium channel blockers in SCN2A early infantile epileptic encephalopathy. *Brain and Development* 39:345–348.
- Dilella R, DiFrancesco JC, Soldovieri MV, Giacobbe A, Ambrosino P, Mosca I, Galli MA, Guez S, Fumagalli M, Miceli F, Cattaneo D, Darra F, Gennaro E, Zara F, Striano P, Castellotti B, Gellera C,

- Varesio C, Veggiotti P, Tagliatela M **(2018)** Early Treatment with Quinidine in 2 Patients with Epilepsy of Infancy with Migrating Focal Seizures (EIMFS) Due to Gain-of-Function KCNT1 Mutations: Functional Studies, Clinical Responses, and Critical Issues for Personalized Therapy. *Neurotherapeutics*;15(4):1112–1126
- Dvir M, Peretz, A Haitin, Y, Attali B **(2014)** Recent molecular insights from mutated  $I_{KS}$  channels in cardiac arrhythmia. *Curr. Opin. Pharmacol.*15, 74-82.
  - Douros A, Bronder E, Andersohn F, Klimpel A, Thomae M, Orzechowski HD, Kreutz R, Garbe E. **(2014)** Flupirtine-induced liver injury-Seven cases from the Berlin Case-Control Surveillance Study and review of the German spontaneous adverse drug reaction reporting database. *Eur J Clin Pharmacol* 70:453–459
  - Dupuis DS, Schroder RL, Jespersen T, Christensen JK, Christophersen P, Jensen BS and Olesen SP **(2002)** Activation of KCNQ5 channels stably expressed in HEK293 cells by BMS-204352. *European journal of pharmacology* 437:129-137.
  - Ekberg J, Schuetz F, Boase NA, Conroy SJ, Manning J, Kumar S, Poronnik P, Adams DJ **(2007)** Regulation of the voltage-gated K<sup>+</sup> channels KCNQ2/3 and KCNQ3/5 by ubiquitination. Novel role for Nedd4-2. *J Biol Chem* 282:12135–12142.
  - Epi4K Consortium & Epilepsy Phenome/Genome Project **(2013)** De novo mutations in epileptic encephalopathies. *Nature* 501: 217–221.
  - Etxeberria A, Aivar P, Rodriguez-Alfaro JA, Alaimo A, Villacè P, Gómez-Posada JC, Areso P, and Villarroel A **(2008)** Calmodulin regulates the trafficking of KCNQ2 potassium channels. *FASEB J* 22: 1135-1143
  - Finlayson K, Turnbull L, January CT, Sharkey J, Kelly JS **(2001)** [3H]Dofetilide binding to HERG transfected membranes: a potential high throughput preclinical screen. *Eur. J. Pharmacol.* 430:147–148
  - Fisher, R. S. van Emde Boas W, Blume W, Elger C, Genton P, Lee P, Jerome Engel J Jr. **(2005)** Epileptic seizures and epilepsy: definitions proposed by the International League Against Epilepsy (ILAE) and the International Bureau for Epilepsy (IBE). *Epilepsia* 46, 470–472
  - Franz DN, Lawson JA, Yapici Z, Ikeda H, Polster T, Nabbout R, Curatolo P, de Vries PJ, Dlugos DJ, Voi M, Fan J, Vauray A, Pelov D, French JA. **(2018)** Everolimus for treatment-refractory seizures in TSC: extension of a randomized controlled trial. *Neurol. Clin. Pract.* 8, 412–420
  - Friedman AK, Juarez B, Ku SM, Zhang H, Calizo RC, Walsh JJ, Chaudhury D, Zhang S, Hawkins A, Dietz DM, Murrough JW, Ribadeneira M, Wong EH, Neve RL, Han MH **(2016)** KCNQ channel openers reverse depressive symptoms via an active resilience mechanism. *Nat. Commun.* 7 :11671.
  - Gamper N, Shapiro MS **(2003)** Calmodulin mediates Ca<sup>2+</sup> -dependent modulation of M-type K<sup>+</sup> channels. *J Gen Physiol* 122:17–31.
  - Gamper N, Li Y, Shapiro MS **(2005)** Structural requirements for differential sensitivity of KCNQ K<sup>+</sup> channels to modulation by Ca<sup>2+</sup>/calmodulin, *Mol Biol Cell* 16: 3538–3551.
  - Gao Z, Zhang T, Wu M, Xiong Q, Sun H, Zhang Y, Zu L, Wang W, Li M **(2010)** Isoform-specific prolongation of Kv7 (KCNQ) potassium channel opening mediated by new molecular determinants for drug-channel interactions. *J Biol. Chem.* 285:28322-28332.
  - Geiger J, Weber YG, Landwehrmeyer B, Sommer C, Lerche H **(2006)** Immunohistochemical analysis of KCNQ3 potassium channels in mouse brain. *Neurosci Lett* 400:101–104.

- Goto A, Ishii A, Shibata M, Ihara Y, Cooper EC, Hirose S **(2019)** Characteristics of KCNQ2 variants causing either benign neonatal epilepsy or developmental and epileptic encephalopathy. *Epilepsia* 60:1870–1880.
- Greene DL, Kosenko A, Hoshi N **(2018)** Attenuating M-current suppression in vivo by a mutant Kcnq2 gene knock-in reduces Pflugers Arch - Eur J Physiol seizure burden and prevents status epilepticus-induced neuronal death and epileptogenesis. *Epilepsia* 59:1908–1918.
- Gribkoff VK, Starrett JE, Dworetzky SI, Hewawasam P, Boissard CG, Cook DA, Frantz SW, Heman K, Hibbard JR, Huston K, Johnson G, Krishnan BS, Kinney GG, Lombardo LA, Meanwell NA, Molinoff PB, Myers RA, Moon SL, Ortiz A, Pajor L, Pieschl RL, Post-Munson DJ, Signor LJ, Srinivas N, Taber MT, Thalody G, Trojnacki JT, Wiener H, Yeleswaram K, Yeola SW **(2001)** Targeting acute ischemic stroke with a calcium-sensitive opener of maxi-K potassium channels. *Nat. Med.* 7:471-477.
- Griffin A, Hamling KR, Knupp K, Hong S, Lee LP, Baraban SC **(2017)** Clemizole and modulators of serotonin signalling suppress seizures in Dravet syndrome. *Brain* 140, 669–683
- Groseclose MR, Castellino S **(2019)** An investigation into retigabine (ezogabine) associated dyspigmentation in rat eyes by MALDI imaging mass spectrometry. *Chem. Res. Toxicol* 32: 294–303.
- Grozeva D, Carss K, Spasic-Boskovic O et al **(2015)** Targeted next-generation sequencing analysis of 1,000 individuals with intellectual disability. *Hum Mutat* 36:1197–1204
- Halliwell JV, Adams PR **(1982)** Voltage-clamp analysis of muscarinic excitation in hippocampal neurons. *Brain Res* 250:71–92.
- Hansen HH, Waroux O, Seutin V, Jentsch TJ, Aznar S, Mikkelsen JD **(2008)** Kv7 channels: Interaction with dopaminergic and serotonergic neurotransmission in the CNS. *J. Physiol.*, , 586(7), 1823-1832
- Hansen HH, Andreasen JT, Weikop P, Mirza N, Scheel-Krüger J, Mikkelsen JD **(2007)** The neuronal KCNQ channel opener retigabine inhibits locomotor activity and reduces forebrain excitatory responses to the psychostimulants cocaine, methylphenidate and phencyclidine. *Eur. J. Pharmacol* 570:77-88
- Helbig I and N Tayoun AA **(2016)** Understanding Genotypes and Phenotypes in Epileptic Encephalopathies *Mol Syndromol* 7:172-181.
- Hernandez CC, Zaika O, Shapiro MS **(2008)** A carboxy-terminal inter-helix linker as the site of phosphatidylinositol 4,5-bisphosphate action on Kv7 (M-type) K channels. *J. Gen. Physiol.* 132:361–381
- Hirose S, Tanakab Y, Shibatab M, Kimurab Y, Ishikawac M, Higurashid N, Yamamotoe T, Ichisef E, Chiyonobuf T, Ishii A **(2020)** Application of induced pluripotent stem cells in epilepsy. *Mol Cell Neurosci* 108:103535.
- Hoshi N, Zhang J S, Omaki M, Takeuchi T, Yokoyama S, Wanaverbecq N, Langeberg LK, Yoneda Y, Scott JD, Brown DA, Higashida H **(2003)** AKAP150 signaling complex promotes suppression of the M-current by muscarinic agonists. *Nat Neurosci* 6: 564-571.
- Housley GD, Ashmore JF **(1992)** Ionic currents of outer hair cells isolated from the guinea-pig cochlea. *J. Physiol* 448:73-98
- Hu HN, Zhou PZ, Chen F, Li M, Nan FJ, Gao ZB **(2013)** Discovery of a retigabine derivative that inhibits KCNQ2 potassium channels. *Acta Pharmacol. Sin* 34:1359-1366.

- Iannotti FA, Panza E, Barrese V, Viggiano D, Soldovieri MV, Taglialatela M **(2010)** Expression, localization, and pharmacological role of Kv7 potassium channels in skeletal muscle proliferation, differentiation, and survival after myotoxic insults. *J Pharmacol Exp Ther* 332:811–820.
- Iannotti FA, Barrese V, Formisano L, Miceli F, Taglialatela M **(2013)** Specification of skeletal muscle differentiation by repressor element-1 silencing transcription factor (REST)-regulated Kv7.4 potassium channels. *Mol Biol Cell* 24:274–284.
- Ihara, Y.; Tomonoh, Y.; Deshimaru, M.; Zhang, B.; Uchida, T.; Ishii, A.; Hirose, S. Retigabine, a Kv7.2/Kv7.3-channel opener, attenuates drug-induced seizures in knock-in mice harboring KCNQ2 mutations. *PLoS One*, 2016, 11(2), e0150095
- Ipavec V, Martire M, Barrese V, Taglialatela M, Currò D (2011) KV7 channels regulate muscle tone and nonadrenergic noncholinergic relaxation of the rat gastric fundus. *Pharmacol Res* 64:397–409
- Jiang Y, Lee A, Chen J, Cadene M, Chait BT, and MacKinnon R **(2002a)** Crystal structure and mechanism of a calcium-gated potassium channel. *Nature* 417:515–522
- Jiang Y, Lee A, Chen J, Cadene M, Chait BT, MacKinnon R **(2002b)** The open pore conformation of potassium channels. *Nature* 417:523–526
- Jiang Y, Lee A, Chen J, Ruta V, Cadene M, Chait BT, et al. **(2003)** X-ray structure of a voltage dependent K<sup>+</sup> channel. *Nature* 423:33–41
- Jensen BS **(2002)** BMS-204352: a potassium channel opener developed for the treatment of stroke. *CNS Drug Rev* 8:353-360.
- Jepps TA, Chadha PS, Davis AJ, Harhun MI, Cockerill GW, Olesen SP, Hansen RS, Greenwood IA **(2011)** Downregulation of Kv7.4 channel activity in primary and secondary hypertension. *Circulation* 124:602–611.
- Kalappa BI, Soh H, Duignan KM, Furuya T, Edwards S, Tzingounis AV and Tzounopoulos T **(2015)** Potent KCNQ2/3-specific channel activator suppresses in vivo epileptic activity and prevents the development of tinnitus. *J. Neurosci* 35:8829-8842.
- Kanaumi T, Takashima S, Iwasaki H, Itoh M, Mitsudome A, Hirose S **(2008)** Developmental changes in KCNQ2 and KCNQ3 expression in human brain: possible contribution to the age-dependent etiology of benign familial neonatal convulsions. *Brain Dev* 30:362–369.
- Kasimova MA, Zaydman MA, Cui J, M Tarek **(2015)** PIP2-dependent coupling is prominent in Kv7.1 due to weakened interactions between S4-S5 and S6. *Sci. Rep.* 5; 7474
- Kass HR, Winesett SP, Bessone SK, Turner Z, Kossoff EH **(2016)** Use of dietary therapies amongst patients with GLUT1 deficiency syndrome. *Seizure* 35:83–7.
- Kato M, Yamagata T, Kubota M, Arai H, Yamashita S, Nakagawa T, Fujii T, Sugai K, Imai K, Uster T, Chitayat D, Weiss S, Kashii H, Kusano R, Matsumoto A, Nakamura K, Oyazato Y, Maeno M, Nishiyama K, Koderah NM, Tsurusaki Y, Miyake N, Saito K, Hayasaka K, Matsumoto N, Saitsu H **(2013)** Clinical spectrum of early onset epileptencephalopathies caused by KCNQ2 mutation. *Epilepsia* 54:1282–1287.
- Kim EC, Patel J, Zhang J, Soh H, Rhodes JS, Tzingounis AV, Chung HJ **(2019)** Heterozygous loss of epilepsy gene KCNQ2 alters social, repetitive and exploratory behaviors. *Genes Brain Behav J* 19:e12599.
- Kim RY, Yau MC, Galpin JD, Seeböhm G, Ahern CA, Pless SA, Kurata HT **(2015)** Atomic basis for therapeutic activation of neuronal potassium channels. *Nat. Commun.* 6,8116.

- Kimitsuki T, KomuneNoda T, Takaiwa K, Ohashi M, Komune S **(2010)** Property of I(K<sub>v</sub>)<sub>n</sub> in inner hair cells isolated from guinea-pig cochlea. *Hear. Res* 261:57-62.
- Ko A, Jung DE, Kim SH, Kang HC, Lee JS, Lee ST, et al. **(2018)** The Efficacy of Ketogenic Diet for Specific Genetic Mutation in Developmental and Epileptic Encephalopathy. *Front. Neurol.* 9:530.
- Korsgaard MP, Hartz BP, Brown WD, Ahning PK, Strobaek D, Mirza NR **(2005)** Anxiolytic effects of Maxipost (BMS-204352) and retigabine via activation of neuronal Kv7 channels. *J. Pharmacol. Exp. Ther.* 314:282- 292.
- Kosenko A, Kang S, Smith IM, Greene DL, Langeberg LK, Scott JD, Hoshi N **(2012)** Coordinated signal integration at the M-type potassium channel upon muscarinic stimulation. *EMBO J* 31(14):3147–3156. doi:10.1038/emboj.2012.156.
- Kothur K, Holman K, Farnsworth E, Ho G, Lorentzos M, Troedson C, Gupta S, Webster R, Procopis PG, Menezes MP, Antony J, Ardern-Holmes S, Dale RC, Christodoulou J, Gill D, Bennetts B **(2018)** Diagnostic yield of targeted massively parallel sequencing in children with epileptic encephalopathy. *Seizure.* 59: 132–140.
- Kubisch C, Schroeder BC, Friedrich T, Lütjohann B, El-Amraoui A, Marlin S, Petit C, Jentsch TJ **(1999)** KCNQ4, a novel potassium channel expressed in sensory outer hair cells, is mutated in dominant deafness. *Cell* 96:437–446
- Kumar M, Reed N, Liu R, Aizenman E, Wipf P and Tzounopoulos T **(2016)** Synthesis and Evaluation of Potent KCNQ2/3-Specific Channel Activators. *Mol. Pharmacol.* 89:667-677
- Lange W, Geissendörfer J, Schenzer A, Grotzinger J, Seeböhm G, Friedrich T, Schwake M **(2009)** Refinement of the binding site and mode of action of the anticonvulsant retigabine on KCNQ K<sup>+</sup> channels. *Mol Pharmacol* 75:272–280.
- Lauritano A, Moutton S, Longobardi E, Tran Mau-Them F, Laudati G, Nappi P, Soldovieri MV, Ambrosino P, Cataldi M, Jouan T, Lehalle D, Maurey H, Philippe C, Miceli F, Vitobello A, Taglialetela M **(2019)** A novel homozygous KCNQ3 loss-of-function variant causes non-syndromic intellectual disability and neonatal-onset pharmacodependent epilepsy. *Epilepsia Open* 4: 464–475.
- Lehman A, Thouta S, Mancini GM, Naidu S, van Slegtenhorst M, McWalter K, Person R, Mwenifumbo J, Salvarinova R, CAUSES Study; EPGEN Study, Guella I, MB MK, Datta A, Connolly MB, Kalkhoran SM, Poburko D, Friedman JM, Farrer MJ, Demos M, Desai S, Claydon T **(2017)** Loss-of-function and gain-of-function mutations in KCNQ5 cause intellectual disability or epileptic encephalopathy. *Am J Hum Genet* 101:65–74.
- Lerche C, Scherer CR, Seeböhm G, Derst C, Wei AD, Busch AE, Steinmeyer K **(2000)** Molecular cloning and functional expression of KCNQ5, a potassium channel subunit that may contribute to neuronal M-current diversity. *J Biol Chem* 275:22395–22400.
- Li T, Wu K, Yue Z, Wang Y, Zhang F, Shen H **(2021)** Structural Basis for the Modulation of Human KCNQ4 by Small-Molecule Drugs. *Mol Cell* 81:25-37.e4.
- Li X, Zhang Q, Guo P, Fu J, Mei L, Lv D, Wang J, Lai D, Ye S, Yang H, Guo J. (2021) Molecular basis for ligand activation of the human KCNQ2 channel. *Cell Res* 31:52-61.
- Li Y, Gamper N, Hilgemann DW & Shapiro MS **(2005)** Regulation of Kv7 (KCNQ) K<sup>+</sup> channel open probability by phosphatidylinositol 4,5-bisphosphate. *JNeurosci* 25:9825–9835.
- Liu R, Tzounopoulos T, Wipf P. Synthesis and Optimization of Kv7 (KCNQ) **(2019)** Potassium Channel Agonists: The Role of Fluorines in Potency and Selectivity. *ACS Med Chem Lett.* May 8;10:929-935

- Liu W, Devaux JJ **(2014)** Calmodulin orchestrates the heteromeric assembly and the trafficking of KCNQ2/3 (Kv7.2/3) channels in neurons. *Mol Cell Neurosci* 58: 40–52.
- Liu Y, Xu X, Gao J, Naffaa MM, Liang H, Shi J, Wang HZ, Yang ND, Hou P, Zhao W, White KM, Kong W, Dou A, Cui A, Zhang G, Cohen IS, Zou X, Cui J. **(2020)** A PIP 2 substitute mediates voltage sensor-pore coupling in KCNQ activation. *Commun Biol* 16;3:385.
- Long, SB, Campbell EB, and Mackinnon R **(2005a)** Crystal structure of a mammalian voltage-dependent Shaker family K<sup>+</sup> channel. *Science* 309:897–903.
- Long, SB, Campbell EB, and Mackinnon R **(2005b)** Voltage sensor of Kv1.2: structural basis of electromechanical coupling. *Science* 309: 903–908
- Long, SB, Tao X, Campbell EB, and Mackinnon R **(2007)** Atomic structure of a voltage-dependent K<sup>+</sup> channel in a lipid membrane-like environment. *Nature* 450:376–382
- Main MJ, Cryan JE, Dupere JR, Cox B, Clare JJ and Burbidge SA **(2000)** Modulation of KCNQ2/3 potassium channels by the novel anticonvulsant retigabine. *Molecular pharmacology* 58:253-262.
- Martire M, Castaldo P, D'Amico M, Preziosi P, Annunziato L, Taglialatela M **(2004)** M channels containing KCNQ2 subunits modulate norepinephrine, aspartate, and GABA release from hippocampal nerve terminals. *J Neurosci* 24:592-7
- Martire M, D'Amico M, Panza E, Miceli F, Viggiano D, Lavergata F, Iannotti FA, Barrese V, Preziosi P, Annunziato L, Taglialatela M **(2007)** Involvement of KCNQ2 subunits in [3H]dopamine release triggered by depolarization and pre-synaptic muscarinic receptor activation from rat striatal synaptosomes. *J Neurochem* 102:179-93.
- Manville RW, and Abbott GW **(2018a)** Ancient and modern anticonvulsants act synergistically in a KCNQ potassium channel binding pocket. *Nat. Commun.* 9:3845
- Manville RW Papanikolaou M, Abbott GW **(2018b)** Direct neurotransmitter activation of voltage-gated potassium channels. *Nat. Commun.* 9:1847
- Manville RW, and Abbott GW **(2018c)** Gabapentin Is a Potent Activator of KCNQ3 and KCNQ5 Potassium Channels *Mol Pharmacol*, 94 :1155-1163
- Manville RW, and Abbott GW **(2019a)** Cilantro leaf harbors a potent potassium channel-activating anticonvulsant. *FASEB J.* 33:11349–11363
- Manville RW, Van Der Horst J, Redford KE, Katz BB, Jepps TA, and Abbott GW **(2019b)** KCNQ5 activation is a unifying molecular mechanism shared by genetically and culturally diverse botanical hypotensive folk medicines. *Proc. Natl. Acad. Sci. U.S.A.* 116:21236–21245
- Manville RW Papanikolaou M, Abbott GW **(2020)** M-channel activation contributes to the anticonvulsant action of the ketone body betahydroxybutyrate. *J. Pharmacol. Exp. Ther.* 372:148–156
- McCammon JA, Gelin BR, Karplus M **(1977)** Dynamics of folded proteins. *Nature* 267:585-590.
- McRae JF, Clayton S, Fitzgerald TW et al **(2017)** Prevalence and architecture of de novo mutations in developmental disorders. *Nature* 542:433–438
- Miceli F, Soldovieri MV, Ambrosino P, Barrese V, Migliore M, Cilio MR, Taglialatela M **(2013)** Genotype-phenotype correlations in neonatal epilepsies caused by mutations in the voltage sensor of K(v)7.2 potassium channel subunits. *PNAS* 110:4386– 4391.



- Miceli F, Soldovieri MV, Ambrosino P, De Maria M, Migliore M, Migliore R, Taglialatela M **(2015a)** Early-onset epileptic encephalopathy caused by gain-of-function mutations in the voltage sensor of Kv7.2 and Kv7.3 potassium channel subunits. *J Neurosci* 35: 3782–3793.
- Miceli F, Striano P, Soldovieri MV, Fontana A, Nardello R, Robbiano A, Bellini G, Elia M, Zara F, Taglialatela M, Mangano S **(2015b)** A novel KCNQ3 mutation in familial epilepsy with focal seizures and intellectual disability. *Epilepsia* 56:e15–e20.
- Miceli F, Soldovieri MV, Nishtha J et al **(2017)** KCNQ3-related disorders. In: Adam MP, Ardinger HH, Pagon RA et al (eds) *GeneReviews®* [Internet]. University of Washington, Seattle
- Miceli F, Soldovieri MV, Joshi N, Weckhuysen S, Cooper E, Taglialatela M **(2018)** KCNQ2-related disorders. In: Adam MP, Ardinger HH, Pagon RA et al (eds) *GeneReviews®* [Internet]. Seattle University of Washington
- Miceli F, Carotenuto L, Barrese V, Soldovieri MV, Heinzen EL, Mandel AM, Lipa N, Bier L, Goldstein DB, Cooper EC, Cilio MR, Taglialatela M, Sands TT. **(2020)** A Novel Kv7.3 Variant in the Voltage-Sensing S4 Segment in a Family With Benign Neonatal Epilepsy: Functional Characterization and *in vitro* Rescue by  $\beta$ -Hydroxybutyrate. *Front Physiol.* Sep 4;11:1040.
- Milh M, Lacoste C, Cacciagli P, Abidi A, Sutura-Sardo J, Tzelepis I, Colin E, Badens C, Afenjar A, Dieux Coeslier A, Dailland T, Lesca G, Philip N, Villard L **(2015)** Variable clinical expression in patients with mosaicism for KCNQ2 mutations. *Am J Med Genet A* 167A:2314–2318.
- Milh M, Roubertoux P, Biba N, Chavany J, Spiga Ghata A, Fulachier C, Collins SC, Wagner C, Roux JC, Yalcin B, Félix MS, Molinari F, Lenck-Santini PP, Villard L **(2020)** A knock-in mouse model for KCNQ2-related epileptic encephalopathy displays spontaneous generalized seizures and cognitive impairment. *Epilepsia*.
- Millichap JJ, Park KL, Tsuchida T, Ben-Zeev B, Carmant L, Flamini R, Joshi N, Levisohn PM, Marsh E, Nangia S, Narayanan V, Ortiz-Gonzalez XR, Patterson MC, Pearl PL, Porter B, Ramsey K, McGinnis EL, Taglialatela M, Tracy M, Tran B, Venkatesan C, Weckhuysen S, Cooper EC **(2016)** KCNQ2 encephalopathy: features, mutational hot spots, and ezogabine treatment of 11 patients. *Neurol Genet* 2:e96.
- Millichap JJ, Miceli F, De Maria M, Keator C, Joshi N, Tran B, Soldovieri MV, Ambrosino P, Shashi V, Mikati MA, Cooper EC, Taglialatela M **(2017)** Infantile spasms and encephalopathy without preceding neonatal seizures caused by KCNQ2 R198Q, a gain-of-function variant. *Epilepsia* 58:e10–e15
- Misura KM, Bock JB, Gonzalez LC Jr, Scheller RH, Weis WI **(2002)** Three-dimensional structure of the amino-terminal domain of syntaxin 6, a SNAP-25 C homolog. *PNAS* 99(14): 9184-9189.
- Mulkey SB, Ben-Zeev B, Nicolai J, Carroll JL, Grønborg S, Jiang YH, Joshi N, Kelly M, Koolen DA, Mikati MA, Park K, Pearl PL, Scheffer IE, Spillmann RC, Taglialatela M, Vieker S, Weckhuysen S, Cooper EC, Cilio MR **(2017)** Neonatal nonepileptic myoclonus is a prominent clinical feature of KCNQ2 gain-of-function variants R201C and R201H. *Epilepsia* 58:436–445.
- Munro G, Dalby-Brown W Kv7 **(2007)** (KCNQ) channel modulators and neuropathic pain. *J. Med. Chem* 50:2576-2582
- Nappi P, Miceli F, Soldovieri MV, Ambrosino P, Barrese V, Taglialatela M **(2020)** Epileptic channelopathies caused by neuronal Kv7 (KCNQ) channel dysfunction. *Pflugers Arch* 472:881-898.
- Orhan G, Bock M, Schepers D, Ilina EI, Reichel SN, Löffler H, Jezutkovic N, Weckhuysen S, Mandelstam S, Suls A, Danker T, Guenther E, Scheffer IE, De Jonghe P, Lerche H, Maljevic S **(2014)** Dominant-negative effects of KCNQ2 mutations are associated with epileptic encephalopathy. *Ann Neurol* 75:382–394.

- Ostacolo C, Miceli F, Di Sarno V, Nappi P, Iraci N, Soldovieri MV, Ciaglia T, Ambrosino P, Vestuto V, Lauritano A, Musella S, Pepe G, Basilicata MG, Manfra M, Perinelli DR, Novellino E, Bertamino A, Gomez-Monterrey IM, Campiglia P, Taglialatela M **(2020)** Synthesis and pharmacological characterization of conformationally restricted retigabine analogues as novel neuronal Kv7 channel activators. *J Med Chem* 63:163–185
- **Oyrer J**, Maljevic S, Scheffer IE, Berkovic SF, Petrou S, Reid CA. **(2018)** Ion Channels in Genetic Epilepsy: From Genes and Mechanisms to Disease-Targeted Therapies. *Pharmacol Rev.* 70:142-173,
- Padilla K, Wickenden A.D, Gerlach A.C, McCormack K **(2009)** The KCNQ2/3 selective channel opener ICA-27243 binds to a novel voltage-sensor domain site. *Neurosci. Lett.* 465, (2), 138-142.
- Pan Z, Kao T, Horvath Z, Lemos J, Sul JY, Cranstoun SD, Bennett V, Scherer SS, Cooper EC **(2006)** A common ankyrin-G-based mechanism retains KCNQ and NaV channels at electrically active domains at the axon. *J Neurosci* 26: 2599-2613.
- Peters HC, Hu H, Pongs O, Storm JF, Isbrandt D **(2005)** Conditional transgenic suppression of M channels in mouse brain reveals functions in neuronal excitability, resonance and behavior. *Nat Neurosci* 8:51–60.
- Peretz A, Degani-Katzav N, Talmon M, Danieli E, Gopin A, Malka E, Nachman R, Raz A, Shabat D, Attali B **(2007)** A tale of switched functions: from cyclooxygenase inhibition to M-channel modulation in new diphenylamine derivatives. *PloS one* 2, (12), e1332.
- Peretz A, Degani N, Nachman R, Uziyel Y, Gibor G, Shabat D, Attali B **(2005)** Meclofenamic acid and diclofenac, novel templates of KCNQ2/Q3 potassium channel openers, depress cortical neuron activity and exhibit anticonvulsant properties. *Mol. Pharmacol* 67:1053- 1066.
- Pierson, T. M. et al. GRIN2A mutation and early-onset epileptic encephalopathy: personalized therapy with memantine. *Ann. Clin. Transl. Neurol.* 1, 190–198 (2014).
- Plouin P **(1994)** Benign familial neonatal convulsions. In: Malafosse A, Hirsch E, Marescaux C, Broglin D, Bernasconi R (ed) *Idiopathic generalized epilepsies: clinical, experimental and genetic aspects*. London John Libbey, p. 39–44
- Postma T, Krupp E, Li XL, Post RM, Weiss SR. **(2000)** Lamotrigine treatment during amygdala-kindled seizure development fails to inhibit seizures and diminishes subsequent anticonvulsant efficacy. *Epilepsia* 41:1514–1521
- Raol YH, Lapidus DA, Keating JG, Brooks-Kayal AR, Cooper EC **(2009)** A KCNQ channel opener for experimental neonatal seizures and status epilepticus. *Ann Neurol.* 2009 Mar;65(3):326-36.
- Rauch A, Wiczorek D, Graf E, Wieland T, Ende S, Schwarzmayr T, Albrecht B, Bartholdi D, Beygo J, Di Donato N, Dufke A, Cremer K, Hempel M, Horn D, Hoyer J, Joset P, Röpke A, Moog U, Riess A, Thiel CT, Tzschach A, Wiesener A, Wohlleber E, Zweier C, Ekici AB, Zink AM, Rump A, Meisinger C, Grallert H, Sticht H, Schenck A, Engels H, Rappold G, Schröck E, Wieacker P, Riess O, Meitinger T, Reis A, Strom TM **(2012)** Range of genetic mutations associated with severe nonsyndromic sporadic intellectual disability: an exome sequencing study. *Lancet* 380:1674–1682.
- Regev N, Degani-Katzav N, Korngreen A, Etzioni A, Siloni S, Alaimo A, Chikvashvili D, Villarroel A, Attali B, Lotan I **(2009)** Selective interaction of syntaxin 1A with KCNQ2: possible implications for specific modulation of presynaptic activity. *Plos One* 4(8): e6586.
- Rockwood K, Beattie BL, Eastwood MR, Feldman H, Mohr E, Pryse-Phillips W, Gauthier S **(1997)** A randomized, controlled trial of linopirdine in the treatment of Alzheimer's disease. *Can. J. Neurol. Sci* 24:140-145.

- Roeloffs R, Wickenden A.D, Crean C, Werness S, McNaughton-Smith G, Stables J, McNamara JO, Ghodadra N, Rigdon GC **(2008)** In vivo profile of ICA-27243 [N-(6-chloro-pyridin-3-yl)-3,4-difluorobenzamide], a potent and selective KCNQ2/Q3 (Kv7.2/Kv7.3) activator in rodent anticonvulsant models. *J. Pharmacol. Exp. Ther* 326:818-828.
- Roepke TK, Anantharam A, Kirchhoff P, Busque SM, Young JB, Geibel JP, Lerner DJ, Abbott GW (2006) The KCNE2 potassium channel ancillary subunit is essential for gastric acid secretion. *J. Biol. Chem.* 281:23740-23747.
- Rosati A, De Masi S, Guerrini R (2015) Antiepileptic drug treatment in children with epilepsy *CNS Drugs* 29:847-63
- Rostock A, Tober C, Rundfeldt C, Bartsch R, Engel J, Polymeropoulos E.E, Kutscher B, Loscher W, Honack D, White H.S, Wolf H.H **(1996)** D-23129: a new anticonvulsant with a broad-spectrum activity in animal models of epileptic seizures. *Epilepsy Res.* 23:211-223.
- Sadewa AH, Sasongko TH, Gunadi LMJ, Daikoku K, Yamamoto A, Yamasaki T, Tanaka S, Matsuo M, Nishio H **(2008)** Germ-line mutation of KCNQ2, p.R213W, in a Japanese family with benign familial neonatal convulsion. *Pediatr Int* 50:167–171
- Safiulina VF, Zacchi P, Taglialatela M, Yaari Y, Cherubini E **(2008)** Low expression of Kv7/M channels facilitates intrinsic and network bursting in the developing rat hippocampus. *J Physiol* 586:5437–5453.
- Sands TT, Miceli F, Lesca G, Beck AE, Sadleir LG, Arrington DK, Schönewolf-Greulich B, Moutton S, Lauritano A, Nappi P, Soldovieri MV, Scheffer IE, Mefford HC, Stong N, Heinzen EL, Goldstein DB, Perez AG, Kossoff EH, Stocco A, Sullivan JA, Shashi V, Gerard B, Francannet C, Bisgaard AM, Tümer Z, Willems M, Rivier F, Vitobello A, Thakkar K, Rajan DS, Barkovich AJ, Weckhuysen S, Cooper EC, Taglialatela M, Cilio MR **(2019)** Autism and developmental disability caused by KCNQ3 gain-of-function variants. *Ann Neurol* 86:181–192.
- Sanguinetti MC, Curran ME, Zou A, Shen J, Spector PS, Atkinson DL, Keating MT **(1996)** Coassembly of K(V)LQT1 and minK (IsK) proteins to form cardiac I(Ks) potassium channel. *Nature* 384:80–83.
- Scheffer IE, Berkovic S, Capovilla G, Connolly MB, French J, Guilhoto L, Hirsch E, Jain S, Mathern GW, Moshé SL, Nordli DR, Perucca E, Tomson T, Wiebe S, Zhang YH, Zuberi SM. (2017) ILAE classification of the epilepsies: Position paper of the ILAE Commission for Classification and Terminology. *Epilepsia* 58 :512-521.
- Schenzer A, Friedrich T, Pusch M, Saftig P, Jentsch TJ, Grotzinger J and Schwake M et al. **(2005)** Molecular determinants of KCNQ (Kv7) K<sup>+</sup> channel sensitivity to the anticonvulsant retigabine. *J Neurosci* 25:5051–5060.
- Schroeder BC, Kubisch C, Stein V, Jentsch TJ **(1998)** Moderate loss of function of cyclic-AMP-modulated KCNQ2/KCNQ3 K<sup>+</sup> channels causes epilepsy. *Nature* 396:687–690.
- Schroeder BC, Hechenberger M, Weinreich F, Kubisch C, Jentsch TJ **(2000)** KCNQ5, a novel potassium channel broadly expressed in brain, mediates M-type currents. *J Biol Chem* 275:24089–24095.
- Schroeder RL, Jespersen T, Christophersen P, Strobaek D, Jensen BS, Olesen SP **(2001)** KCNQ4 channel activation by BMS-204352 and retigabine. *Neuropharmacology* 40:888-898.
- Seeböhm G, Strutz-Seeböhm N, Ureche ON, Baltaev R, Lampert A, Kornichuk G, Kamiya K, Wuttke TV, Lerche H, Sanguinetti MC, Lang F **(2006)** Differential roles of S6 domain hinges in the gating of KCNQ potassium channels. *Biophys. J.* 90:2235–2244.

- Sharawat IK, Kasinathan A, Sahu JK, Sankhyan N **(2019)** Response to carbamazepine in KCNQ2 related early infantile epileptic encephalopathy. *Indian J Pediatr* 86:301–302.
- Singh NA, Charlier C, Stauffer D, DuPont BR, Leach RJ, Melis R, Ronen GM, Bjerre I, Quattlebaum T, Murphy JV, McHarg ML, Gagnon D, Rosales TO, Peiffer A, Anderson VE, Leppert M (1998) A novel potassium channel gene, KCNQ2, is mutated in an inherited epilepsy of newborns. *Nat Genet* 18:25–29.
- Singh NA, Westenskow P, Charlier C, Pappas C, Leslie J, Dillon J, Anderson VE, Sanguinetti MC, Leppert MF **(2003)** KCNQ2 and KCNQ3 potassium channel genes in benign familial neonatal convulsions: expansion of the functional and mutation spectrum. *Brain* 126:2726–2737.
- Singh NA, Otto JF, Dahle EJ, Pappas C, Leslie JD, Vilaythong A, Noebels JL, White HS, Wilcox KS, Leppert MF **(2008)** Mouse models of human KCNQ2 and KCNQ3 mutations for benign familial neonatal convulsions show seizures and neuronal plasticity without synaptic reorganization. *J Physiol* 586:3405–3423.
- Soh H, Tzingounis A.V **(2010)** The specific slow afterhyperpolarization inhibitor UCL2077 is a subtype-selective blocker of the epilepsy associated KCNQ channels. *Mol. Pharmacol.* 78, (6), 1088-1095.
- Soh H, Pant R, LoTurco JJ, Tzingounis AV **(2014)** Conditional deletions of epilepsy-associated KCNQ2 and KCNQ3 channels from cerebral cortex cause differential effects on neuronal excitability. *J Neurosci* 34:5311–5321.
- Soh H, Park S, Ryan K, Springer K, Maheshwari A, Tzingounis AV **(2018)** Deletion of KCNQ2/3 potassium channels from PV+ interneurons leads to homeostatic potentiation of excitatory transmission. *Elife* 1(7):e38617.
- Soldovieri MV, Boutry-Kryza N, Milh M, Doummar D, Heron B, Bourel E, Ambrosino P, Miceli F, De Maria M, Dorison N, Auvin S, Echenne B, Oertel J, Riquet A, Lambert L, Gerard M, Roubergue A, Calender A, Mignot C, Taglialatela M, Lesca G **(2014)** Novel KCNQ2 and KCNQ3 mutations in a large cohort of families with benign neonatal epilepsy: first evidence for an altered channel regulation by syntaxin-1A. *Hum Mutat* 35(3): 356–367
- Soldovieri MV, Freri E, Ambrosino P, Rivolta I, Mosca I, Binda A, Murano C, Ragona F, Canafoglia L, Vannicola C, Solazzi R, Granata T, Castellotti B, Messina G, Gellera C, Labalme A, Lesca G, DiFrancesco JC, Taglialatela M **(2020)** Gabapentin treatment in a patient with KCNQ2 developmental epileptic encephalopathy. *Pharmacol Res.* 160:105200.
- Steinlein OK, Mulley JC, Propping P, Wallace RH, Phillips HA, Sutherland GR, Scheffer IE, Berkovic SF (1995) A missense mutation in the neuronal nicotinic acetylcholine receptor alpha 4 subunit is associated with autosomal dominant nocturnal frontal lobe epilepsy. *Nat Genet* 11:201-3
- Sun & MacKinnon **(2017)** Cryo-EM Structure of a KCNQ1/CaM Complex Reveals Insights into Congenital Long QT Syndrome. *Cell* 169:1042–1050.
- Sun & MacKinnon **(2017)** Structural Basis of Human KCNQ1 Modulation and Gating. *Cell* 180:340–347.
- Svalø J, Bille M, Parameswaran Theepakaran N, Sheykhzade M, Nordling J, Bouchelouche P **(2013)** Bladder contractility is modulated by Kv7 channels in pig detrusor. *Eur J Pharmacol* 715:312– 320.
- Syrbe S, Hedrich UBS, Riesch E, Djémié T, Müller S, Møller RS, et al. **(2015)** De novo loss- or gain-of-function mutations in KCNA2 cause epileptic encephalopathy. *Nat Genet* 47:393–9.
- Szelenyi I **(2013)** Flupirtine, a re-discovered drug, revisited. *Inflam. Res* 62:251-258.

- Tao X, Lee A, Limapichat W, Dougherty DA, MacKinnon R **(2010)** A gating charge transfer center in voltage sensors. *Science* 328:67–73.
- Tatulian L, Delmas P, Abogadie FC and Brown DA **(2001)** Activation of expressed KCNQ potassium currents and native neuronal M-type potassium currents by the anti-convulsant drug retigabine. *The Journal of neuroscience : the official journal of the Society for Neuroscience* 21:5535-5545.
- Tatulian L and Brown DA **(2003)** Effect of the KCNQ potassium channel opener retigabine on single KCNQ2/3 channels expressed in CHO cells. *The Journal of physiology* 549:57-63.
- Tinel N, Lauritzen I, Chouabe C, Lazdunski M, Borsotto M **(1998)** The KCNQ2 potassium channel: splice variants, functional and developmental expression. Brain localization and comparison with KCNQ3. *FEBS Lett* 438:171–176
- Tober C, Rostock A, Rundfeldt C, Bartsch R **(1996)** D-23129: A potent anticonvulsant in the amygdala kindling model of complex partial seizures. *Eur J Pharmacol* 303:163–169.
- Tombola F, Pathak MM, and Isacoff EY **(2006)** How does voltage open an ion channel? *Annu. Rev. Cell Dev. Biol.* 22, 23–52.
- Tomonoh Y, Deshimaru M, Araki K, Miyazaki Y, Arasaki T, Tanaka Y, Kitamura H, Mori F, Wakabayashi K, Yamashita S, Saito R, Itoh M, Uchida T, Yamada J, Migita K, Ueno S, Kitaura H, Kakita A, Lossin C, Takano Y, Hirose S **(2019)** The kick-in system: a novel rapid knock-in strategy. *PLoS One* 2014 9: e88549.
- Tykocki NR, Heppner TJ, Dalsgaard T, Bonev AD, Nelson MT **(2019)** The Kv7 channel activator retigabine suppresses mouse urinary bladder afferent nerve activity without affecting detrusor smooth muscle K<sup>+</sup> channel currents. *J Physiol* 597:935-950
- Tzingounis AV, Nicoll RA **(2008)** Contribution of KCNQ2 and KCNQ3 to the medium and slow after hyperpolarization currents. *PNAS* 105:19974–19979
- Tzingounis AV, Heidenreich M, Kharkovets T, Spitzmaul G, Jensen HS, Nicoll RA, Jentsch TJ **(2010)** The KCNQ5 potassium channel mediates a component of the after-hyperpolarization current in mouse hippocampus. *PNAS* 107:10232–10237
- Vawter-Lee M, Franz DN, Fuller CE, Greiner HM **(2019)** Clinical letter: a case report of targeted therapy with sirolimus for NPRL3 epilepsy. *Seizure* 73, 43–45).
- Wang AW, Yau MC, Wang CK, Sharmin N, Yang RY, Pless SA, Kurata HT **(2018)** Four drug-sensitive subunits are required for maximal effect of a voltage sensor-targeted KCNQ opener. *J Gen Physiol.* Oct 1;150(10):1432-1443.
- Wang HS, Pan Z, Shi W, Brown BS, Wymore RS, Cohen IS, Dixon JE, McKinnon D **(1998)** KCNQ2 and KCNQ3 potassium channel subunits: molecular correlates of the M-channel. *Science* 282:1890-1893.
- Wang HS, Brown BS, McKinnon D, Cohen IS **(2000)** Molecular basis for differential sensitivity of KCNQ and I(Ks) channels to the cognitive enhancer XE991. *Mol. Pharmacol.* 57:1218-1223.
- Wang HW, Wang JW **(2017)** How cryo-electron microscopy and X-ray crystallography complement each other. *Protein Sci* 26:32–39
- Wang K, McIlvain B, Tseng E, Kowal D, Jow F, Shen R, Zhang H, Shan QJ, He L, Chen D, Lu Q, Dunlop J **(2004)** Validation of an atomic absorption rubidium ion efflux assay for KCNQ/M-channels using the Ion Channel Reader 8000. *Assay Drug Dev. Technol.* 2:525–534
- Wang L, Qiao GH, Hu HN, Gao ZB, Nan FJ. **(2018)** Discovery of Novel Retigabine Derivatives as Potent KCNQ4 and KCNQ5 Channel Agonists with Improved Specificity. *ACS Med Chem Lett.* Dec 19;10:27-33

- Watanabe H, Nagata E, Kosakai A, Nakamura M, Yokoyama M, Tanaka K, Sasai H **(2000)** Disruption of the epilepsy KCNQ2 gene results in neural hyperexcitability. *J Neurochem* 75:28–33.
- Weber YG, Geiger J, Kämpchen K, Landwehrmeyer B, Sommer C, Lerche H (2006) Immunohistochemical analysis of KCNQ2 potassium channels in adult and developing mouse brain. *Brain Res* 1077:1–6.
- Weckhuysen S, Mandelstam S, Suls A, Audenaert D, Deconinck T, Claes LR, Deprez L, Smets K, Hristova D, Yordanova I, Jordanova A, Ceulemans B, Jansen A, Hasaerts D, Roelens F, Lagae L, Yendle S, Stanley T, Heron SE, Mulley JC, Berkovic SF, Scheffer IE, de Jonghe P **(2012)** KCNQ2 encephalopathy: emerging phenotype of a neonatal epileptic encephalopathy. *Ann Neurol* 71:15–25
- Weckhuysen S, Marsan E, Lambrecq V, et al **(2016)** Involvement of GATOR complex genes in familial focal epilepsies and focal cortical dysplasia. *Epilepsia* 57:994–1003.
- Wickenden AD, Krajewski JL, London B, Wagoner PK, Wilson WA, Clark S, Roeloffs R, McNaughton-Smith G, Rigdon GC **(2008)** N-(6-chloro-pyridin-3-yl)-3,4-difluoro-benzamide (ICA-27243): a novel, selective KCNQ2/Q3 potassium channel activator. *Mol. Pharmacol.* 73:977–986.
- World Health Organization. Epilepsy: a public health imperative (WHO, 2019).
- Wu N, Nishioka WK, Derecki NC, Maher MP **(2019)** High-throughput-compatible assays using a genetically encoded calcium indicator *Sci Rep* 9:12692.
- Wu YJ, Davis CD, Dworetzky S, Fitzpatrick WC, Harden D, He H, Knox RJ, Newton AE, Philip T, Polson C, Sivarao DV, Sun LQ, Tertyshnikova S, Weaver D, Yeola S, Zoeckler M, Sinz MW **(2003)** Fluorine substitution can block CYP3A4 metabolism-dependent inhibition: identification of (S)-N-[1-(4-fluoro-3- morpholin-4-ylphenyl)ethyl]-3- (4-fluorophenyl)acrylamide as an orally bioavailable KCNQ2 opener devoid of CYP3A4 metabolism-dependent inhibition. *J. Med. Chem* 46:3778–3781.
- Wu YJ, Boissard CG, Chen J, Fitzpatrick W, Gao Q, Gribkoff VK, Harden DG, He H, Knox R.J, Natale J, Pieschl RL, Starrett JE Jr, Sun LQ, Thompson M, Weaver D, Wu D, Dworetzky SI **(2004)** (S)-N-[1-(4-cyclopropylmethyl-3,4-dihydro-2H-benzo[1,4]oxazin-6-yl)- ethyl]-3-(2-fluoro-phenyl)-acrylamide is a potent and efficacious KCNQ2 opener which inhibits induced hyperexcitability of rat hippocampal neurons. *Bioorg. Med. Chem. Lett* 14:1991–1995.
- Wu YJ, He H, Sun LQ, L'Heureux A, Chen J, Dextraze P, Starrett JE, Boissard CG, Gribkoff VK, Natale J, Dworetzky SI **(2004)** Synthesis and structure-activity relationship of acrylamides as KCNQ2 potassium channel openers. *J. Med. Chem* 47:2887–2896.
- Wu YJ, Sun LQ, He H, Chen J, Starrett JE, Dextraze P, Daris JP, Boissard CG, Pieschl RL, Gribkoff VK, Natale J, Knox RJ, Harden DG, Thompson MW, Fitzpatrick W, Weaver D, Wu D, Gao Q, Dworetzky SI **(2004)** Synthesis and KCNQ2 opener activity of N-(1-benzo[1,3]dioxol-5-yl-ethyl, N-[1-(2,3-dihydro-benzofuran-5-yl)-ethyl, and N-[1-(2,3-dihydro-1H-indol-5-yl)-ethyl acrylamides. *Bioorg. Med. Chem. Lett.*, 14, (17), 4533–4537.
- Wu YJ, Conway CM, Sun LQ, Machet F, Chen J, Chen P, He H, Bourin C, Calandra V, Polino JL, Davis CD, Heman K, Gribkoff VK, Boissard CG, Knox RJ, Thompson MW, Fitzpatrick W, Weaver D, Harden DG, Natale J, Dworetzky SI, Starrett JE **(2013)** Discovery of (S,E)-3-(2-fluorophenyl)-N-(1-(3-(pyridin-3-yloxy)phenyl)ethyl)-acrylamide as a potent and efficacious KCNQ2 (Kv7.2) opener for the treatment of neuropathic pain. *Bioorg. Med. Chem. Lett* 23:6188–6191.
- Wuttke TV, Seeböhm G, Bail S, Maljevic S and Lerche H **(2005)** The new anticonvulsant retigabine favors voltage-dependent opening of the Kv7.2 (KCNQ2) channel by binding to its activation gate. *Molecular pharmacology* 67:1009–1017.
- Xiong Q, Sun H, Li M **(2007)** Zinc pyrithione-mediated activation of voltage-gated KCNQ potassium channels rescues epileptogenic mutants. *Nat. Chem Biol.* 3, (5), 287–296.

- Xiong Q, Gao Z, Wang W, Li M **(2008)** Activation of Kv7 (KCNQ) voltage-gated potassium channels by synthetic compounds. *Trends Pharmacol. Sci.* 29:99-107.
- Yang Y, Beyer BJ, Otto JF, O'Brien TP, Letts VA, White HS, Frankel WN **(2003)** Spontaneous deletion of epilepsygene orthologs in a mutant mouse with a low electroconvulsive threshold. *Hum Mol Genet* 12:975–984.
- Yang S, Lu D, Ouyang P **(2018)** Design, synthesis and evaluation of substituted piperidine based KCNQ openers as novel antiepileptic agents. *Bioorg Med Chem Lett* 28:1731-1735.
- Yang S, Lu D, Ouyang P **(2018)** Design, synthesis and evaluation of novel N-phenylbutanamide derivatives as KCNQ openers for the treatment of epilepsy. *Bioorg Med Chem Lett* 28:3004-3008
- Yau MC, Kim RY, Wang CK, Li J, Ammar T, Yang RY, Pless SA, Kurata HT **(2018)** One drug-sensitive subunit is sufficient for a near-maximal retigabine effect in KCNQ channels. *J Gen Physiol.* 150:1421-1431.
- Yeghiazaryan NS, Zara F, Capovilla G, Brigati G, Falsaperla R, Striano P **(2012)** Pyridoxine-dependent epilepsy: an under-recognised cause of intractable seizures. *J Paediatr Child Health* 48: E113–5. 50.
- Yeghiazaryan NS, Striano P, Spaccini L, et al. **(2011)** Long-term follow-up in two siblings with pyridoxine-dependent seizures associated with a novel ALDH7A1 mutation. *Eur J Paediatr Neurol* 15:547–50
- Yue C, Yaari Y **(2004)** KCNQ/M channels control spike afterdepolarization and burst generation in hippocampal neurons. *The Journal of Neuroscience: The Official Journal of the Society for Neuroscience*, 24:4614:4624.
- Yue JF, Qiao GH, Liu N, Nan FJ, Gao ZB **(2016)** Novel KCNQ2 channel activators discovered using fluorescence-based and automated patch-clamp-based high-throughput screening techniques. *Acta Pharmacol. Sin* 37:105-110
- Yus-Nájera E, Santana-Castro I, Villarroel A (2002) The identification and characterization of a noncontinuous calmodulin-binding site in noninactivating voltage-dependent KCNQ potassium channels. *The Journal of Biological Chemistry*, 277: 28545-28553.
- Zara F, Specchio N, Striano P, Robbiano A, Gennaro E, Paravidino R, Vanni N, Beccaria F, Capovilla G, Bianchi A, Caffi L, Cardilli V, Darra F, Bernardina BD, Fusco L, Gaggero R, Giordano L, Guerrini R, Incorpora G, Mastrangelo M, Spaccini L, Laverda AM, Vecchi M, Vanadia F, Veggiotti P, Viri M, Occhi G, Budetta M, Taglialatela M, Coviello DA, Vigeveno F, Minetti C **(2013)** Genetic testing in benign familial epilepsies of the first year of life: clinical and diagnostic significance. *Epilepsia* 54: 425–436
- Zaydman MA, Silva JR, Delaloye K, Li Y, Liang H, Larsson HP, Shi J, and Cui J **(2013)** Kv7.1 ion channels require a lipid to couple voltage sensing to pore opening. *Proc. Natl. Acad. Sci. USA* 110: 13180–13185.
- Zhang H, Craciun LC, Mirshahi T, Roha'cs T, Lopes C, M Jin, Logothetis DE **(2003)** PIP2 activates KCNQ channels, and its hydrolysis underlies receptor-mediated inhibition of M currents. *Neuron* 37: 963–975
- Zhang Q, Zhou P, Chen Z, Li M, Jiang H, Gao Z & Yang H **(2013)** Dynamic PIP2 interactions with voltage sensor elements contribute to KCNQ2 channel gating. *PNAS* 110: 20093-20098.
- Zhou X, Ma A, Liu X, Huang C, Zhang Y, Shi R, Mao S, Geng T, Li S **(2006)** Infantile seizures and other epileptic phenotypes in a Chinese family with a missense mutation of KCNQ2. *Eur J Pediatr* 165:691–695.

- Zhou P, Zhang Y, Xu H, Chen F, Chen X, Li X, Pi X, Wang L, Zhan L, Nan F and Gao Z **(2015)** P-retigabine: an N-propargyld retigabine with improved brain distribution and enhanced antiepileptic activity. *Molecular pharmacology* 87:31-38.